

**GCES OFFICE COPY
DO NOT REMOVE!**

**MONITORING OF SAND BAR INSTABILITY DURING THE INTERIM FLOWS:
A SEEPAGE EROSION APPROACH**

FINAL REPORT

**GLEN CANYON ENVIRONMENTAL
STUDIES OFFICE**

NOV 15 1995

**RECEIVED
FLAGSTAFF, AZ**

by
Muniram Budhu and Roger Gobin,
Department of Civil Engineering and Engineering Mechanics,
University of Arizona,
Tucson, Arizona 85721.

Cooperative Agreement: 2-FC-40-13270
Principal Investigator: **Muniram Budhu**

Effective date of Cooperative Agreement: 9-18-92
Termination date of Cooperative Agreement: 12-31-94.

Funded by: The U.S. Department of Interior
Bureau of Reclamation
Glen Canyon Environmental Studies

500.03
PAT-10.00
6558
23681 copy 2

phydep-fulver

U

TABLE OF CONTENTS

ABSTRACT	5
1. INTRODUCTION	8
1.1 Background	8
1.2 Problem Statement	11
1.3 Objectives	12
2. STABLE SEEPAGE SLOPE FOR SANDBARS IN GRAND CANYON	13
2.1 Introduction	13
2.2 Stable Seepage Slope	14
2.3 A "Simple" Model to Predict the Stable Seepage Slope	16
2.4 Determination of the Groundwater Surface	19
2.4.1. Formulation	19
2.4.2 Comparison of Predicted Groundwater Surface with Field Data ..	21
2.5 Comparison of the Predictions of the "Simple" Model with Field Data ...	24
2.6 Summary	32
3. EFFECTS OF DAM OPERATION PARAMETERS ON THE STABLE SEEPAGE PROFILE	34
3.1 Introduction	34
3.2 Effects of Upramping Rates	35
3.3 Effects of Permeability	37
3.4 Effects of Slope Angle	38
3.5 Effects of Downramping Rate	39

3.6 Combined Effects of Ramping Rates, Range of Discharge, Soil Permeability and Slope Angle	41
3.7 Effects of Duration of Peak Discharge	41
3.8 Procedures to Determine Stable Seepage Slopes for a Given Dam Discharge Regime	43
3.9 Illustrative Example	44
3.10 Reduction of Usable Width of Sandbars for Campsites and Riparian Habitat	46
3.11 Reduction of Volume of Sandbars for Campsites and Riparian Habitat .	49
3.11 Summary	49
4. FINITE ELEMENT MODEL FOR SEEPAGE EROSION	52
4.1 Introduction	52
4.2 Observed Aggradation/Erosion Pattern on Sandbar 172L	52
4.3 Comparison of Finite Element Model Predictions with Field Data for Sandbar 172L	56
4.4 Effects of Interim Flow Alternatives	64
4.5 Comparison of Conventional Stability Analyses with Field Data	65
4.6 Summary	66
5. AGGRADATION/EROSION OF SANDBARS IN GRAND CANYON	69
5.1 Introduction	69
5.2 General Conceptual Model	69
5.3 Comparison of Field Data with the General Aggradation/Erosion Conceptual Model	74

5.4 Aggradation/Erosion Within Recirculating Zones	81
5.6 Summary	87
6. SUMMARY AND CONCLUSIONS	88
Equilibrium Profile	89
Effects of Dam Operation Parameters on the Equilibrium Profile	89
Research Flows and Interim Low flows	90
Aggradation/Erosion of Sediments in Grand Canyon	90
Control Flood	92
REFERENCES	93
LIST OF FIGURES	97
NOTATION	101
APPENDIX I	104
Formulation of 'Simple' Model	104
APPENDIX II	119
Formulation of Finite Element Model for Seepage Erosion	119

ABSTRACT

The emphasis of this study is on the effects of seepage erosion (bank cuts, slumping, slope instability and mass wasting) on the stability of sandbars within Grand Canyon. Two models are developed to investigate the effects of seepage erosion on sandbar stability. One, a "simple" model, is intended to provide a method that can be used by dam operators, environmentalists, planners and others to obtain an approximation of the changes in the riparian and recreation environment resulting from changes in dam operation. The other is a finite element model which provides better insights into seepage erosion from fluctuating dam discharges than the "simple" model and can predict the rate of erosion from different discharge regimes. Both models are restricted to two dimensions. The simple model is based on limit equilibrium considerations and assumes worst case seepage conditions, which occur when seepage is parallel to the sandbar face.

Sandbars in Grand Canyon exist in a stable condition when the lower seepage slope is between 11° and 14° (or lower) and the upper seepage slope is less than or equal to the angle of friction of the soil (30° to 32°). Sediments deposited on the stable seepage profile becomes unstable due to seepage forces and collapse during falling river stage. Predictions from the theoretical models are consistent with field data from twenty-eight of twenty-nine regularly monitored sandbars. The use of the simple model requires a knowledge of the groundwater level within the sandbar. The finite element method is shown to predict groundwater levels which agree with field data. A set of equations and

procedures is developed to determine the stable seepage slope for any given dam discharge regime and soil conditions.

Detailed analyses of failures observed on sandbars show that there is a preferred failure plane that delineates the stable seepage profile from freshly deposited sediments (transient sediments). Sediments below the stable seepage profile are well consolidated and denser than the freshly deposited sediments. The boundary between the two different types of sediments forms a natural discontinuity along which failure occurs. Analyses performed with the aid of the finite element model and conventional slope stability programs confirm that failures are indeed occurring along a predefined failure surface.

The relationship between seepage erosion and eddy dynamics is examined and a conceptual model that couples seepage erosion with eddy dynamics is presented. Variations in dam discharge regime cause changes in the recirculating zones (zones which are partially sheltered from the dynamics of the main channel, within which eddy systems operate) resulting in cycles of erosion and deposition of transient sediments. The aggradation/erosion of transient sediments in Grand Canyon involves both dam operation and natural phenomena.

The conceptual model shows that if the Colorado River downstream of Glen Canyon Dam were a single channel then the sandbars would have existed in a stable state. Since several tributaries are present and natural events such as snow melts, rainfall, debris flow occur frequently, perturbations about the stable state occur.

Controlling dam discharge regimes would not prevent the aggradation/erosion of sandbars in Grand Canyon. By lowering the peak discharge, the amount of sediments

involved in the cycles of aggradation/erosion would reduce. Floods (natural and deliberate) are likely to deposit sediments at higher elevations and widen sandbars. However, when the floods recede and normal dam operation recommences, slope failures would recur and the initial volume of sediments involved is likely to be much greater than that involved in pre-flood events.

CHAPTER 1

INTRODUCTION

1.1 Background

Glen Canyon Dam, located in the northeastern corner of Arizona (Fig. 1.1), was commissioned in 1963 to provide flood control, water storage and hydroelectric power for some western states in the USA (Stevens, 1983). The dam is operated as a peaking facility; that is; it produces electrical power when there is a demand. Dam discharge varies during the day, creating a daily tide. Peak dam discharge usually occurs at about the middle of the day. Typical daily river stage fluctuation is between 1 m to 3 m with some narrow river sections reaching 4 m.

Before the construction of Glen Canyon Dam, the unregulated Colorado River was laden with sediments. During periods of heavy precipitation, large volumes of sand, silt and mud were transported by the tumultuous murky flow in the channel. In the post dam era, most of the sediments are trapped upstream of the dam in Lake Powell. The water downstream of the dam is almost clear with very little sediment. Sediment concentration near Lees Ferry was in excess of 10,000 parts per million prior to the construction of the dam. Now, the sediment concentration there is about 200 parts per million (Schmidt and Graf, 1990).

In the pre-dam era, the mean annual maximum flow , for the period in which flow has been measured, was 2439 cubic meters per second (m^3/s) with a record flow of 5660 m^3/s in 1921 (Howard and Dolan, 1981). The river banks were continuously scoured, especially during the spring snow melt and periods of heavy precipitation. However, some of the scoured areas were rebuilt during the receding flood waters because of the large sediment load in the river. Regular scouring of the river banks prevented the development of vegetation below the old high water line in the pre-dam period.

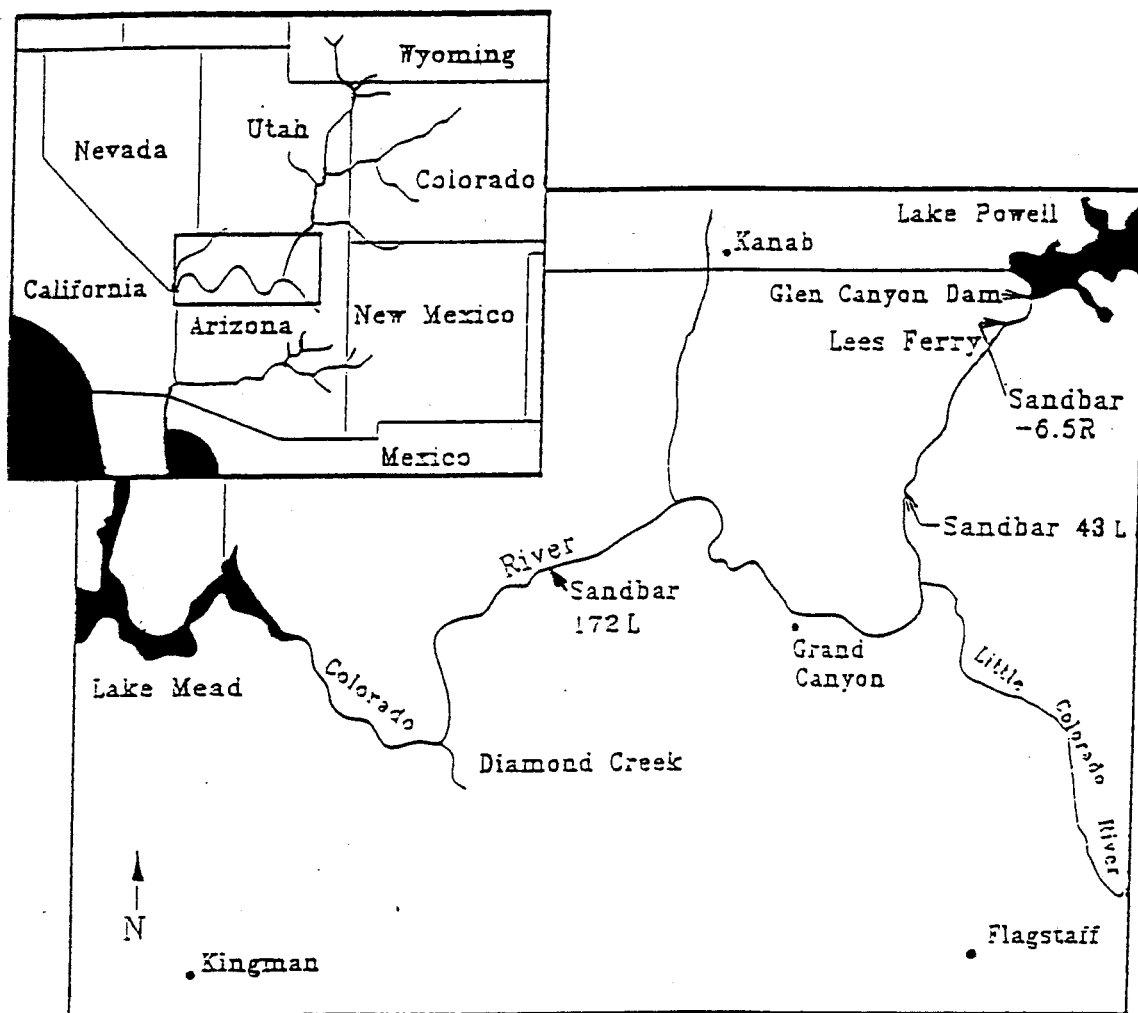


Fig. 1.1. Map of the study area.

Glen Canyon Dam regulates the flow of the Colorado River, which varies between 57 m³/s and 849 m³/s. A lush, vibrant, band of vegetation supporting a rich and diverse riparian life exists along the Colorado River (Turner and Karpiscak, 1980). The continued existence of this new riparian habitat is challenged by erosion processes. Daily tidal variations in river stage encourage seepage which results in bank slumps, rilling, and other erosion features on many of the sandbars used for recreation and riparian habitat. These sandbars are scattered along the banks of the main channel but are more common at the confluences of ephemeral tributaries and the main channel. During floods or high dam releases, deposits at the confluences and fresh sediments from the ephemeral tributaries are transported and then redeposited at locations conducive to aggradation. At these locations, where the velocity is much lower than the average velocity, new sandbars are formed and existing sandbars are either replenished, if prior erosion occurred, or increased in size. The sandbars form a natural environment for riparian habitat and campsites for rafters and hikers.

In response to public concerns on the environmental impact of the operation of Glen Canyon Dam, special flow regimes termed 'research flows' were conducted by the Bureau of Reclamation from June 1990 to July 1991. These research flows were intended to evaluate the effects of alternative flows on downstream resources and to provide data for an environmental impact statement. The results from the research flows and an environmental assessment led the Bureau of Reclamation to begin testing 'interim flow' regimes in August 1991. The purpose of the interim flows was to protect downstream resources pending the completion of the environmental impact statement. Following the

interim flow regimes, a set of interim operating criteria was introduced in November 1991 to reduce, if not eliminate, the negative impacts on downstream resources while still providing some measures of flexibility for power generation until the completion of the environmental impact statement. The minimum and maximum releases were restricted to 226.5 m³/s (8000 cfs) and 566.3 m³/s (20,000 cfs) respectively while daily fluctuations were kept to below 169.9 m³/s (6000 cfs). The releases, known as 'interim low fluctuations flow' are summarized in Table 1.1.

Table 1.1 Interim Low Fluctuations Flow

Minimum releases (m ³ /s)	Maximum releases (m ³ /s)	Daily fluctuations (m ³ /s/24hrs)	Ramp rate (m ³ /s/hr)
226.5 between 7 a.m. and 7 p.m. 141.6 at night	566.3	141.6, 169.9 or 226.5	70.8 up 42.5 down

1.2 Problem Statement

Three agents - seepage, traction and wave - have been identified as causes of erosion downstream of the Glen Canyon Dam (Budhu, 1992). Seepage erosion has been identified as ubiquitous (Budhu, 1992). Three questions that arise are

- What is the erosion process downstream of Glen Canyon Dam?
- What is the extent of seepage erosion on sand bars that negatively impacts the riparian and recreation environment?
- Does the interim low fluctuating flow regime reduce the rate and amount of seepage erosion?

This report is intended to address these questions.

1.3 Objectives

The objectives of this study are:

- ▶ Determine if there is a dynamic equilibrium slope for Grand Canyon sediment deposits, and relate this information to the proposed bar building flow.
- ▶ Determine the range of dam related fluctuations, downramping rates and duration of minimum flow that will minimize seepage driven erosion.
- ▶ Determine dam discharges that are conducive to sandbar aggradation and degradation.
- ▶ Determine if the interim flows are more conducive to sandbar stability than either the research flows or normal flows.

CHAPTER 2

STABLE SEEPAGE SLOPE FOR SANDBARS IN GRAND CANYON

2.1 Introduction

The negative influence of seepage on slope stability has been recognized for a long time (Casagrande, 1937). Seepage of groundwater has often resulted in catastrophic slope failures. River banks, embankments of canals and reservoirs, and hillside slopes are typical examples of situations where seepage erosion has been observed (Hagerthy, 1991a,b; Iverson and Major, 1986). There are two basic theoretical approaches to deal with seepage problems. These are (a) the particulate approach and (b) the continuum approach.

The particulate approach is only applicable to non-cohesive material, while the continuum approach can be applied to any soil type. In the particulate approach (for example, Howard and McLane, 1988), the stability of a representative grain is considered using force equilibrium. Empirical coefficients are used to account for factors such as packing of the grains and grain size variations.

The continuum approach (eg. Taylor, 1948; Iverson and Major, 1986) involves the consideration of an elemental unit (area or volume) of soil in which the soil properties are taken as lumped values for the entire unit. This approach requires the determination of the angle of internal friction, cohesion and the density of the soil. These properties can be obtained, with reasonably good accuracy, from simple laboratory soil tests.

In this chapter, the continuum approach will be used to determine the maximum stable slope angle for an infinite slope under a given seepage regime. Procedures will be developed to determine the maximum stable seepage slope for sandbars in Grand Canyon and field data will be used to validate these procedures.

2.2 Stable Seepage Slope

Dry sand can form a stable slope at an angle equal to its angle of internal friction. The angle of internal friction for dry and saturated sand is about the same. A sand mass will collapse to a smaller stable slope (stable seepage slope), if water is allowed to seep through it (Taylor, 1948). The stable seepage slope angle depends on the soil properties, the direction and magnitude of the seepage vector (Appendix 1). When the hydraulic and hydrologic conditions are favorable for deposition, existing sandbars tend to enlarge. When submerged, the depositional slopes can grow from the extant slope value to values sometimes greater than the angle of friction of the soil. The latter steep slopes are possible because the lateral water pressure stabilizes the slopes during deposition. When the water level drops, depositional slopes may become unstable.

Sandbar failures can be provoked by two different mechanisms when the external water level is lowered. One occurs when the water level drops very rapidly so that the pore water pressure within the slope may become large enough to cause slope failures to

occur. This type of failure is termed an "undrained" slope failure. It usually occurs on slopes in reservoirs, dams and embankments under rapid drawdown conditions. Failure is sudden and is usually observed when the water level is lowered to a certain threshold value. The other, is caused by a combination of increased pore water pressure and seepage forces. As the river stage is lowered, water accumulated during the rising river stage must drain from the sandbar. During the drainage of bank stored water, seepage forces are developed. The seepage forces now act in combination with the pore water pressures to trigger slope failures.

The formulation of a simple model to determine the maximum stable seepage slope is presented in Appendix 1. The maximum stable seepage slope is defined here as the slope angle below which bank cuts or slope failures would not normally occur from seepage forces. From Appendix I, seepage parallel to the slope ($\lambda = 90^\circ$, where λ is the seepage direction measured from the outwards normal to the sandbar face) produces the maximum stable seepage slope (α_s) given by

$$\alpha_s = \tan^{-1}\left(\frac{\gamma'}{\gamma_{sat}} \tan\phi\right) \quad (2.1)$$

where γ' is the effective unit weight, γ_{sat} is the saturated unit weight and ϕ is the effective angle of friction of the soil.

In deriving equation (2.1), the following assumptions were made

- homogeneous, cohesionless sediments (sand)
- infinite slope

- stress free boundaries
- fully saturated sandbar with the groundwater at the top of the slope

Equation (2.1) is defined for a saturated, cohesionless soil. The effects of cohesion and saturated-unsaturated sediments on slope stability are described in Appendix I.

2.3 A "Simple" Model to Predict the Stable Seepage Slope

Glen Canyon Dam is operated such that water is discharged at a suitable rate to meet peak power demands, which occur for relatively short intervals (about 2 hours). The peak discharge duration is usually not long enough for the groundwater level in sandbars to equilibrate with the peak river stage. Therefore, equation (2.1) cannot be directly applied to the sandbars in Grand Canyon. The assumption of seepage parallel to the slope in deriving equation (2.1) is also only reasonable for the lower portion of the seepage face.

The following procedure is now proposed to determine the stable seepage slope. Consider a sandbar at its maximum depositional slope. Discharge from the dam will cause water to infiltrate into the sandbar and the groundwater level to rise. At peak discharge, the groundwater level in a typical sandbar can be represented by the curve shown in Fig. 2.1. The groundwater level is dependent on dam operation - rate and magnitude of discharge, duration of peak discharge, and the soil condition permeability and homogeneity.

The proposed procedure to determine the stable or equilibrium seepage slope is as follows.

(1) The stable slope of a sandbar below the low water level (AB, Fig. 2.1) would be the angle of friction of the soil. A stable slope greater than the angle of friction can exist below the low water level because of the lateral pressure exerted by the water. However, because deposition usually occurs under flowing water, which imposes a destabilizing shear force on the sandbar face, AB is usually a few degrees less than the angle of friction of the soil.

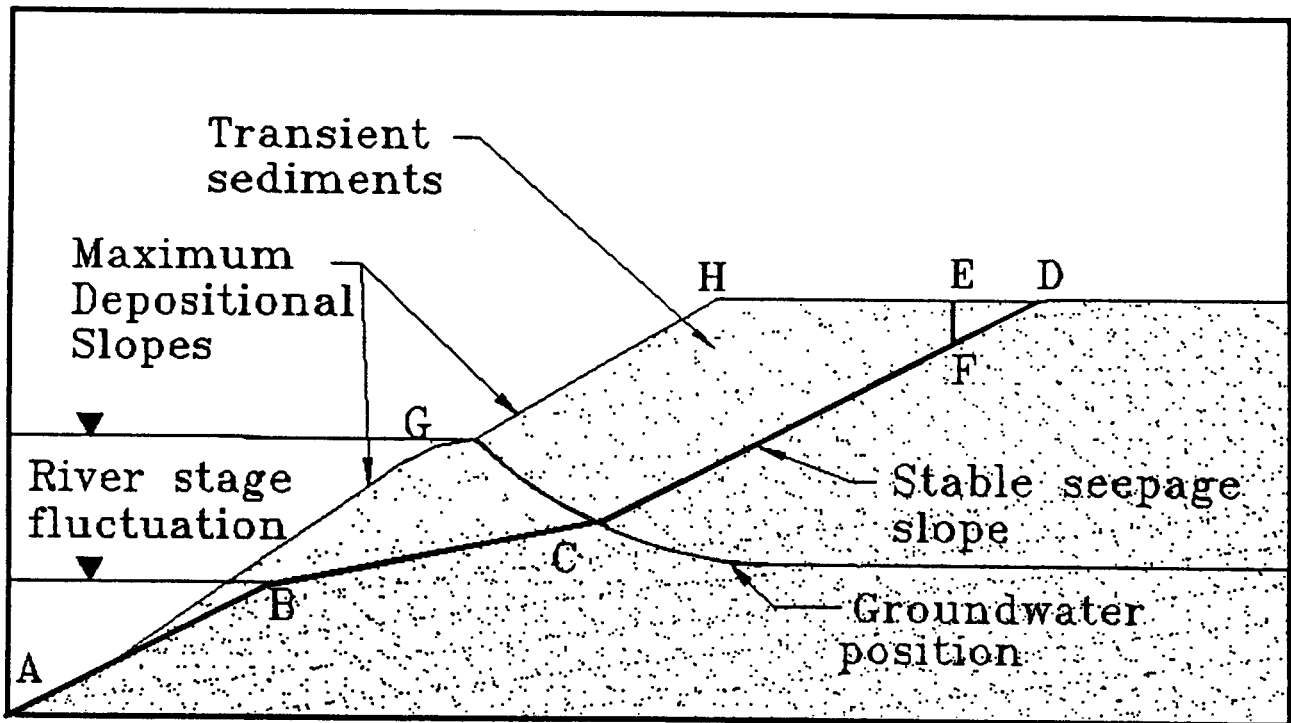


Fig. 2.1. Proposed stable seepage slope.

(2) For the lower part of the seepage face, the stable seepage slope angle (BC) would be approximately equal to α_s . That is, a plane of slope, α_s , drawn from the lowest water level, intersecting the groundwater level at peak river stage at C represents the stable seepage slope of the lower portion of the active sandbar face (Fig. 2.1).

(3) The portion of the sandbar above the groundwater level will not be affected directly by seepage forces. The stable slope for this portion of the sandbar would be its angle of internal friction described by plane CD.

(4) If the soil has some cohesion, then a vertical face (tension crack), EF, of depth

$$h_c = \frac{2c}{\gamma_t \sqrt{K_a}} \quad (2.2)$$

where c is the cohesion of the soil, γ_t is the total unit weight and K_a is the lateral earth pressure coefficient, will intersect the slope CD at F. The presence of vegetation, in particular tree roots, would increase the depth of the vertical face. Capillarity can also result in the formation of vertical faces on the sandbars. However, such faces would be unstable when fully inundated.

The surfaces ABCFD or ABCFE that characterize the stable seepage slopes (stable seepage profile) define the upper limit for slope stability under seepage and can be further degraded by rilling, tractive, wave and other erosion processes. The soil enclosed within

these surfaces and the maximum depositional slopes constitutes sediments that would be in a state of flux undergoing cyclic accretion and erosion. The sharp changes at B, C, and F are unlikely to occur naturally and a gradual transition in slopes is to be expected.

To determine the stable seepage profile, the soil properties and the location of the groundwater surface for a given range and rate of discharge must be known. The key soil properties are the unit weight, permeability and angle of friction. These can easily be determined from standard geotechnical laboratory or field tests. Although the groundwater surface can be measured, using pore water sensors (Carpenter et al., 1992), the expense and time involved are exorbitant. We opted to use numerical methods to predict the groundwater level under various dam discharge regimes.

2.4 Determination of the Groundwater Surface

2.4.1. Formulation

There are various numerical techniques (Taylor and Brown, 1967; Neuman and Witherspoon, 1971; Neuman, 1973; Desai, 1976; Bathe and Khoshgoftaar, 1979; Desai and Li, 1983; Desai, 1984; Lacy and Prevost, 1987; Cividini and Gioda, 1989) available for the prediction of groundwater level for unconfined seepage flows. The differences between the methods stem from the techniques used in solving the governing equations, which involve Darcy's law and continuity. Apart from problems with very simple geometry, where closed-form solutions may be found, these situations usually require the use of

numerical techniques - finite difference method, finite element method and boundary element method. The finite difference method has many drawbacks when dealing with complex boundary geometry , as a result the finite element and boundary element methods are becoming the methods of choice (de Marsily, 1986).

In this investigation a fixed mesh (also called invariant or constant mesh) finite element approach in which the whole domain (saturated and unsaturated zones) is discretized is used. The location of the groundwater surface is found by interpolating between positive and negative pressure heads. The coefficient of permeability for the saturated soil is retained for elements with positive pressure heads but changes according to a pressure-coefficient of permeability relationship for elements with negative pressure heads (Desai and Li, 1983).

The boundary element method (Liggett, 1977) offers less time-consuming data input since only the boundary of the domain is discretized rather than the whole domain as in the finite element method. In the boundary element method, functions are defined which satisfy the governing equations exactly with approximations confined to the boundary conditions. In contrast, with the finite element method, the boundary conditions rather than the governing equations are satisfied exactly.

In transient problems, each cycle of infiltration and seepage imposes stress changes which may influence the location of the groundwater surface in certain types of soils, especially soft normally consolidated clays. A fall in river stage would cause a decrease in the hydrostatic pressure on the face of the river bank and a decrease in pore

water pressure within the bank with a concomitant increase in effective stresses. The soil will consolidate and the permeability will decrease. A rise in river stage would do the opposite. In the conventional approach to groundwater problems, the stress changes are not coupled to the flow equations.

For the purpose of this study, we developed a finite element coupled seepage-stress-consolidation analysis utilizing Biot's (1941) consolidation theory. The details of this analysis are presented in Appendix II. A boundary element solution of the Laplace's flow equation (Budhu, Contractor and Wu, 1994) and groundwater data from sandbar - 6.5R are used to check the capability and validity of the finite element model developed.

2.4.2 Comparison of Predicted Groundwater Surface with Field Data

Sandbar -6.5R (Fig. 1.1), located on the right bank of the Colorado River about 10.5 kilometers upstream from Lees Ferry and some 16 kilometers downstream of Glen Canyon Dam, was used as the test site to provide the groundwater data. It is the smallest sandbar of three test sites (Beus et. al., 1992); its area is about 3700 square meters (Fig. 2.2). This sandbar, at the time when the first batch of groundwater instrumentation was installed, had a gentle slope of approximately 1:6. It is composed of a well-graded sand with an average grain size of 0.13 mm. A thin layer of clayey silt, with an average thickness about 0.3 m in a half bowl shape, separates the sandbar into two similar sand zones (Fig. 2.2). Along three cross sections of the sandbar, a network of pore water

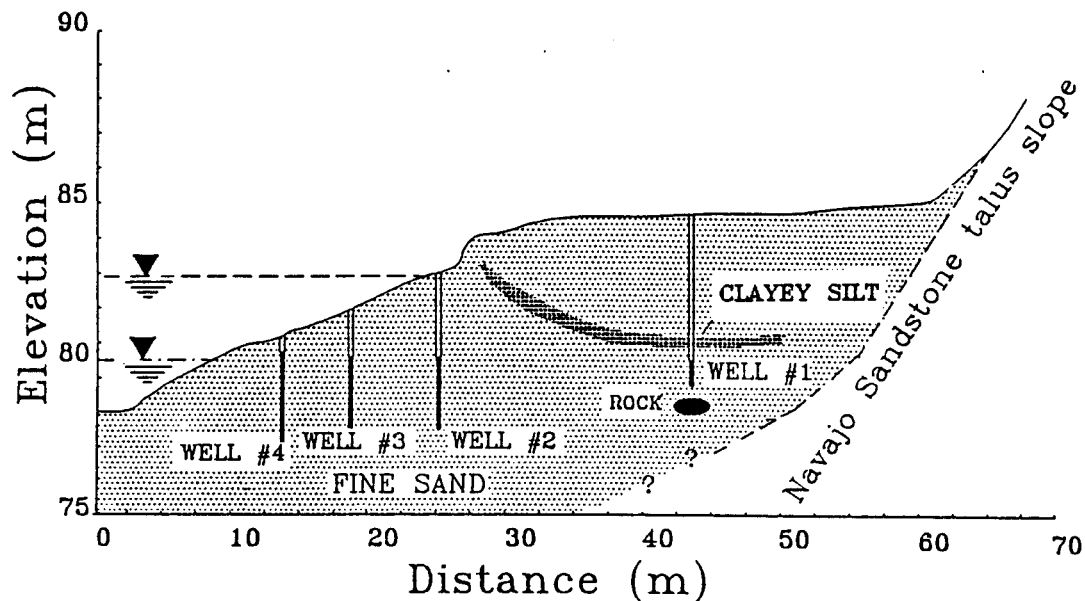


Fig. 2.2. Geological section of sandbar -6.5R.

pressure sensors was installed by Rick Inglis, U.S. National Park Service hydrologist. The outputs from the pore water pressure sensors were monitored every 20 minutes, stored on a memory board, and retrieved by downloading to a portable computer.

Numerical simulations using the finite element and boundary element methods were performed using river stage data supplied by Rick Inglis. Comparisons between the groundwater level predicted by the finite element method for research flows, Flow G and Flow E, and field data, are shown in Figs. 2.3 and 2.4. The groundwater level predicted by both numerical models closely match the field data, especially during the rising river

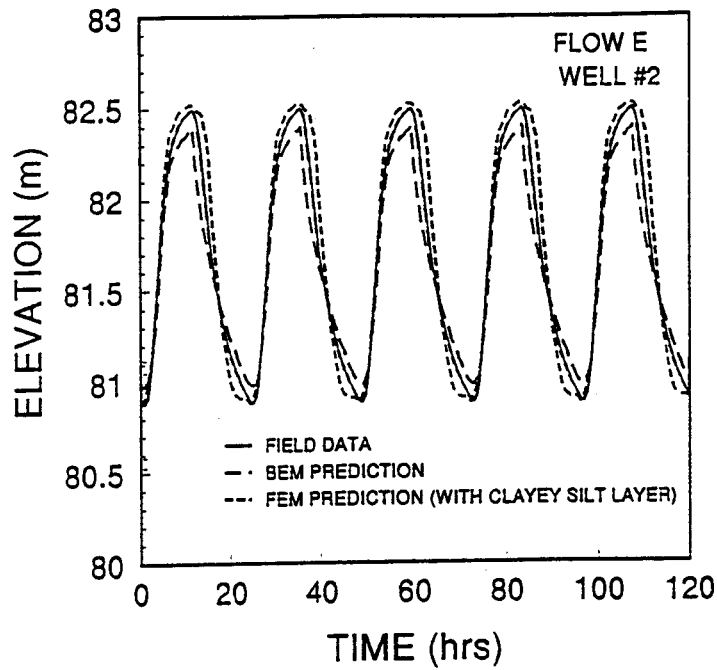


Fig. 2.3. Comparison between model predictions and field data, Flow G.

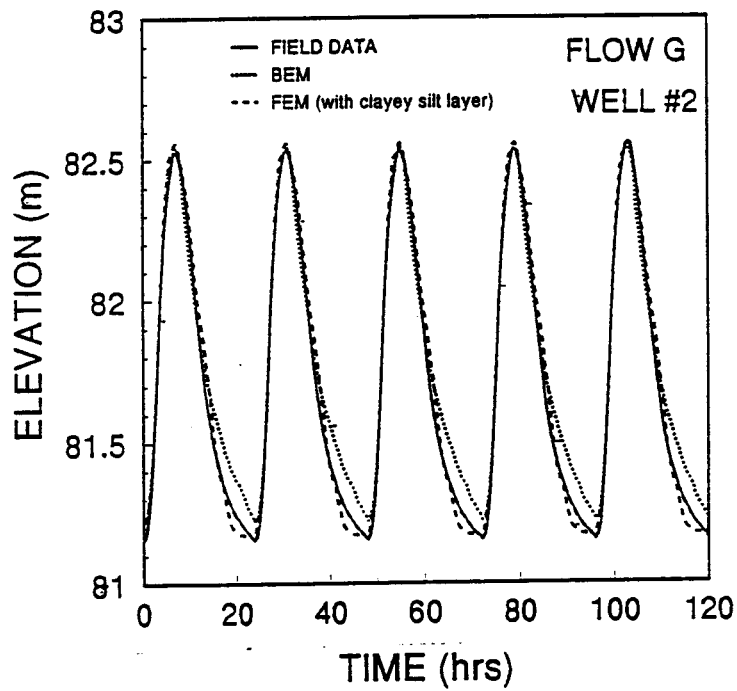


Fig. 2.4. Comparison between model predictions and field data, Flow E.

stage. However, the finite element method's predictions shows better agreement with the field data for the falling river stage than the boundary element method. The finite element method accounts for the clayey silt layer, stress and volumetric changes of the soil from transient river stage. However, the results from the finite element method shows very small volumetric changes (as expected) and neglecting the clayey silt layer did not affect the groundwater level significantly. The possible reason for the differences in the predictions between the two numerical models stems from the effects of saturation-desaturation. The finite element takes account of this but the boundary element does not. The capability of the models to make predictions of the changes in groundwater level due to transient flow was reflected by the good agreement with field data. No calibration run was made and no parameter was varied to provide a good match between the predicted and the field data.

2.5 Comparison of the Predictions of the "Simple" Model with Field Data

Three sites, sandbars - 6.5R, 43L and 172L (Fig. 1.1) - were instrumented by United States Geological Survey (Carpenter et al., 1992) with pore water pressure, temperature and tilt sensors. Ground and bathymetric surveys were periodically conducted at these sites as well as at twenty-six other sandbars by a team of scientists from Northern Arizona University (Beus et. al., 1992). Each sandbar was divided into several transects (between

7 and 10) for detailed ground surveys. Time lapsed photography was conducted by Cluer (1992) to monitor the behavior of some sandbars. Soil properties were obtained from soil tests conducted on samples of sediments from sandbars -6.5R, 43L and 172L (Budhu, 1992)

Sandbar -6.5R has a gentle slope of about 1:6. Rill erosion is evident on the sandbar face but no slope failure was recorded during the two-year study period. The stable slope BC (Fig. 2.5) determined from the survey data is 10° compared with a predicted value of 11.6° using equation (2.1) with the appropriate soil properties, $\gamma_{sat} = 16 \text{ kN/m}^3$ and $\phi = 28^\circ$.

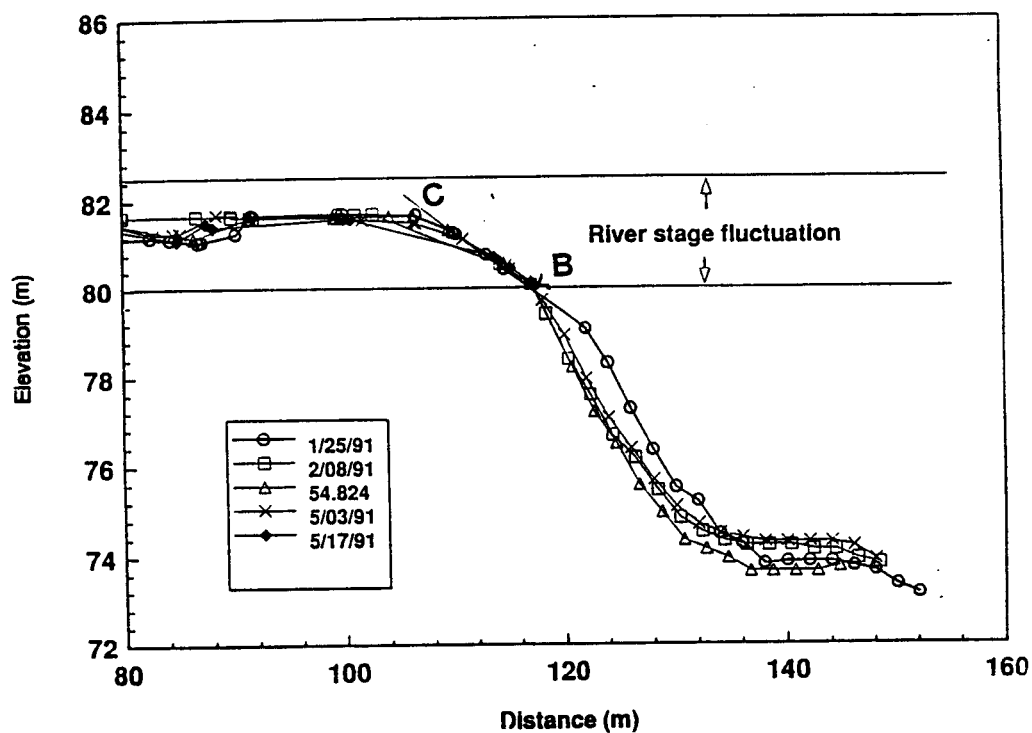


Fig. 2.5. Comparison of predicted stable seepage slope with ground survey data for sandbar -6.5R.

Sandbar 43L is located 69.4 km downstream of Lees Ferry on the left bank of the Colorado River. The soil at this site consists essentially of a fine sand with pockets of coarse sand and gravel (Fig. 2.6). At the back of this sandbar is a redwall limestone talus slope with a narrow but deep return channel. Rill erosion dominated the sandbar face. The predicted stable seepage profile is shown by the plane BCD with the slopes BC and CD of 12.6° and 30° respectively (Fig. 2.7). The predicted stable seepage slope is in good agreement with the profile obtained from the survey data. No slope failure event was recorded on sandbar 43L during the two-year research study period; the sandbar aggradated during this period.

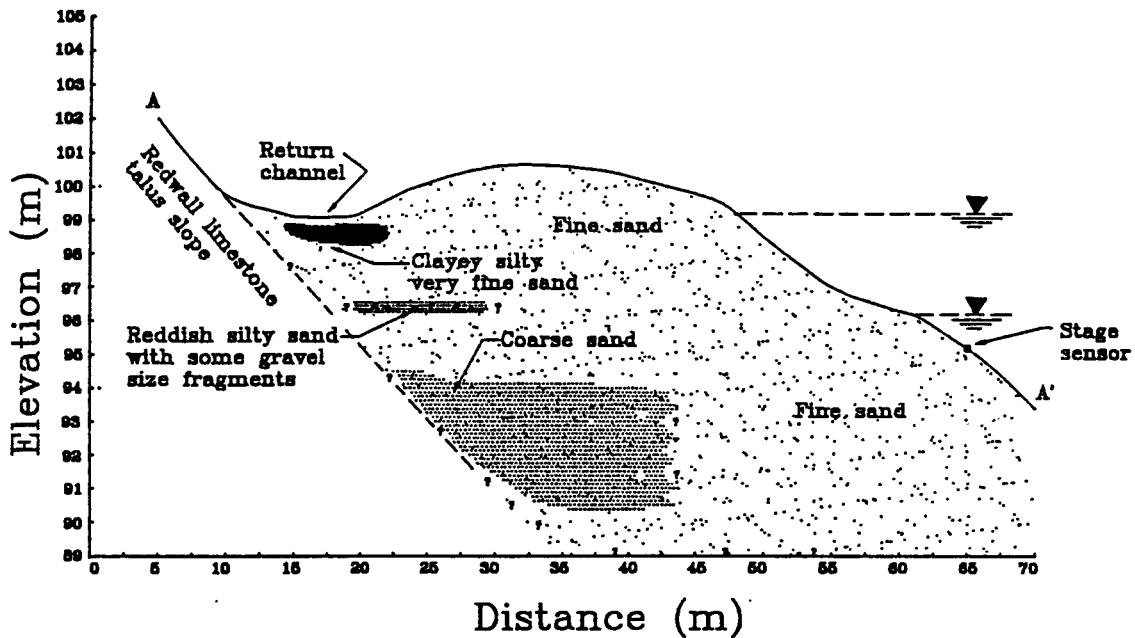


Fig. 2.6. Geological section of sandbar 43L.

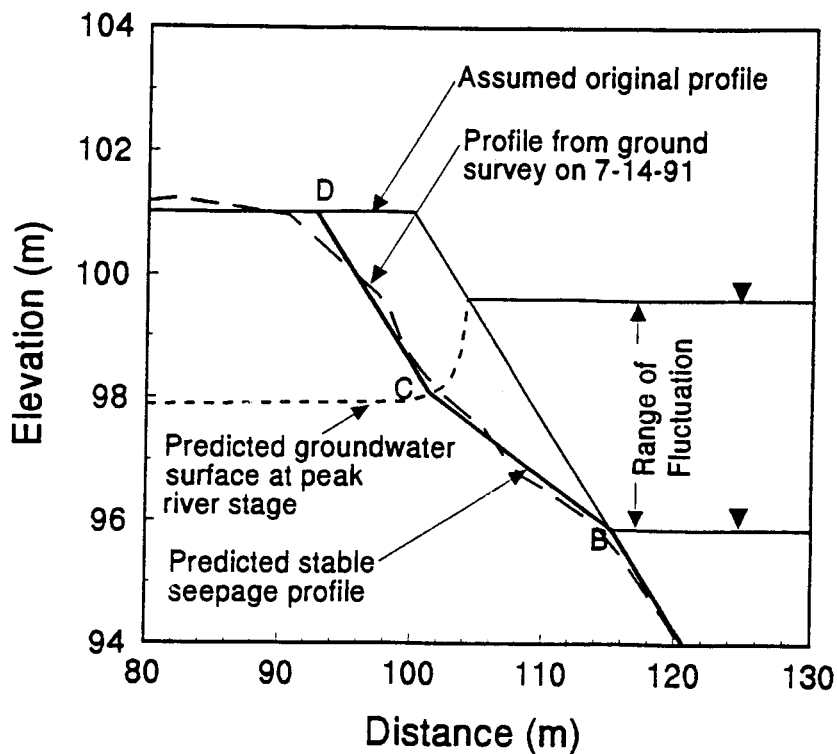


Fig. 2.7. Comparison of predicted stable seepage profile with ground survey data for sandbar 43L.

Sandbar 172L is located 277 kilometers (172 miles) downstream of Lees Ferry on the left bank of the Colorado River in Grand Canyon National Park (Fig. 1.1). This is the most active of the instrumented sandbars. It underwent several cycles of erosion and deposition during the study period. Sandbar 172L is composed of two zones of material (Fig. 2.8). Zone I, a stable zone, is a fine to medium sand with a small amount of silt and clay (<10% by weight). Zone II, an unstable (transient) zone of varying size, is a very fine sand to medium sand with a small amount of silt and clay. The top of the sandbar is capped with a layer of silty sand upon which vegetation and some forms of riparian life

flourish. The saturated unit weight of the soil in Zone II near to the face (dark shaded) is 16 kN/m^3 compared with 17.2 kN/m^3 in Zone I toward the back of the sandbar (lightly shaded).

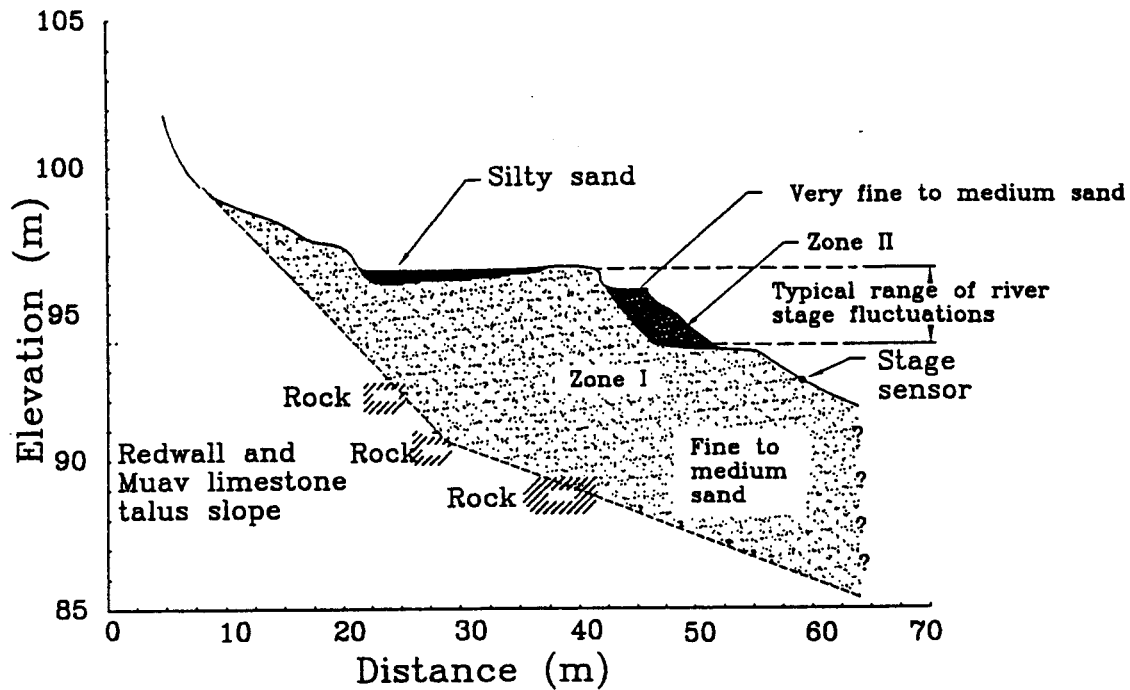


Fig. 2.8. Geological section of sandbar 172L.

The effective angle of friction from simple shear tests was 32° for the soil in Zone I and 30° for the soil in Zone II. Field permeability measurements using a falling head permeameter gave average coefficient of permeability of $2.3 \times 10^{-2} \text{ cm/s}$. for Zone I and $4.2 \times 10^{-2} \text{ cm/s}$. for Zone II. The coefficient of permeability showed insignificant changes under the different research flow regimes.

Prior to a flood in 1983, caused by an unusual springtime release from the dam, the width of sandbar 172L was narrower than the current width as shown in Fig. 2.8. The lowest river stage at that time was about elevation 92.6 m (Stevens, 1992, and from geomorphic features evident in the survey data). It was assumed that sandbar 172L had achieved a maximum slope AD of 26° (Fig. 2.9) during or just prior to the 1983 flood, and subsequently collapsed to the stable slope BCD. Using equation (2.1), the predicted inclination of BC is 12.6° and the inclination of CD is 30° . The predicted stable seepage slope, BCD, is in good agreement with field data (Fig. 2.9). Any further enlargement of this sandbar with slopes greater than the stable seepage slope will eventually collapse back

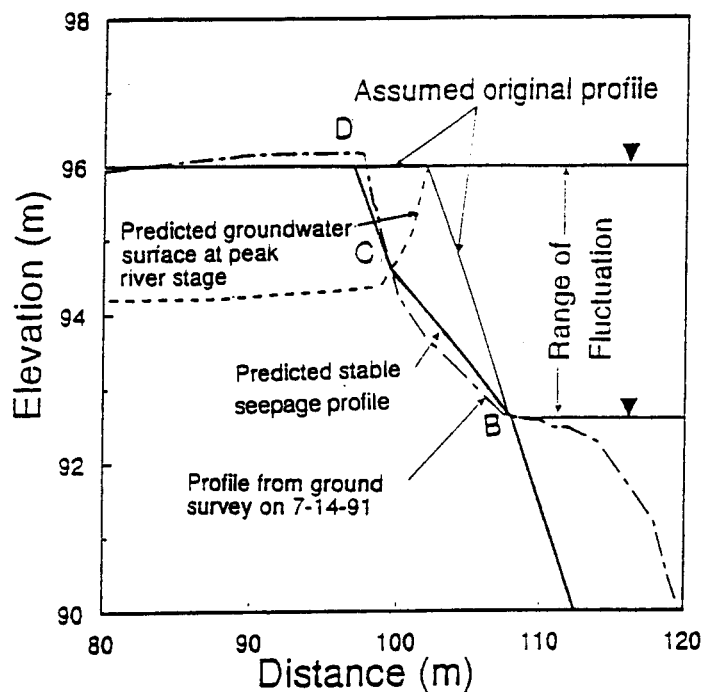


Fig. 2.9. Comparison of predicted stable seepage profile with ground survey data for sandbar 172L.

to the profile BCD. The stable seepage profile, BCD, becomes the preferred failure plane since this plane is a natural discontinuity between the older and the freshly deposited sediments. maximum lower seepage slope (BC) and the maximum upper seepage slope (CD) were extracted from each profile. For each sandbar, the average value of these slopes for each transect was calculated and then the average over all the transects was computed. The results are shown in Table 2.1. On some sandbars, there were some small transition slopes between AB and BC, and BC and CD, these transition slopes were ignored. The predicted values of the stable seepage slopes based on the range of soil properties measured (Budhu, 1992) are compared with the average values for twenty-eight of the twenty-nine sandbars at the bottom of Table 2.1. Sandbar 8, had only a single slope and was excluded from Table 2.1. The agreement between the field data and the model lends credence to the use of the simple model and emphasizes the importance of seepage in shaping the profiles of sandbars below Glen Canyon Dam. The average stable seepage slope (equilibrium profile) for sandbars in Grand Canyon is made up of a lower seepage slope at an angle of approximately 11° starting from the low water level followed by an upper slope of slope angle 30° .

Table 2.1 Slopes (degrees) measured during the study period.

SANDBAR	SLOPE AB	SLOPE BC	SLOPE CD
-6.5	28.93	10.93	30.14
3	26.89	13.88	32.11
16	29.12	9.66	32.26
30	29.05	13.32	27.11
31	28.95	13.50	30.12
43	26.32	19.87	32.81
45	27.41	13.92	31.35
47	28.12	11.31	29.73
50	28.16	13.70	31.12
51	28.42	13.99	29.12
68	28.19	9.95	25.63
81	30.01	10.51	30.08
91	28.15	12.57	31.96
93	28.20	9.80	31.48
104	27.17	15.13	32.62
119	29.95	11.20	32.60
122	27.48	9.83	28.46
123	25.02	6.24	31.91
137	29.63	8.13	32.77
145	28.32	9.2	27.53
172	25.65	10.51	28.17
183	28.34	8.71	33.11
194	27.28	7.21	28.95
203	28.09	7.12	28.80
213	28.28	8.56	28.18
220	28.90	8.10	31.21
Average Slope	28.11	11.17	30.33
Std. Deviation	1.23	2.93	2.07
Predicted by "simple" model	26-32	11-14	26-32

2.6 Summary

In this chapter, an analytical model to predict the extent of seepage erosion on a given sandbar is formulated. This model, termed the simple model, is based on limit equilibrium conditions for a sand mass subjected to seepage and gravitational forces. Seepage effects are critical when seepage is parallel to the slope of the sandbar. In this case, the stable seepage slope is approximately one-half the angle of friction. The simple model relates the position of the groundwater level to the area of the sandbar that will be affected by seepage erosion. This model can be used to obtain a first approximation of the extent to which seepage erosion is likely to affect the stability of a given sandbar. Analysis of the monitored sandbars showed that all but one of the sandbars attained stable seepage profiles that closely matched those predicted by the simple model.

Sandbars in Grand Canyon tend to achieve a stable seepage profile consistent with the dam discharge regime. The stable seepage profile consists of three distinct slopes - a depositional slope below the low river stage ranging between 26 - 32°, a lower seepage slope ranging between 11 - 14° (and lower) and an upper slope ranging from 26 - 32°. The presence of tree roots and cohesion of the soil allow for the development of a vertical face near the sandbar surface. Sediments deposited above the stable seepage profile are unstable and erode readily from seepage forces.

CHAPTER 3

EFFECTS OF DAM OPERATION PARAMETERS ON THE STABLE SEEPAGE PROFILE

3.1 Introduction

The position of the groundwater surface must be known in order to determine the stable seepage profile. Numerical models capable of predicting groundwater level variation within a soil mass when subjected to a transient external water level are not widely available. In addition, reliable predictions with numerical models usually require users that are familiar with numerical modeling techniques and the availability of suitable computer resources. For dam management, a quick, simple and accurate method to locate point C (Fig. 2.1) on the stable seepage profile is required.

The vertical projection of BC, the stable seepage slope, (Fig. 3.1) is related to the variation in river stage (H_w) by a factor β . The factor β is dependent mainly on the stage variation (range of dam discharge), rate of rising river stage (r), rate of drawdown of river stage (d), duration of peak discharge (P_t), coefficient of permeability (k) of the soil and the slope angle (s). In this chapter, the effects of the parameters r , k , d , s and P_t are examined individually and then coupled using optimization techniques. The finite element model described in Appendix II is used to predict the groundwater surface under different dam discharge regimes.

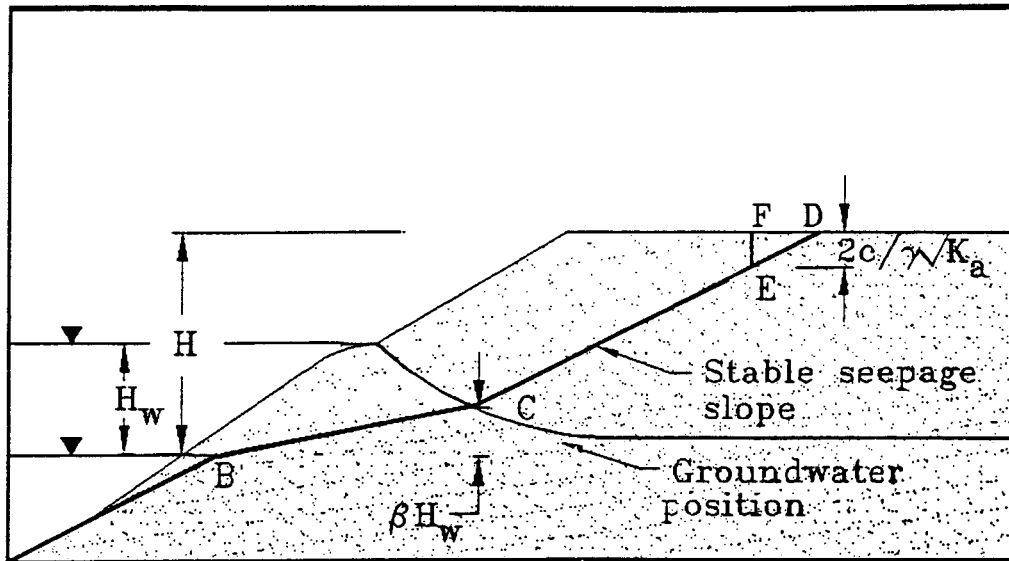


Fig. 3.1. Relationship between groundwater surface and river stage variation.

3.2 Effects of Upramping Rates

Various rates of rise of river stage were imposed on a sandbar with a slope of 26° (a typical depositional slope for sandbars in Grand Canyon) and a soil permeability of 1×10^{-5} m/s. The predicted groundwater surfaces using the finite element method (Appendix II) are shown in Fig. 3.2 together with the stable seepage slope. A plot of the variation of β (extracted from Fig. 3.2) with rate of rise of river stage (Fig. 3.3) shows that β increases rapidly for $r < 0.1$ m/hr and reduces gradually for $r > 0.1$ m/hr. The transition rate of rise river stage $r = 0.1$ m/hr is about 3 times the coefficient of permeability. Thus, it appears that dam discharges that produce river stage rise less than 3 times the permeability of the soil in sandbars are likely to affect a larger area of the sandbar than faster rate of river ($r > 3k$). However, β changes only within a small range for practical ranges (0.3 to 0.5 m/hr)

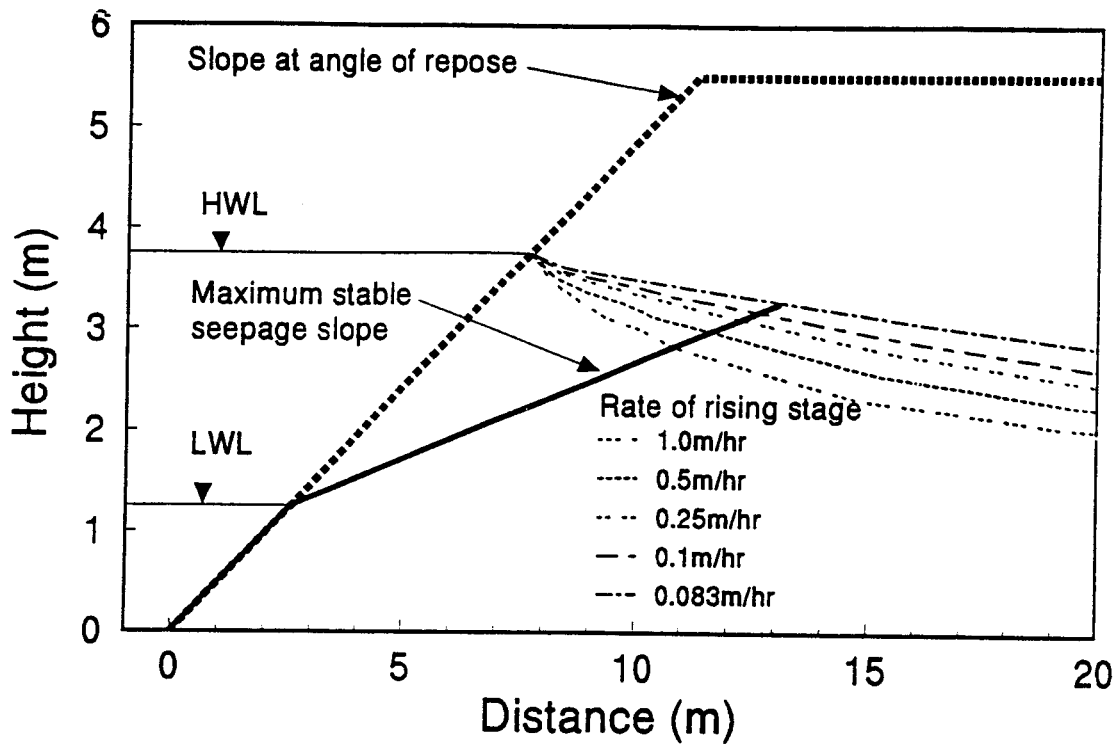


Fig. 3.2. Variation of groundwater surface at high water level with rate of rising river stage.

of rate of rise of river stage. Approximate relationship between β and rate of rise of river stage are:

$$\beta = 0.774 - 0.167r \quad ; r > 0.1\text{m/hr} \quad (3.1)$$

$$\beta = 1.0 - 2.4r \quad ; r < 0.1\text{m/hr} \quad (3.2)$$

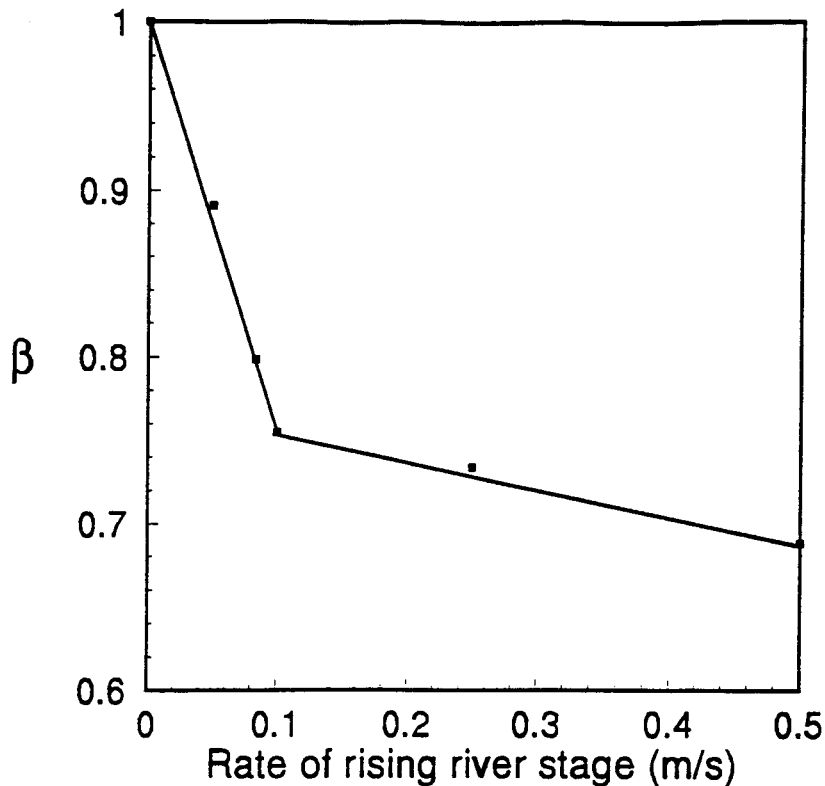


Fig. 3.3. Plot of beta versus rate of rising river stage.

3.3 Effects of Permeability

A second set of analyses was conducted by varying the coefficient of permeability of the soil keeping the slope constant at 26° and the rate of rise of river stage constant at 0.25 m/hr. The parameter β was found to vary linearly with the natural logarithm of the coefficient of permeability (Fig. 3.4). It is expected that with a higher coefficient of permeability, the parameter β would increase as obtained from the analyses. Thus, a larger mass of soil would be involved in bank cuts if the permeability of the soil increases. An approximate relationship between β and the coefficient of permeability is given by

$$\beta = 1.4 + \ln(k) \quad (3.3)$$

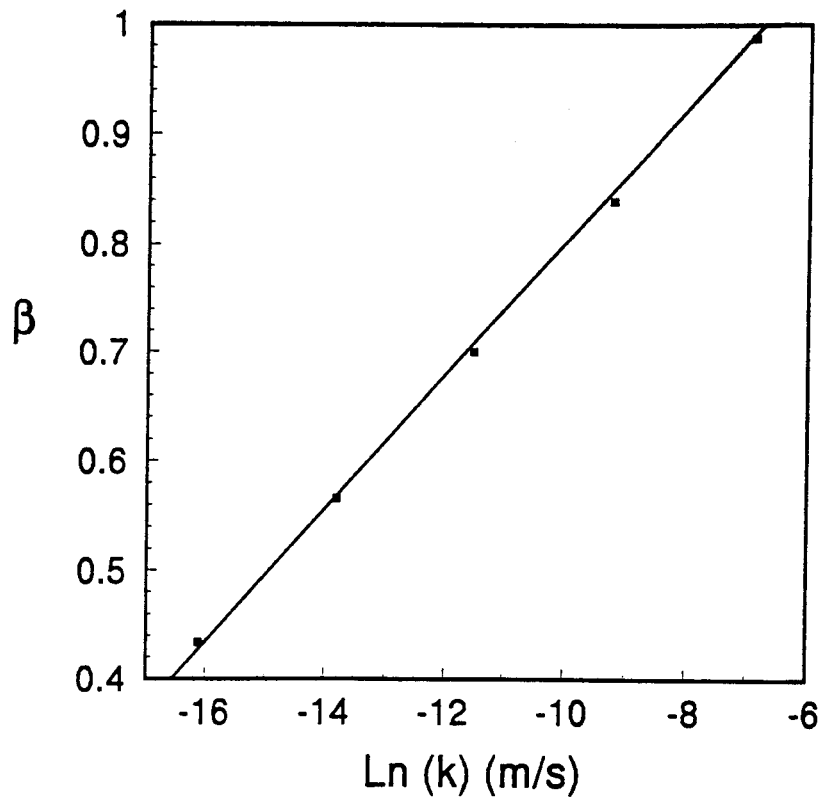


Fig. 3.4. Plot of beta versus permeability

3.4 Effects of Slope Angle

A third set of analyses, in which the slope angle was varied but the coefficient of permeability of the soil was kept constant at 1×10^{-4} m/s and the rate of rise of river stage constant at 0.25 m/hr, was conducted. It was found, within practical ranges of slope angles corresponding to the angles of internal friction of cohesionless materials, that slope angle does not have a significant effect on the parameter β compared to the coefficient of permeability. The relationship between β and slope angle can be approximated as

$$\beta = 1.32 - 0.12 \ln(s) \quad (3.4)$$

3.5 Effects of Downramping Rate

If the river stage falls slowly, water can still infiltrate the sandbar causing the elevation of a part of the groundwater surface, away from the face of the sandbar, to rise. The time for the Glen Canyon Dam to downramp from peak discharge to its lowest discharge on any given day varies between 4 and 16 hours. However, the time for the river stage to fall from high water level to low water level varies with location. Average rate of fall of river stage, calculated from data collected by Carpenter et al. (1992) during research flows, varies between 0.25 m/hr and 0.5 m/hr.

The effects of rate of fall of river stage (downramp rate, d) ranging from 0.25 m/hr to 0.5 m/hr were analyzed for a sandbar of permeability 1.0×10^{-5} m/s and slope angle 30° . The transition of the groundwater surface during the drawdown period for the above rates of fall of river stage are shown in Fig. 3.5 and Fig. 3.6 respectively. The results reveal that β is insensitive to rate of fall of river stage (downramping rate). However, from geotechnical principles, a rapid rate of drawdown could lead to severe bank cuts from undrained slope failures, but this simple model cannot account for this condition. The finite element model discussed in Chapter 4 provides details on the effects of rate of drawdown. With a downramp rate of 0.25 m/hr the bank stored water takes more than 25 hours to drain while for a downramp rate of 0.5 m/hr the drainage time is about 10 hours.

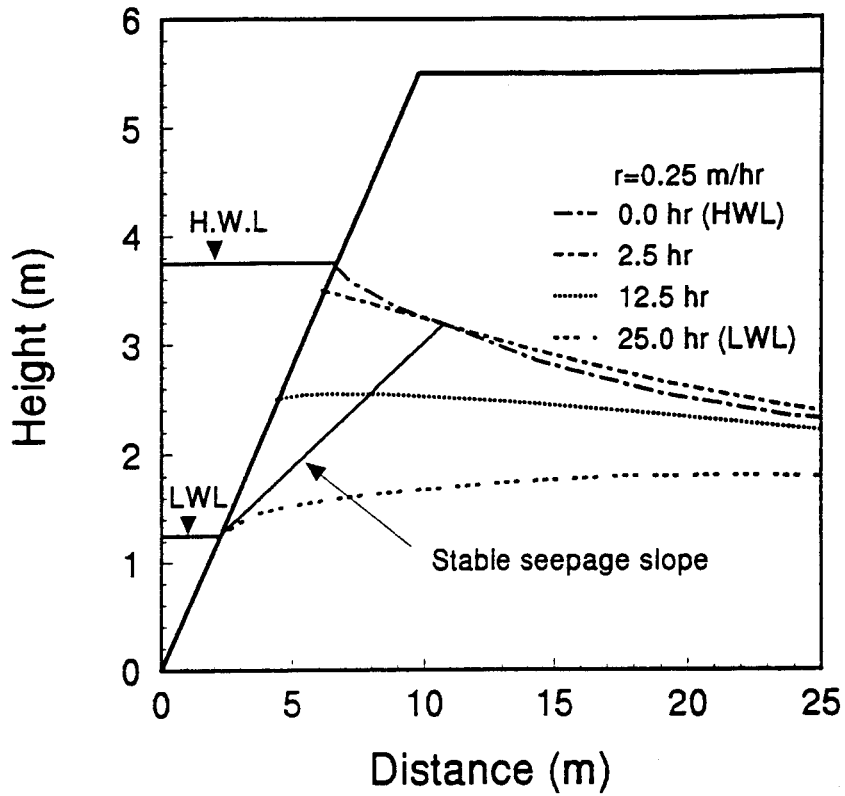


Fig. 3.5. Groundwater surface variation with time for downramping rate of 0.25 m/hr.

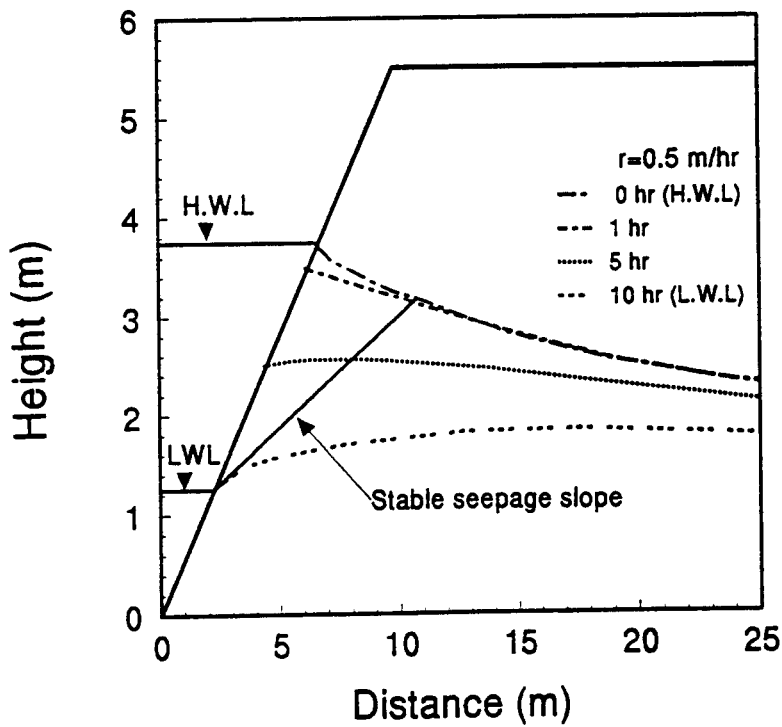


Fig. 3.6. Groundwater surface variation with time for downramping rate of 0.5 m/hr.

3.6 Combined Effects of Ramping Rates, Range of Discharge, Soil Permeability and Slope Angle

Equations (3.1 - 3.4) only give the relationship between β and each of the parameters, rate of rise of river stage, soil permeability and slope angle. Using optimization methods, an approximate general expression for β is

$$\beta = 1.308 - 0.072 \ln\left(\frac{r}{k}\right) - 0.132 \ln(s) \quad ; \quad \frac{r}{k} > 1, s > 10.5 \quad (3.5)$$

It was shown above that β is insensitive to rate of fall of river stage (d). Therefore, equation (3.5) is independent of d .

Equation (3.5) can be used to determine β to delineate the lower stable seepage slope and to estimate the mass of sediments that would undergo cyclic seepage erosion and aggradation under transient flow. The stable seepage slope depends mainly on the permeability of the soil, the range of river stage fluctuation, and the upramping rate.

3.7 Effects of Duration of Peak Discharge

If the dam discharge regime is such that the peak discharge is held constant for a period longer than an instantaneous peak, then the groundwater level will rise with a corresponding increase in the area affected by seepage erosion. The effects of duration of peak discharge were investigated for hypothetical sandbars with slopes varying between

2 ° and 32°, soil permeability ranging from 1.0×10^{-3} and 1.0×10^{-7} m/s and duration of peak discharge ranging from 0 to 8 hours.

The value of β was found to increase rapidly during the first two hours of the peak discharge period and then to increase at a slower rate for a longer duration of peak period (Fig. 3.7). At the beginning of the peak period, a large difference in head exists across the sandbar. However, as the duration of the peak discharge increases, water entering the sandbar causes the groundwater surface to rise, resulting in a decrease in head with time. The net result is a decrease in the rate of change of β with time. Using optimization techniques, the change of β with permeability, slope and duration of peak discharge is given as

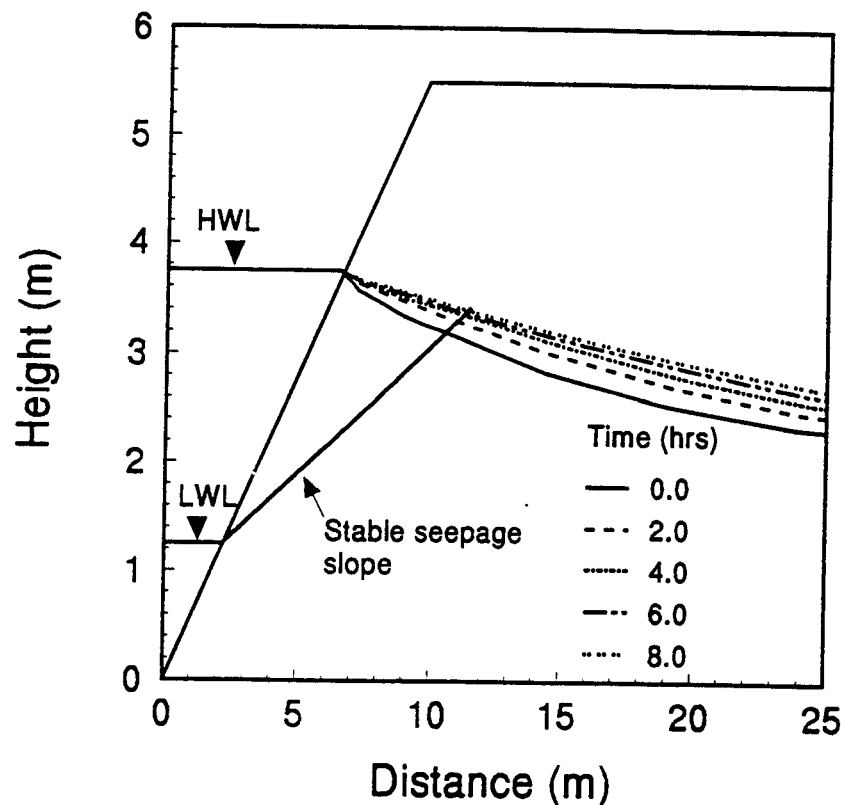


Fig. 3.7. Effects of duration of peak discharge on groundwater surface position.

For $P_t \leq 2$ hrs

$$\Delta\beta = 0.085 - 30k + 0.003s + 0.045P_t \quad (3.6)$$

For $P_t > 2$ hrs

$$\Delta\beta = 0.130 + 40k + 0.006s + 0.020P_t \quad (3.7)$$

The position of the groundwater surface for peak discharge duration greater than zero is obtained by adding β from equation (3.5) to $\Delta\beta$ from the appropriate duration of peak discharge equation (equation 3.6 or 3.7). If β exceeds 1 (because of rounding off errors in the individual equations and the combined equation), β should be set to 1.

3.8 Procedures to Determine Stable Seepage Slopes for a Given Dam Discharge Regime

The following procedures are suggested to determine the stable seepage slopes based on a set of dam operating parameters.

- Determine soil parameters - unit weight (γ), permeability (k) and angle of friction (ϕ)
- from geotechnical laboratory and field tests (see Budhu, 1992).
- Obtain dam operating parameters - upramping rate, total discharge, duration of peak discharge.

- Use routing model (done by others) to predict stage changes from the proposed upramping rate and total discharge.
- Use equation (3.5) to calculate β and, if appropriate, use either equation (3.6) or equation (3.7) to determine $\Delta\beta$; add these components.
- Calculate the height of point C (Fig. 2.1) from the low water elevation and β .
- Determine each of the equilibrium slopes as follows.

The lower stable seepage BC = α_s [equation (2.1)]; and the upper stable seepage slope CD = ϕ .

3.9 Illustrative Example

Determine the stable seepage slope for a sandbar, with the following properties; $\gamma_{\text{sat}} = 16$ kN/m³, $\phi = 30^\circ$, $k = 3 \times 10^{-4}$ m/s, $s = 26^\circ$. The sandbar is to be subjected to the following dam operating parameters:

Total discharge = 708 m³/s

Upramping rate = 142 m³/s/hr

Duration of peak discharge = 2 hrs

Low constant discharge = 85 m³/s (river stage elevation 92.6)

Solution

If the channel characteristics are known then a routing model can be used to determine the stage elevation at maximum discharge. For the purpose of this illustrative example, it will be assumed that for a total discharge of 708 m³/s, the river stage will be 2.5 m above

the low water elevation and that the upramping rate of $142 \text{ m}^3/\text{s}/\text{hr}$ corresponds to a change of river stage of $0.45 \text{ m}/\text{hr}$. From equation (3.5), β can be found as follows :

$$\beta = 1.308 - 0.072 \ln \left(\frac{0.45}{3 \times 10^{-4}} \right) - 0.132 \ln (26) - 0.35 \quad (3.8)$$

From equation (3.6)

$$\Delta\beta = 0.085 - 30(3 \times 10^{-4}) + 0.003(26) + 0.045(2) = 0.24 \quad (3.9)$$

$$\text{Total } \beta = 0.35 + 0.24 = 0.59$$

The lower seepage slope is at an angle given by equation (2.1)

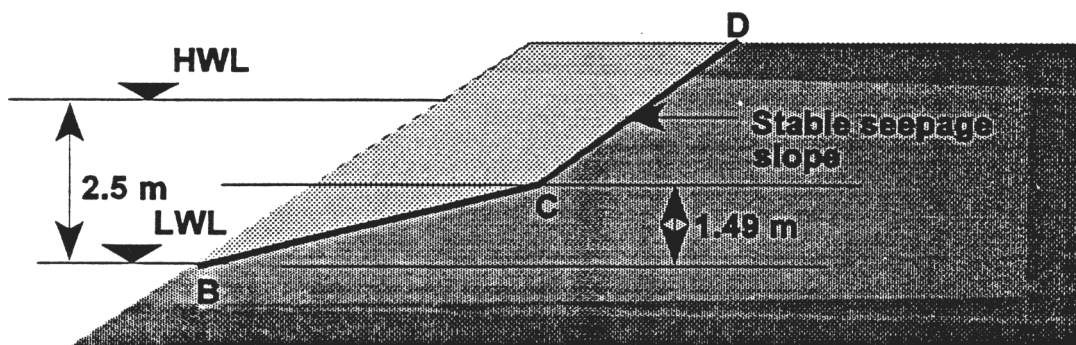


Fig. 3.8. Stable seepage profile for the illustrative example.

$$\alpha_s = \tan^{-1} \left(\frac{16 - 9.81}{16} \right) \tan 30^\circ = 12.6^\circ \quad (3.10)$$

Draw a horizontal line at a distance $\beta H_w = 0.59 (2.5) = 1.49$ m above the low water level. (Fig. 3.8). From the low water level, point B (Fig. 3.8), draw a line at an angle 12.6° to the horizontal to intersect the horizontal line. The intersection of the two lines is point C. From C draw a line at an angle $\phi = 30^\circ$ to the horizontal to intersect the surface at D. The stable seepage slope is BCD.

3.10 Reduction of Usable Width of Sandbars for Campsites and Riparian Habitat

The concerns for riparian habitat and recreation use are reflected in reduction in height and width of the sandbars from bank cuts. From the geometry of Fig. 3.9, the width B is

$$B = \beta H_w \cot \alpha_s + (H - \beta H_w) \cot \phi - H \cot \phi - \beta H_w (\cot \alpha_s - \cot \phi) \quad (3.11)$$

By substituting equation (2.1) into equation (3.11), we obtain

$$B = \beta H_w \cot \phi \left(\frac{\gamma_{sat}}{\gamma'} - 1 \right) \quad (3.12)$$

As a first approximation, for most common soils, $\gamma_{sat}/\gamma' \approx 2$ and

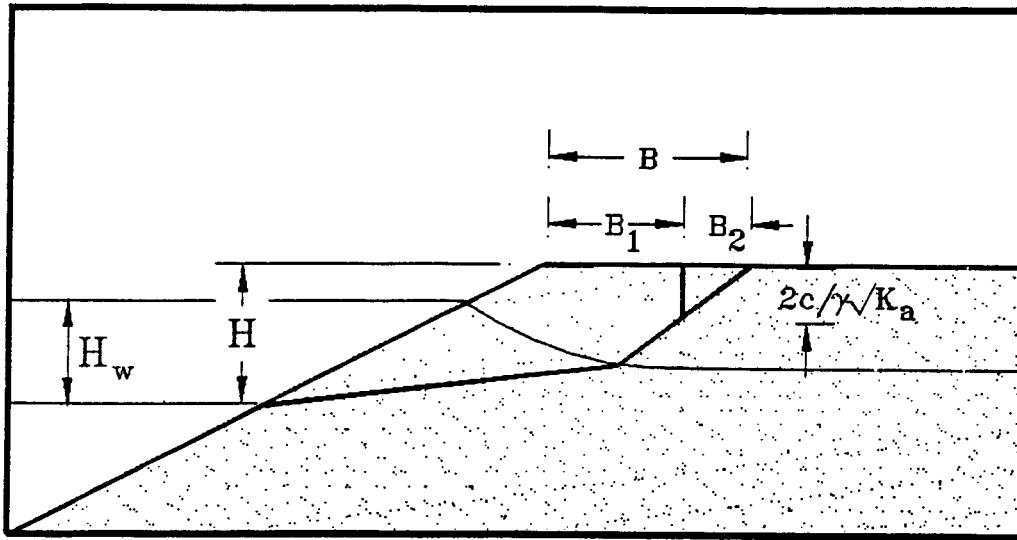


Fig. 3.9. Geometry of width of sandbar affected by seepage erosion.

$$B = \beta H_w \cot \phi \quad (3.13)$$

If the soil has some cohesion, then

$$B_1 = B - B_2 = \cot \phi \left[\beta H_w \left(\frac{\gamma_{sat}}{\gamma'} - 1 \right) - \frac{2c}{\gamma \sqrt{K_a}} \right] \quad (3.14)$$

where

$$B_2 = \frac{2c}{\gamma \sqrt{K_a}} \cot \phi \quad (3.15)$$

Equation (3.14) can be used to predict the reduction of the widths of sandbars at campsites from slope failures. The variation of the angle of internal friction of the soil with

the width B normalized to the fluctuation depth for $\gamma_{\text{sat}}/\gamma' = 2$ and $\gamma_{\text{sat}}/\gamma' = 2.5$ is shown in Fig. 3.10. The latter value is the average value from unit weight measurements from three sandbars. If the soil has some cohesion then B is reduced by the amounts shown in Fig. 3.11 for some typical values of soil cohesion in Grand Canyon.

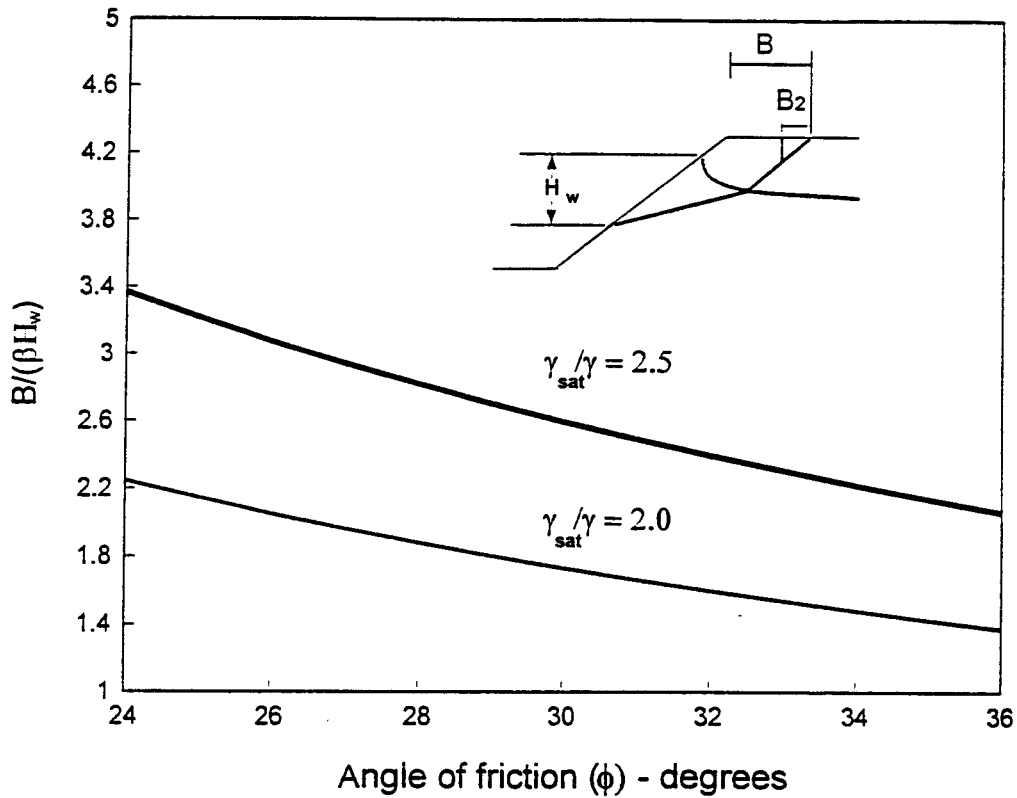


Fig. 3.10. Reduction of sandbar width with angle of friction.

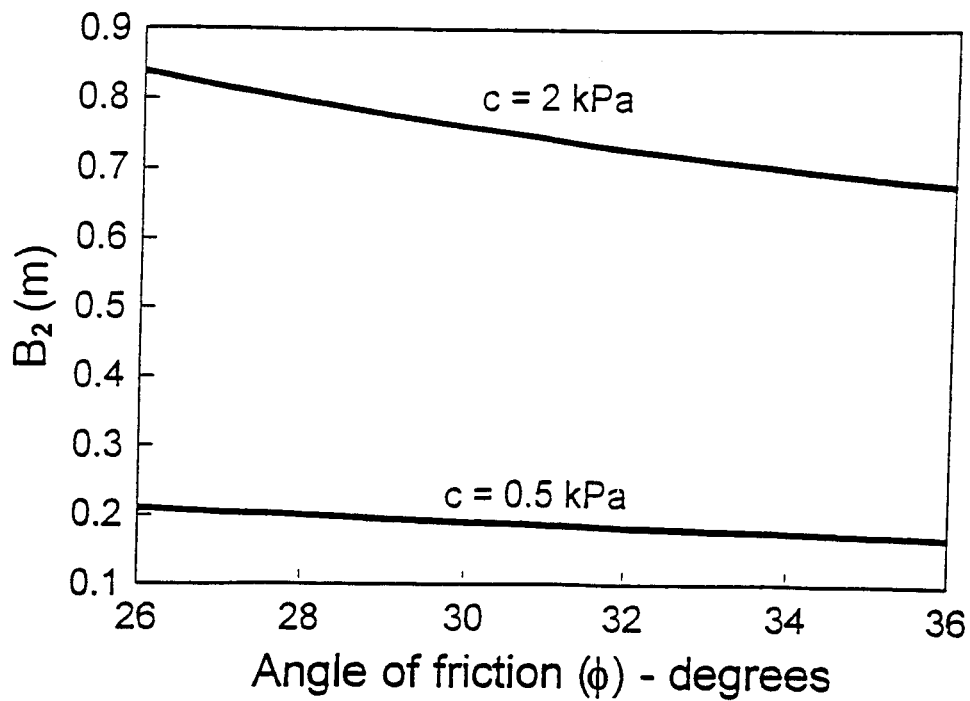


Fig. 3.11. Variation of width with cohesion and angle of friction.

3.11 Reduction of Volume of Sandbars for Campsites and Riparian Habitat

The upramping rates and the range of stage variations will govern the extent to which seepage erosion will affect a given sandbar. A hypothetical sandbar with a slope angle of 26° , angle of friction 30° and coefficient of permeability $1 \times 10^{-4} \text{ m/s}$ is used to illustrate the effects of dam parameters on the volume (per meter length) of a sandbar.

The effect of variations in the range of river stage on the volume of a sandbar is shown in Fig. 3.12. As the range of river stage fluctuation increases seepage erosion can now operate on a larger portion of the sandbar and there is a corresponding increase in the area of the sandbar affected by seepage. As expected, increasing the rate of rise of river stage reduces the volume of sand that will be eroded from seepage forces.

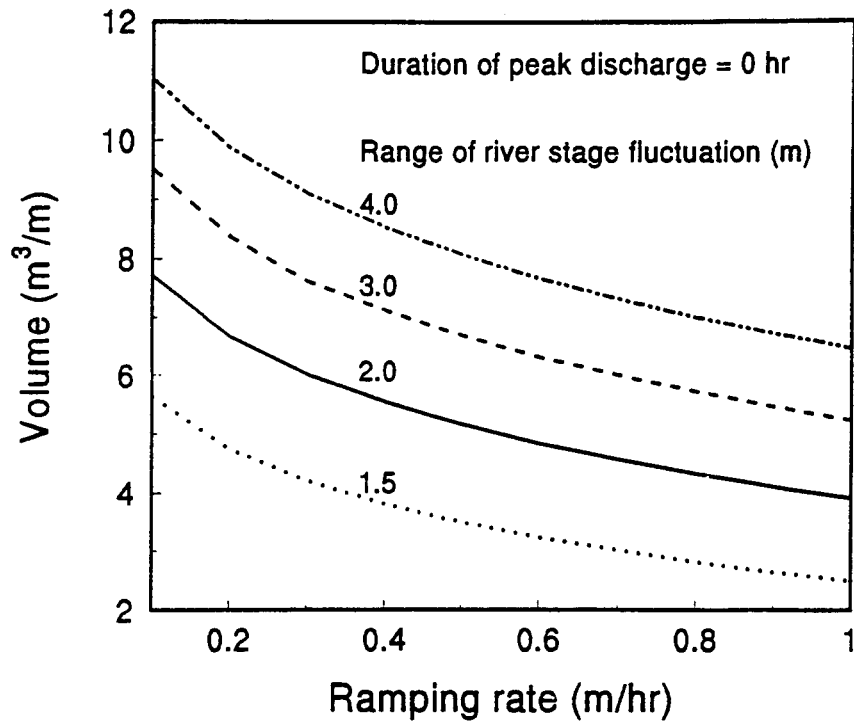


Fig. 3.12. Volume changes due to river stage fluctuations.

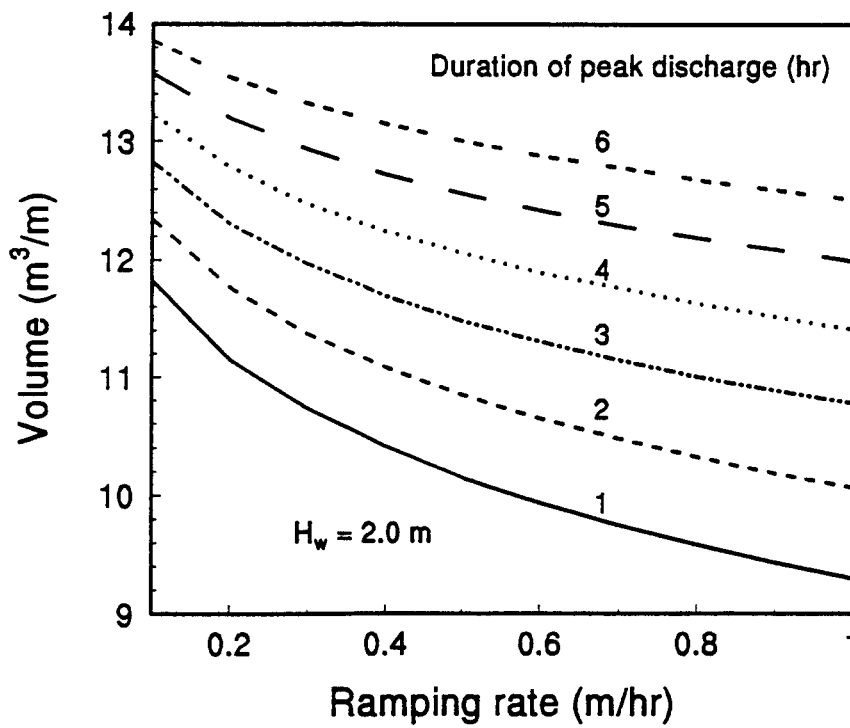


Fig. 3.13. Volume changes due to duration of peak discharge.

Changes in volume for the above sandbar with the duration of the peak discharge are shown in Fig. 3.13. Increases in the duration of the peak discharge causes decreases in the volume of the sandbar. As the duration of the peak discharge increases then the groundwater level of within the sandbar rises since more water can infiltrate into the sandbar. Seepage erosion can again operate on a greater portion of the sandbar, causing a corresponding decrease in sandbar volume.

3.12 Summary

The extent to which seepage erosion will affect a sandbar, under a given set of dam discharge parameters, is governed by the elevation of the groundwater level. The effects of rate of rising and falling river stage, duration of peak discharge, coefficient of permeability and slope angle on seepage erosion were examined theoretically in this chapter. Equations to account for the influence of these factors were developed from curve fitting numerical results from a finite element model. These equations are intended to be used to obtain a first approximation of the potential effects of seepage erosion on a sandbar resulting from dam operation. An example illustrating the application of these equations to a typical situation within Grand Canyon is also presented.

The volume of the sandbar that will be affected by any given dam discharge scenario was related to the range of river stage fluctuation, duration of peak discharge and rate of rise of river stage. Increases in river stage fluctuation and in duration of peak discharge lead to increases in volume of sand that will be eroded by seepage. Increases

in the rate of rise of river stage lead to decreases in volume of sand that will be eroded by seepage.

CHAPTER 4

FINITE ELEMENT MODEL FOR SEEPAGE EROSION

4.1 Introduction

The "simple" model can predict the extent of seepage erosion. However, it is incapable of predicting the time sequence of failures and the effects of the rate of drawdown of river stage. Consequently, a complete evaluation of the effects of different dam discharge scenarios cannot be obtained from the simple model. A finite element model embracing Biot's coupled stress - pore water pressure theory was developed to predict groundwater level variations and slope instability from transient groundwater seepage. The details of the formulation are presented in Appendix II. The finite element model is capable of predicting what dam operating conditions provoke slope failures and when such failures would occur. In this chapter, the predictions of the finite element model are evaluated using ground survey data (Bues et. al., 1992) and time lapsed photography (Cluer, 1992) for sandbar 172L. Calculations from conventional slope stability analysis are also compared with the finite element model predictions. The effects of various dam discharge alternatives on sandbar stability are also examined.

4.2 Observed Aggradation/Erosion Pattern on Sandbar 172L

A particular event on sandbar 172L will be described and later used to test the

predictions from the finite element model. On December 8, 1990, Cluer (1992) installed an automatic 35mm camera on a rock outcrop overlooking sandbar 172L. He programmed the camera to take one photograph each day at 5:00 p.m. corresponding to, approximately, the lowest daily river stage. Image processing of the photographs captured by the camera gave the daily exposed sandbar areas at low river stage. Ground surveys were conducted by Bues et. al. (1992) to reveal geometric changes in the sandbar before and soon after each research flow regime. Typical changes as represented by ground survey data on a cross-section in the middle of sandbar 172L are shown in Fig. 4.1.

From May 22 to May 30, 1991, a research flow with a constant discharge of 426 m³/s was released from Glen Canyon Dam. On the initiation of this constant flow, Cluer (1992) measured, from his time lapsed photographs, a constant rate of deposition on

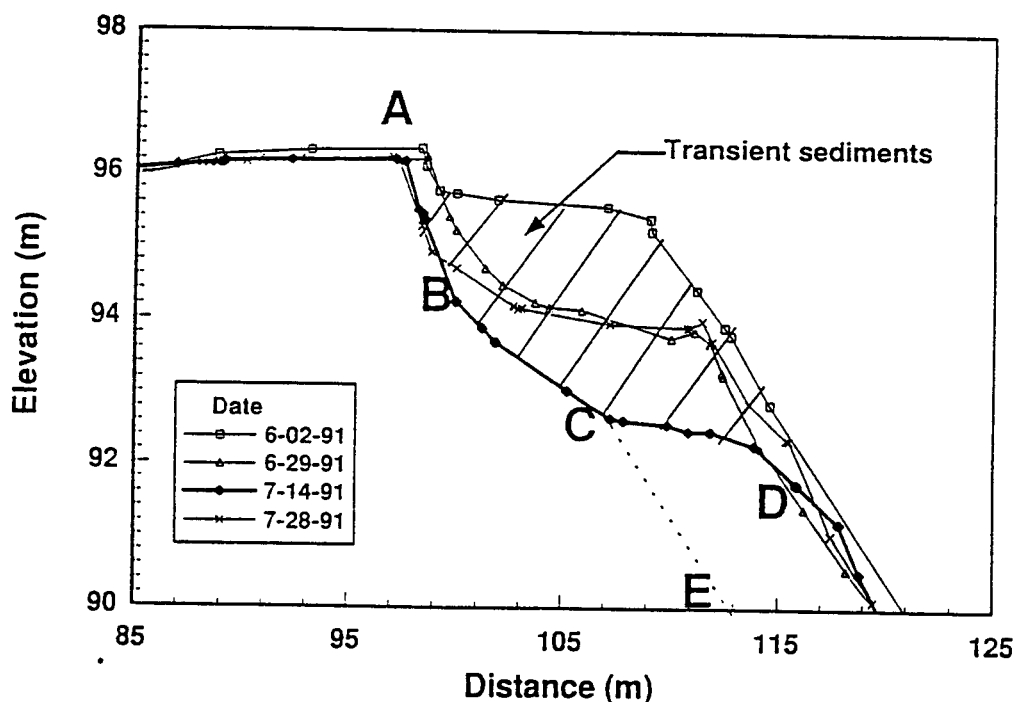


Fig. 4.1 Typical changes on the profile of sandbar 172L.

sandbar 172L. On June 4, 1991, another research flow consisting of 27 days of widely fluctuating discharges was initiated. The minimum discharge was $68 \text{ m}^3/\text{s}$ and the maximum was $836 \text{ m}^3/\text{s}$ with a mean value of $380 \text{ m}^3/\text{s}$. This series of experimental discharges, called "normal summer" was designed to replicate discharges released during usual summer periods. The minimum and maximum flow, and ramping rates were constrained by agreements, but daily range was driven by changing electrical demands. Fluctuations during the summer months are generally the greatest of any season, this held true during this "normal summer" experimental period.

During the "normal summer" research flow regime, deposition occurred at a slower rate than during the constant flow regime. On June 18, 1991, Cluer's (1992) daily photographs revealed that the sandbar area increased significantly and achieved a slope of 26° . The profile of the sandbar on June 18, 1991, (Fig. 4.2a) is similar to the ground survey measurements made on June 2 as shown in Fig. 4.1. On June 19, a slope failure of the sandbar was captured by Cluer's automatic camera. An approximately vertical bank cut traversed the vegetation zone along the length of the sandbar (Fig. 4.2b). The time when the event occurred is unknown, but it is assumed from prior observations that it may have occurred sometime between 5:00 p.m. on June 18 and 8:00 a.m. on June 19, 1991.

On June 20, with widely fluctuating discharges continuing, deposition resumed but at a much greater rate than before the slope failure. The sandbar grew wider and higher with each daily fluctuation. Slope failures recurred but since the sandbar grew well into the channel, tractive forces were assumed to play a large role in triggering these failures. Undercutting of the slope was observed during rising river stage (Cluer, 1992).

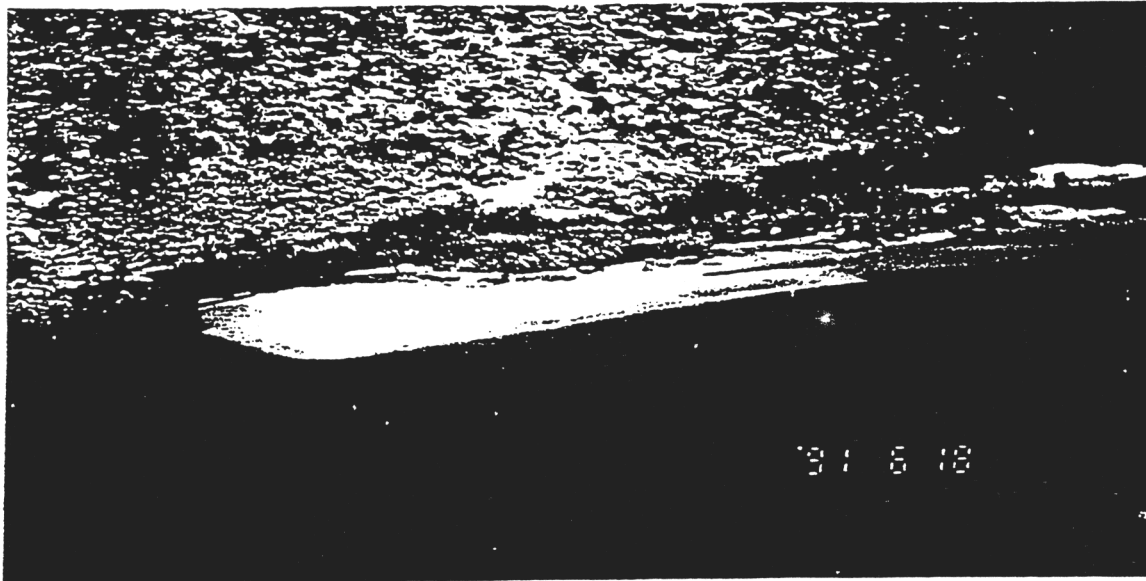


Fig. 4.2a. Photograph of sandbar 172L on June 18, 1991 (courtesy of B. Cluer).

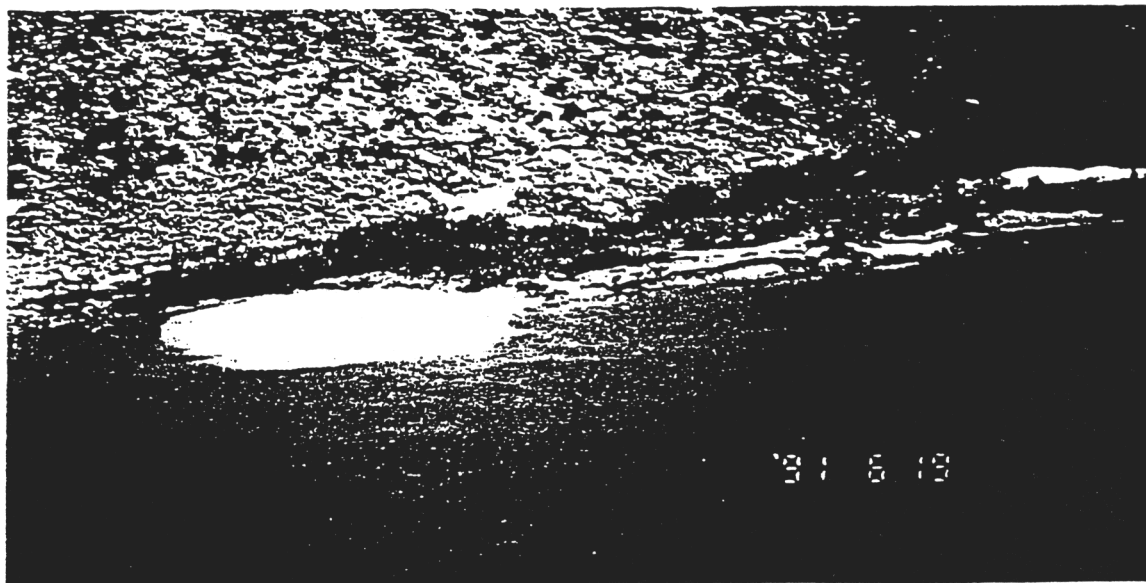


Fig. 4.2b. Photograph of sandbar 172L on June 19, 1991 (courtesy of B. Cluer).

Sandbar profiles were recorded before and after each research flows by one or two survey crews (Beus et. al., 1992) and, thus, ground surveys gave only geometric changes in a sandbar at a given time. They rarely capture the real sequence of events before, during and after failures occurred. For example, the survey measurements on June 29, 1991 (Fig. 4.1) can be interpreted as the sandbar profile after a failure occurred some time between June 2, 1991 and June 28, 1991. However, the time lapsed photographs showed that the sandbar collapsed to the profile ABCD (Fig. 4.1) between 5.00 pm on June 18, 1991 and 8.00 am on June 19, 1991, and then redeposition resumed. Thus, the survey measurements of June 29, 1991, represent the sandbar in an aggradational mode. During the study period, slope failures on sandbar 172L occurred frequently and progressively but never extended beyond ABCD in Fig. 4.1.

4.3 Comparison of Finite Element Model Predictions with Field Data for Sandbar 172L

The cross section of sandbar 172L measured on June 2, 1991 (Fig. 4.1) was discretized into 318 isoparametric quadrilateral elements. Field and laboratory tests were conducted to obtain the soil parameters needed for the numerical model. A summary of the soil properties of the two soil zones - zones I and II - (Fig. 2.8) is given in Table 4.1.

On June 18-19, 1991, when the failure event occurred sensors within the observation wells (Carpenter et. al. 1992) were shifted off scale, and therefore, the groundwater fluctuations measured after this date are unreliable. Consequently, the

numerical model was used to predict groundwater variations within the sandbar just prior to the failure event

Table 4.1. Soil properties used in finite element analysis

Soil Parameters	Zone 1	Zone 2
Shear Modulus, G, kPa	3700	3500
Permeability, k, cm/s	2.3×10^{-2}	4.2×10^{-2}
Angle of friction, ϕ	32°	30°
Cohesion, c, kPa	2.0	4.0
Saturated unit weight, γ_{sat} , kPa	17.2	16.0

to test its reliability. The groundwater level on June 14, 1994, was deemed to be reliable (Carpenter, 1994) and was selected to compare with numerical predictions. The river stage variation on June 14, 1994, (Fig. 4.3) is approximated as shown in Fig. 4.4 for the finite element model. Hydrostatic stresses were imposed on the face of the slope following the rate of rise and fall of the river stage on June 14, 1991 (Fig. 4.4). The predictions of the numerical model are compared with field data in Fig. 4.5. The comparison between the numerical predictions and the field data is good, and this lends further confidence in the numerical model to predict groundwater changes from river stage variations.

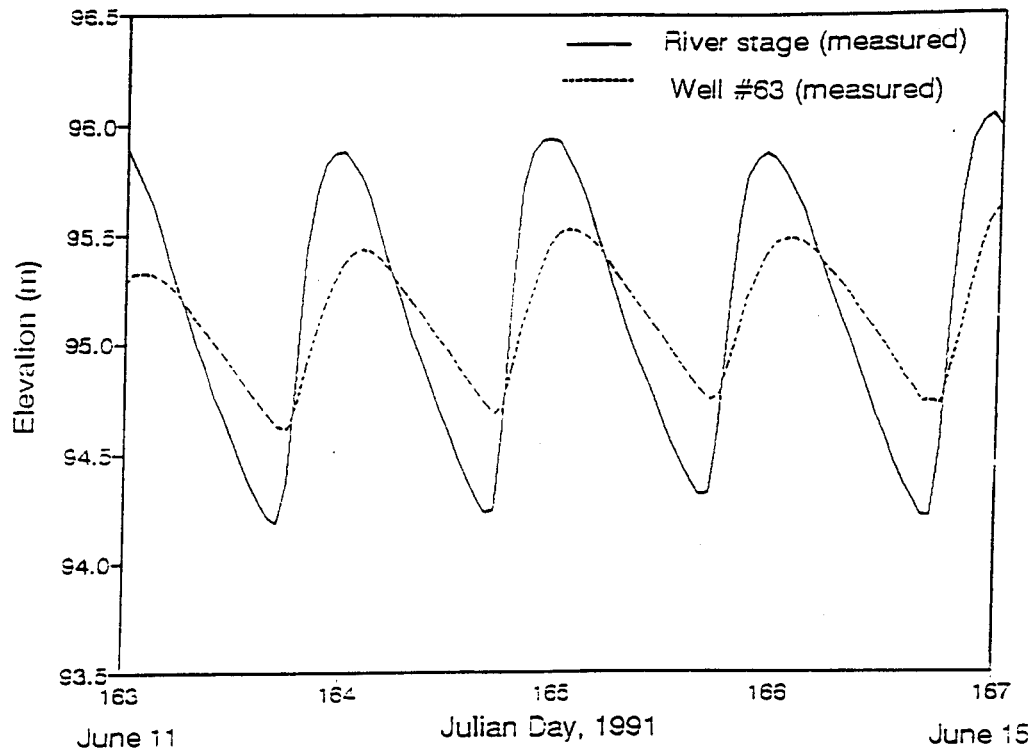


Fig. 4.3 River stage and water level variation in well #63 from June 11 to June 15, 1991.

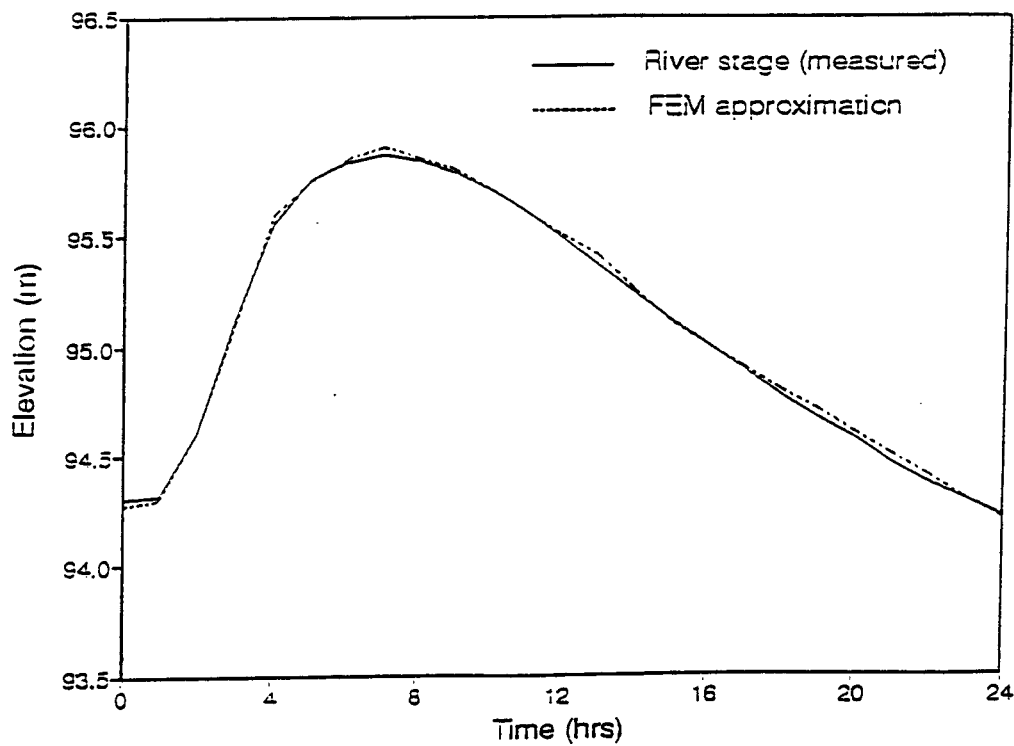


Fig. 4.4 Finite element approximation of river stage on June 14, 1991.

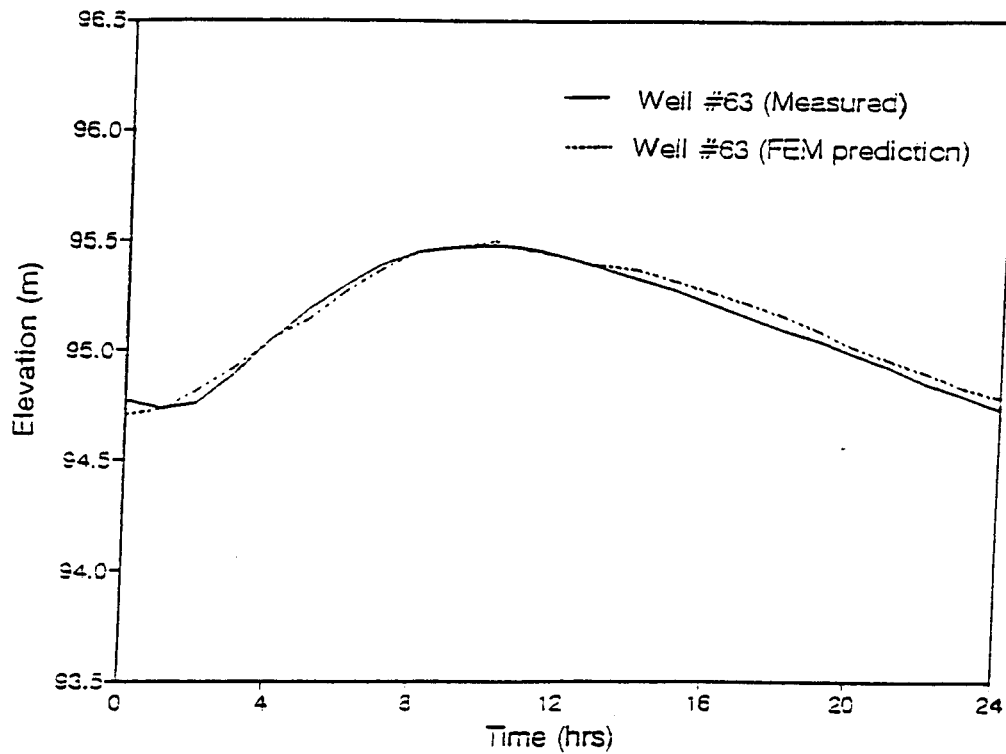


Fig. 4.5 Comparison between finite element prediction of groundwater and well #63 on June 18, 1991.

The finite element model was then used to predict the failure event captured by time lapsed photography (Cluer, 1992) on June 18 - 19, 1991, at sandbar 172L. The river stage on June 18 - 19, 1991 at sandbar 172L was obtained by correcting the measured values (Carpenter et al., 1992) using data from a nearby R200 gauging station. It appears that the slope failure on June 18 - 19, caused the river stage sensor to drop to an elevation of about 1m below its original position. The sensor then remained stable in this new position. The following procedure was followed in the finite element algorithm.

- ◆ The soil was assumed to be elastic since the river stage for the flow regime that produced failure on June 18-19, 1991 was lower than the maximum river stage recorded (Appendix II).
- ◆ Hydrostatic stresses were imposed on the face of the slope following the rise and fall of the river stage as measured on June 18 (Fig. 4.6).

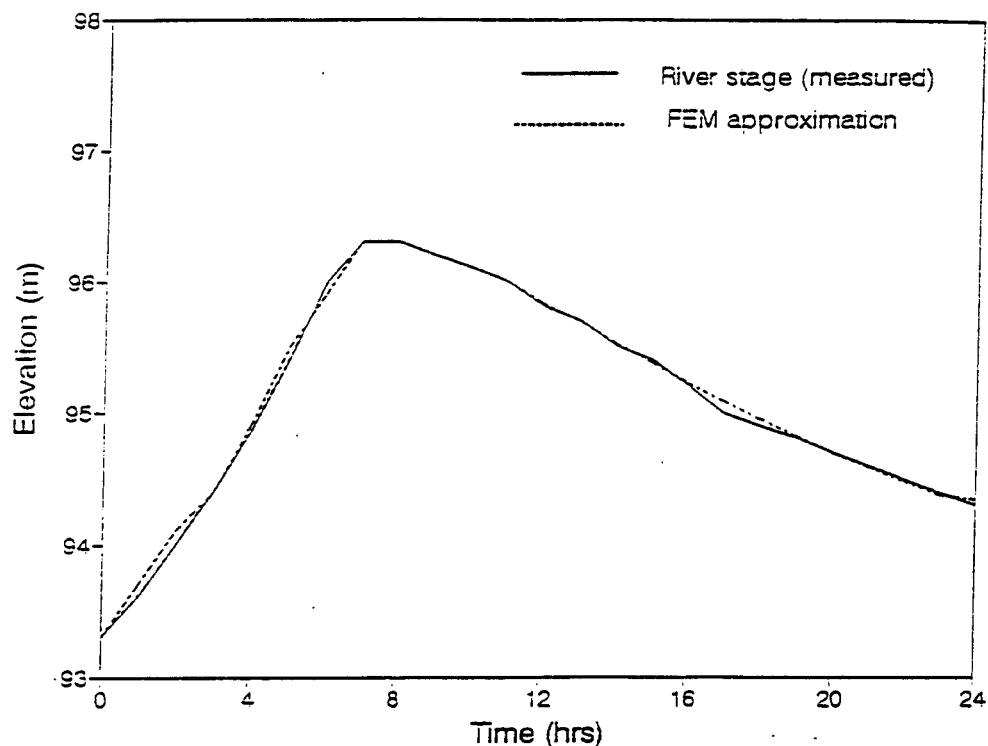


Fig. 4.6 Finite element approximation of river stage on June 18, 1991.

- ◆ The effective unit weight (γ') of the soil was reduced or increased by the seepage force per unit volume (j) depending on the direction of the velocity vector. If the velocity vector were upward directed, the effective unit weight was reduced to $\gamma'_c = \gamma' - j$, whereas if the velocity vector was downward directed, the effective unit

weight was increased to $\gamma'_c = \gamma' + j'$ where γ'_c is the current effective unit weight and j' is the vertical component of the seepage vector. The corresponding upwards or downwards forces were computed for each element and used as vertical nodal forces. The forces corresponding to the horizontal component of the seepage vector were used as horizontal nodal forces.

- ◆ Failure was governed by the Mohr-Coulomb failure criterion.

- ◆ A check was made at each Gaussian point - nine in the isoparametric quadrilateral elements used in the algorithm - to determine whether the failure state is reached or the mean effective stress approaches zero. In the former case, the Gaussian points were flagged to delineate the failure surface. Each Gaussian point was taken to represent 1/9 th of the area of the element. For the latter case, the element was removed (eroded element) when at least eight of the nine Gaussian points show that the mean effective stress was near to zero. In preliminary numerical tests, it was found that there was a reduction in computational time, if instead of removing eroded elements, they were left in the mesh but the stiffness was reduced by at least one-thousandth and the permeability was increased by one thousand times their original values. There was no significant practical difference (<5%) between the results from reducing the stiffness and leaving the mesh intact, and removing the element and reforming the mesh.

It was observed during the study period that the slope failures only extended as far back as ABCD (Fig.4.1). This line delinates the two distinct soil unit weight zones. For the finite element model, an interface approximately following ABCD (Fig. 4.1) was introduced between these two zones. The soil properties assumed for the interface were the same as for zone I but with the cohesion taken as zero.

The predicted failure zone at the end of the stage variation (Fig. 4.6) and the displacement field are shown in Figs. 4.7 and 4.8 respectively. The introduction of an interface predefines the failure surface. Thus, the agreement between the predicted and the measured failure plane (Fig. 4.7) is not surprising. What would be the result if an interface was not used? The analysis was repeated by removing the interface and using the soil properties for the two zones as shown in Table 4.1. The results of this analysis showed a shallow slope failure (Fig. 4.9) which did not agree with the field observations and measurements. It appears that the stable seepage slope indeed defines a preferred failure plane for newly deposited sediments when acted on by seepage forces.

Elements close to the sandbar face are subjected to large hydraulic gradients. Consider a slope , α , and a surface of seepage AB in which the seepage vector exits the slope at an angle λ to an outwardly directed normal to the slope (Fig. I-1). Harr (1962) showed that at the discharge point B, the hydraulic gradient $i \rightarrow \infty$; that is the hydraulic gradient is unbounded and Darcy's law is not valid. However, in practice this would not occur (Harr, 1962). Instead, the hydraulic gradient would be sufficiently large to cause static liquefaction of the sand. Static liquefaction is identified in our algorithm when the mean effective stress of an element approaches zero. Elements of soil that have statically

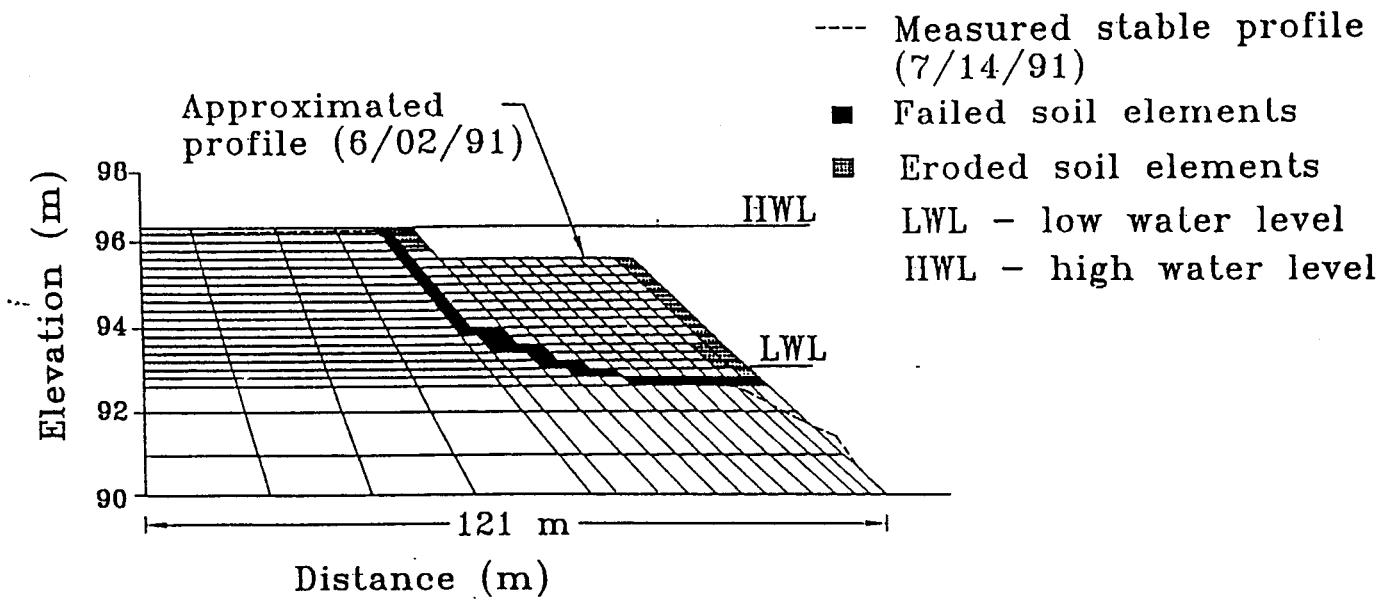


Fig. 4.7 Finite element prediction of failure zone when interface elements are included.

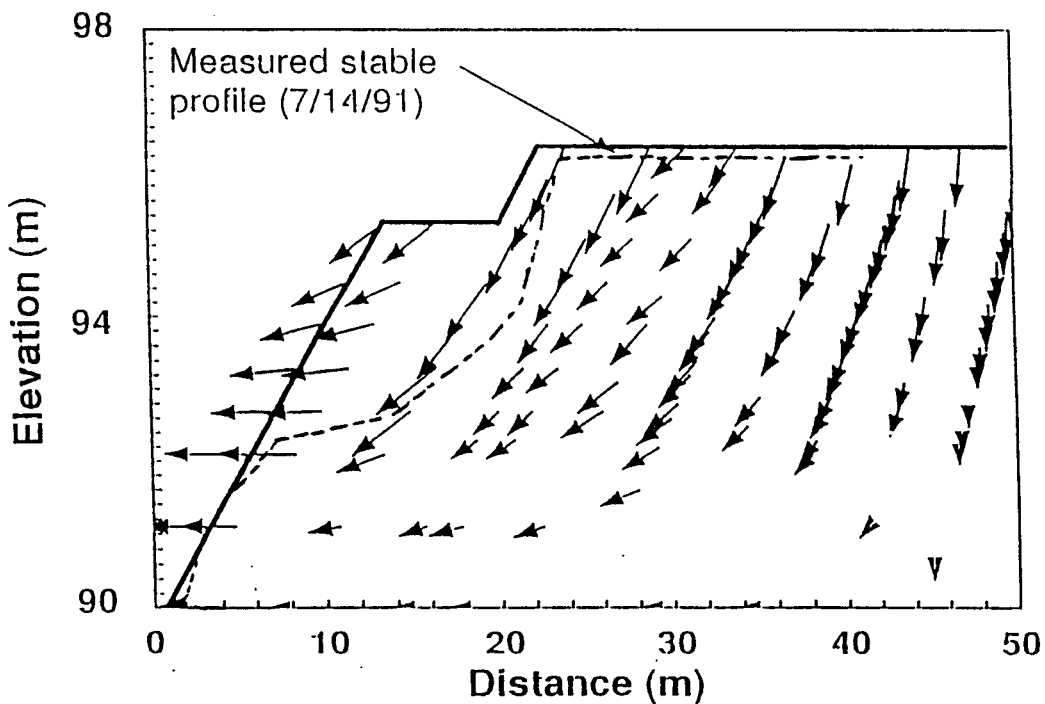


Fig. 4.8 Displacement vectors at low water level.

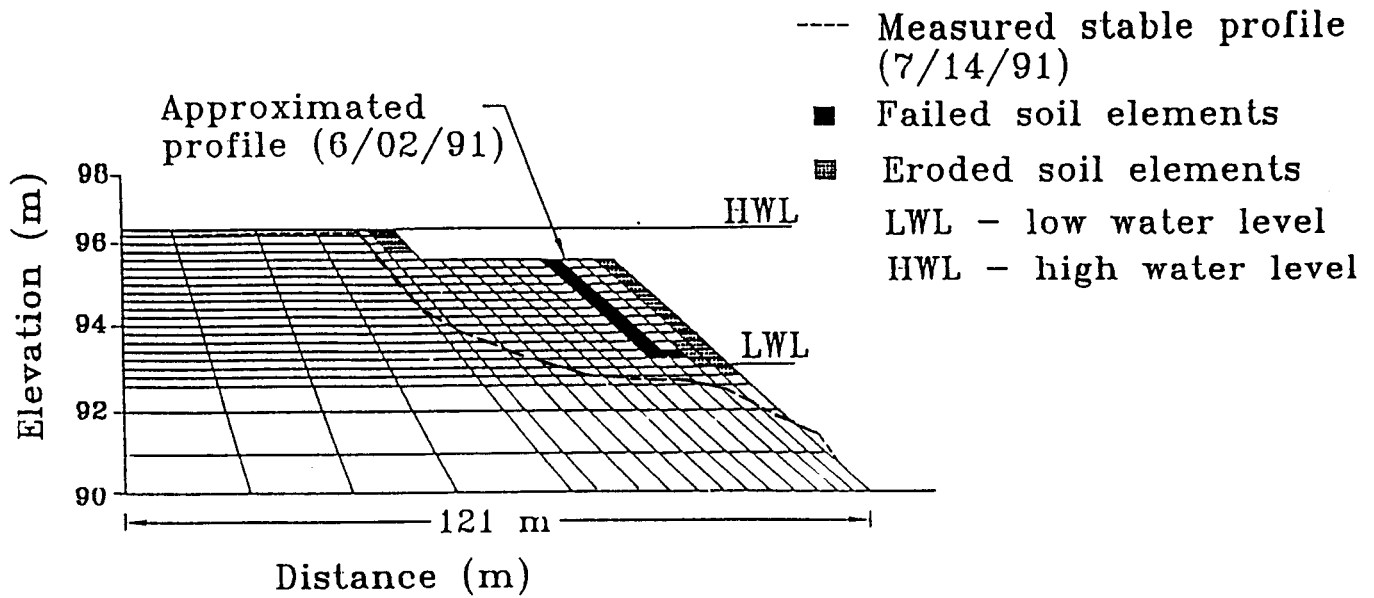


Fig. 4.9 Finite element prediction of failure zone without interface elements

liquefied would flow out of the sandbar. The sand mass just above the cavity created by the outflow of the sand would normally collapse into the cavity as was observed on sandbars in Grand Canyon. The elements of sand that have statically liquefied prior to the slope failure on sandbar 172L are shown by the hatched area (eroded area) in Figs. 4.7 and 4.9. All these elements are on or near to the face of the sandbar where the hydraulic gradient is expected to be large enough to cause static liquefaction.

4.4 Effects of Interim Flow Alternatives

Numerical simulations of the interim low flow regimes were performed by subjecting the profile used in the previous analysis to the following variations in discharge :

- a) Low water level of 142 m³/s (5000 cfs), high water level of 283 m³/s (10000 cfs).
- b) Low water level of 142 m³/s (5000 cfs), high water level of 368 m³/s (13000 cfs).
- c) Low water level of 340 m³/s (12000 cfs), high water level of 566 m³/s (20000 cfs).

The range of discharge given above represents conditions of low, medium and high discharge under the interim low flow regime. Upramping rates and downramping rates were maintained at the specified values of 70.8 and 42.5 m³/s/hr respectively. Numerical simulations were performed with (a) interface elements and (b) without interface elements. With the inclusion of interface elements, slope failures occurred along the interface under all three discharge scenarios as shown in Fig. 4.7. Without the interface elements shallow slope failures similar to that shown in Fig. 4.9, were predicted for the interim flow alternatives. The interface between the two material zone again dictates where failure would occur. Along the interface there is a discontinuity in material properties and a given stress change will produce different displacements at the boundary between the different materials. The difference in the displacement along the interface could cause a crack to form, leading to the development of a failure plane and eventually to slope failure.

4.5 Comparison of conventional stability analyses with field data

A few conventional slope stability analyses were used to examine the factor of safety of sandbar 172L under two conditions.

RD1. A rapid drawdown condition using the groundwater surface predicted by the finite element model at peak river stage with the external water level at elevation 92.6m (low water level).

RD2. A rapid drawdown condition with the groundwater level at the same horizontal elevation as the peak river stage and the external water level at elevation 92.6m (low water level).

We employed stability analysis that utilized a non-circular failure surface and specified the observed failure surface (discontinuity between Zone I and Zone II soil) as the failure surface for which a factor of safety is being sought. The results of the slope stability analysis are summarized in Table 4.2. As expected, the factors of safety for RD2 are much lower than RD1 because of the high pore water pressures in RD2. The conditions imposed by RD2 are unusual because the peak discharge holding time was too short for the groundwater elevation to rise to the river stage elevation. The intention of using the conditions specified in RD2 was to investigate the worst case scenario. It is known that although these conventional analyses are based on the same fundamental principles, they give different results for the factor of safety mainly because of the differences in interslice forces (Whitman and Bailey, 1967). Further review of some of the conventional slope stability analyses by Duncan et. al. (1990) showed that differences could arise from different representation of soil strength. None of the conventional analyses examined here predicted failure. We repeated these analyses without specifying a failure surface; all predicted shallow slope failures (Fig. 4.10) similar to the finite element analyses. The disagreement is not surprising since the conditions under which failures

Table 4.2. Results from conventional stability analyses

Method of Analysis	Factor of safety	
	RD1	RD2
Spencer (1967)	4.15	1.75
Janbu (1954)	4.18	1.60
Modified Swedish (USACE, 1970)	4.10	1.72
Lowe and Karafiath (1960)	3.90	1.70

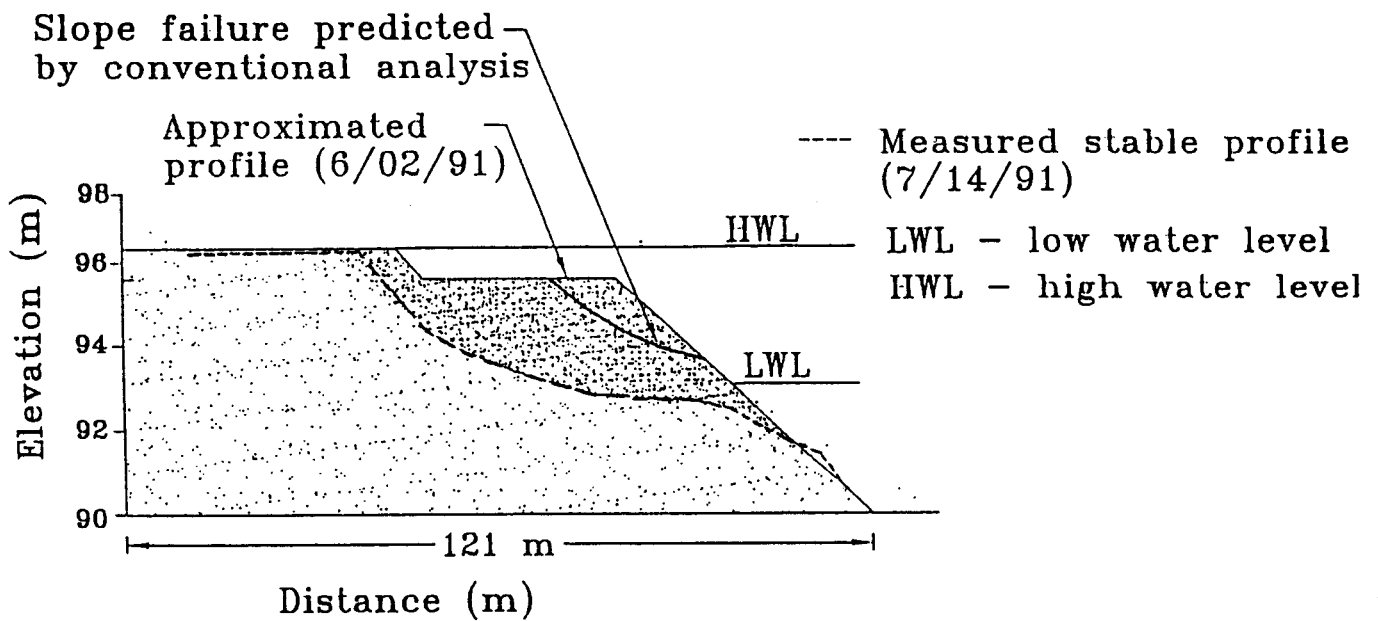


Fig. 4.10 Slope failure predicted by Spencer's method other conventional methods gave a similar failure surface.

occur on sandbars in Grand Canyon are different from the classical undrained failures under rapid drawdown where high pore water pressures are responsible for failures. For sandbars in Grand Canyon, seepage forces and high pore water pressures are responsible for slope failures.

4.6 Summary

The ability of the finite element model (Appendix II) to accurately predict the effects of dam discharge parameters on sandbar stability was demonstrated by modelling a well documented failure event on sandbar 172L, on June 18-19, 1991. The finite element model prediction showed good agreement with ground survey information and images captured by time lapsed photography only when an interface between the stable sandbar face and the freshly deposited sediments is included. The finite element model shows the importance of the interface in dictating where failures will occur. Slope stability analysis using conventional methods were incapable of accurately modelling the observed failure event on sandbar 172L.

Simulation of different dam discharge regimes under the guidelines of the interim low flow were performed with the finite element model. It was found that regardless of the dam discharge pattern, sandbars that have aggraded to a certain size will eventually collapse back to the stable seepage slope. Therefore controlling the dam discharge parameters (range, ramping rates and duration of the peak) will not prevent bankcuts or slope instability from occurring on sandbars in Grand Canyon.

CHAPTER 5

AGGRADATION/EROSION OF SANDBARS IN GRAND CANYON

5.1 Introduction

Seepage is only one of three major mechanisms that contribute to the erosion of sandbars in Grand Canyon. In this report, only one manifestation of seepage induced erosion, that is, bank cuts (mass wasting, slumping, slope instability) is considered. There are other manifestations of seepage, such as rilling, that are active on sandbars downstream of Glen Canyon Dam. In addition, none of the three major mechanisms act alone; they act together, but only one predominates at a given time period depending on the hydrologic and hydraulic conditions. In this chapter, a general conceptual model is presented to understand some key features of the erosion/aggradation process of sandbars in Grand Canyon. Field data is compared with the predictions from the model.

5.2 General Conceptual Model

If the Colorado River downstream of the Glen Canyon Dam were a single channel with no tributaries, and seepage erosion in the form of bank cuts was dominant, then the sandbars would achieve equilibrium profiles compatible with the dam discharge regime. The equilibrium profile will change by a small amount due to rilling and other seepage

related processes. The changes in sandbars with time would then be negligible with respect to the equilibrium profile (Fig. 5.1). However, the Colorado River is endowed with tributaries. Rains cause the tributaries to flow, bringing sediments into the main channel (Schmidt and Graf, 1990). These sediments are then available for the replenishment of eroded sandbars or to build new ones. Rock fall and debris flow can constrict the main channel near to an existing sandbar changing the local hydraulic conditions which may result in erosion.

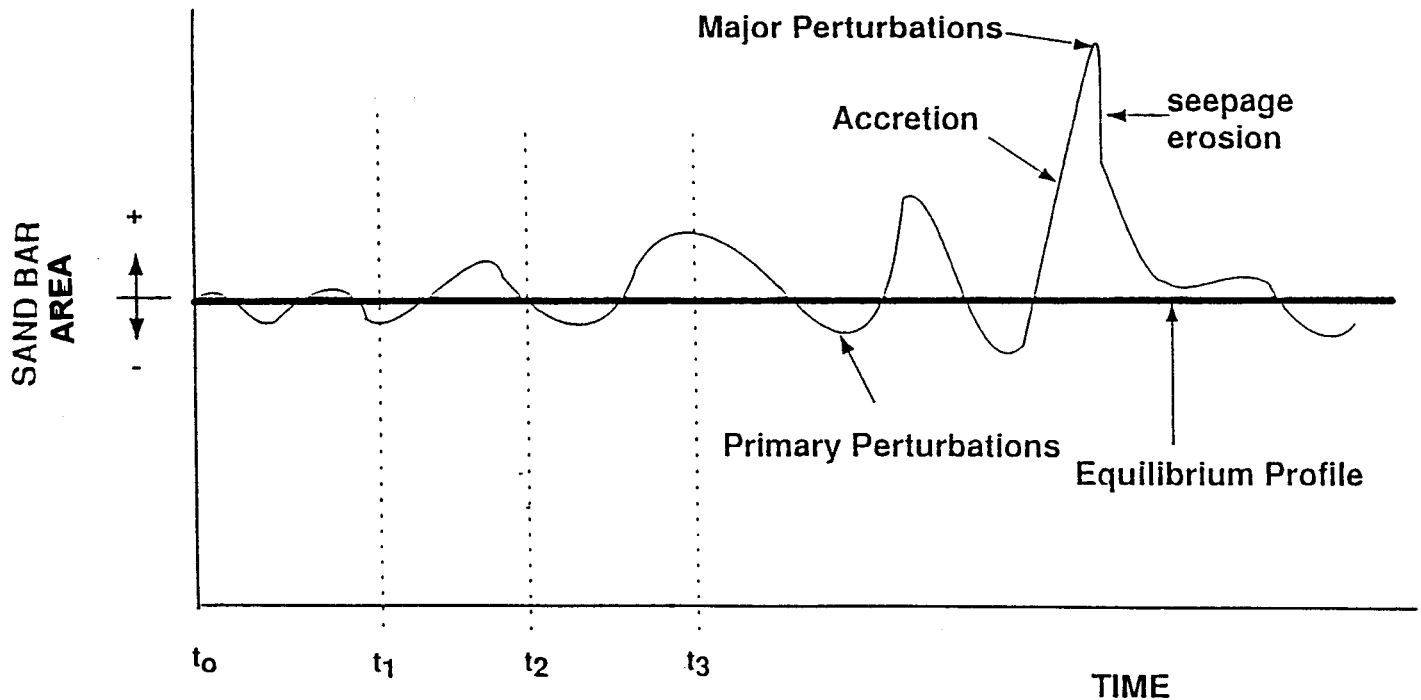


Fig. 5.1 General concept of erosion/aggradation

The transport of sediments from the tributaries during and after periods of low rainfall, debris flow, rock fall, reworking of sediments by eddies, wave action, tractive forces, rilling, small bank cuts, etc., cause perturbations (called primary perturbations here) in the equilibrium profile of a typical sandbar (Fig. 5.1). If the profile of a sandbar is measured at a given time, t_1 , the sandbar would show erosion or sand loss with reference to some initial measured profile (in this case, the equilibrium profile) at time, t_0 (Fig. 5.1). At a different time, t_2 , no change would be measured; the sandbar would be at its equilibrium profile compatible with the dam discharge regime. At another time, t_3 , measurement of the profile of the sandbar would show aggradation. Thus, over a certain period, T , the net sand loss balances the net sand gain, while for intermediate periods sand losses or sand gains may be measured. The effect, then, of sediments from the tributaries, debris flow, rock fall, reworking of sediments by eddies, wave action, tractive forces, rilling and other seepage phenomena, etc., is to upset the equilibrium profile through accretion followed by erosion or vice-versa.

Major perturbations (Fig. 5.1) to the equilibrium profile result from floods caused by heavy rains and/or snow melts or high dam discharges. During periods of floods, large volumes of sediments from the tributaries are transported into the main channel rebuilding and enlarging the sandbars (Schmidt et al.1992). Significant sand losses would occur due to bank cuts during the recession of the floods. Subsequently, other agents of erosion would act in partnership with seepage but the rate of erosion would be less than that due to bank cuts just after the floods. Sand losses would continue to occur towards the equilibrium profile unless another perturbation occurs. A summary of the factors

responsible for the perturbations is presented in Table 5.1. Two agents are described. One is due to natural phenomena causing perturbations following the vagaries of the natural world. The other is due to dam management practice.

Table 5.1. Factors governing the equilibrium profile and perturbations

	AGENTS	
	Natural	Dam Related
Equilibrium Profile	————	Seepage erosion (bank cuts, slumping, mass wasting, slope instability)
Primary perturbations	Rock fall, debris flow, transport of sediments from tributaries, eddy dynamics, reworking of bed load sediments, waves (boats and wind generated), transport of sediments from the canyon face and the top of sandbars from rain and wind.	Seepage erosion (rilling, bank cuts), tractive force
Major perturbations	Floods, transport of large volume of sediments from the tributaries, transport of sediments from the canyon face and the top of sandbars from rain, bank cuts, tractive forces, wave action.	High dam discharges, seepage erosion (bank cuts, rilling), tractive force.

A sandbar with an initial profile, carved by seepage erosion (bank cuts) from a given set of dam discharge regimes, would exist in a dynamically stable state. A different set of dam discharge regimes would rework the current equilibrium profile to a new dynamically stable state. There are special cases in which the local hydraulic conditions change significantly, for example, debris flow or rock fall which can result in severe erosion or the complete destruction of an extant sandbar. Floods may deposit sediments forming sandbars in locations incompatible with the current set of dam discharge regimes. These sandbars may then be completely eroded following the recession of the flood and the resumption of normal dam operation.

It appears that many sandbars in Grand Canyon (e.g. 172L) were built up under flood conditions. Following recession of the flood and resumption of normal dam operation, slope failures from seepage forces carved the stable seepage profile. The shape of the stable seepage profile is dictated by the highest and lowest river stage, the upramp rate and the duration of peak discharge. The sand behind the stable seepage profile becomes compacted under the cyclic river stage variation resulting from fluctuating dam discharges. If new sediments are deposited, a natural discontinuity at the interface of the stable seepage profile and the new sediments is formed. The unit weight of the new sediments is usually lower than that of the older sediments. If the slope of the new sediments is lower than that of the stable seepage profile, failure from seepage forces will not occur. However, if the slope of the new sediments is greater than the stable seepage slope, failure will eventually occur (Fig. 5.2). The slopes do not have to be rebuilt to the maximum profile previously attained but may fail at intermediate profiles.

The natural discontinuity between the older and the fresh sediments becomes the preferred failure plane. If the new sediments are deposited to enlarge the sandbar toward the main channel, tractive forces are likely to scour and undercut the lower part of the slope and cause slope failures (Fig. 5.3). These slope failures would continue to occur as more freshly deposited sediments at the lower part of the slope are scoured out. Eventually, the scouring may proceed close to the lower stable seepage slope triggering a slope failure along the discontinuity (Fig. 5.3). Although, the agent of erosion is scour, the extent of failure is dictated by the stable seepage slope.

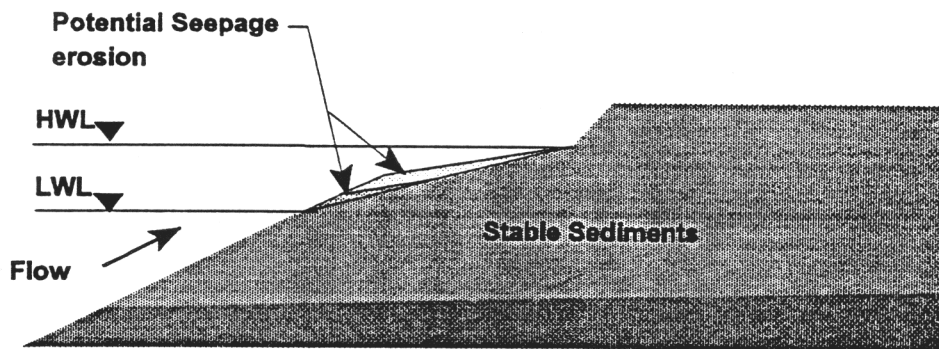


Fig. 5.2 Instability of sediments due to seepage.

5.3 Comparison of Field Data with the General Aggradation/Erosion Conceptual Model

Sandbar 172L was selected to compare the effects of the different flow regimes on aggradation and degradation to compare with the predictions of the general conceptual model. This sandbar is located in a hydraulically active zone and has been profoundly affected by changes in flow regime (Cluer, 1992; Beus et. al., 1992; Beus et. al., 1994). Several cycles of aggradation and erosion occurred during the research and interim flow periods.

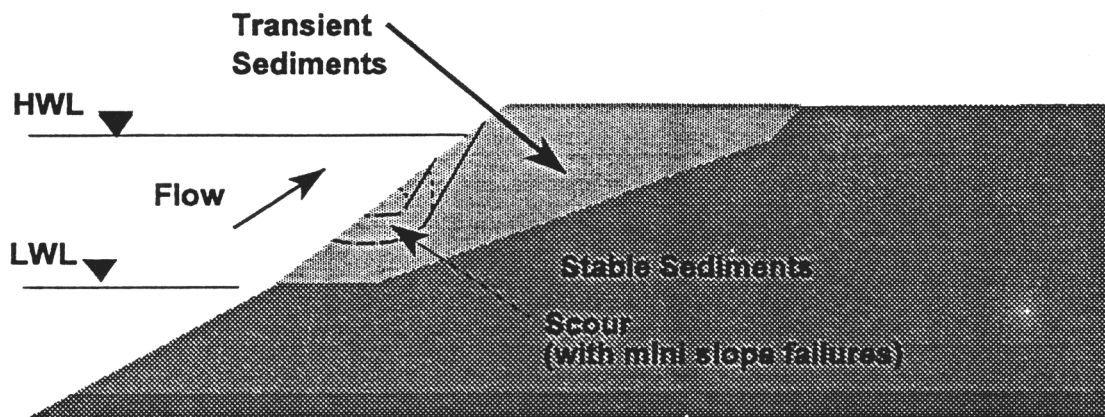


Fig. 5.3 Instability of sediments due to scour

The profiles along five transects (2, 4, 6, 8 and 10) along sandbar 172L (Fig. 5.4) were regularly monitored by ground surveys (Beus et. al., 1992; Beus et. al., 1994). Profile 10, which has a large return channel at the back of the sandbar was not considered in this

analysis since this represents a complex hydraulic condition that is addressed by neither the simple model nor the finite element model.

Changes in profile areas of each transect were calculated using the ground survey generated profiles developed by Beus et. al. (1992) and Beus et. al.,(1994). The lowest river stage elevation on sandbar 172L was taken as 92.6m based on discussions with and data presented by Beus et. al.,1994. A horizontal line at elevation 92.6m was drawn on the profile plots to intersect the lowest recorded profile in a transect. This point of intersection was used as the coordinate of point B (Fig. 2-1). The lower stable seepage slope $\alpha_s = 12.6^\circ$ (equation (2.1), for $\gamma_{sat} = 16 \text{ kN/m}^3$, $\phi = 30^\circ$) was drawn from B to intersect the projection of the upper slope DC at C (Fig. 5.5). The areas of sand above and below this stable seepage slope (BCD) for each profile in each transect were determined using a digitizer and the computer program AUTOCAD (R12).

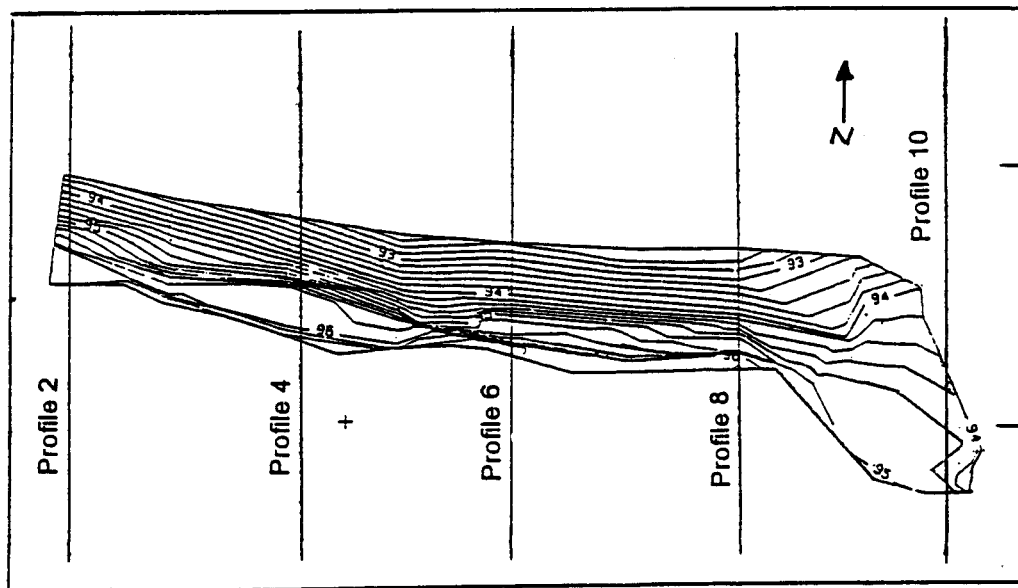


Fig. 5.4 Plan of sandbar 172L.

Field surveys were only performed at discrete time intervals and consequently the largest erosion event might not have been captured. In most cases, surveys were conducted some time after the failure events, when the bar was again in an aggradational mode. In addition, when field surveys were conducted, the coordinates of only a few points were recorded. The points measured in the field are assumed to be connected by straight lines in the plotted profiles. Consequently, the exact location of point B and, therefore, the preferred failure plane or stable seepage slope is uncertain.

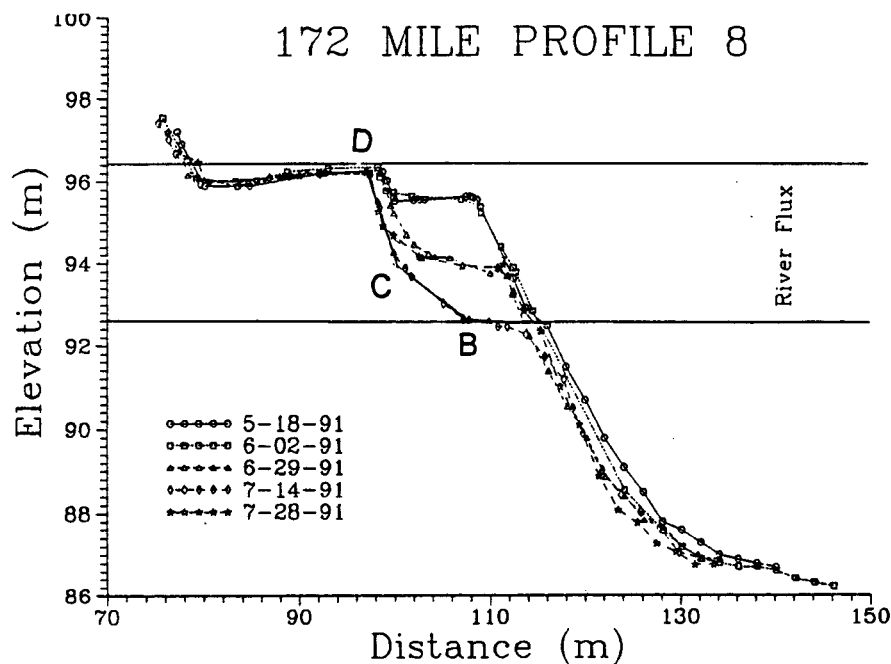


Fig. 5.5 Diagram showing how the changes in profile area were determined.

Plots of the areas above (positive quantity) and below (negative quantity) the stable seepage slope (equilibrium profile) for each transect during the research flows, interim flow

and interim low flow periods are shown in Figs. 5.6 to 5.9. These areas can be interpreted as volume per meter length of sandbar.

An examination of the plots reveal that none of the profiles undergo continuous erosion or continuous aggradation during any of the different flow regimes. Rather, the sandbar show a pattern of accretion followed by erosion. The research flows included many different flow regimes, each lasting for approximately 10 days. Each flow regime has to rework the river sustem to an equilibrium position compatible with that flow regime. Consequently, during the research flows more pronounced changes in sandbar area occured than during the interim and interim low flow periods. The high water level for the interim flows is less than that of the other flow regimes. Consequently, the upper part of the sandbar is not replenished with sediments. Mass wasting events and accretion are still observed in the interim low flow period, but there is a decrease in the amount of material involved.

The volume per meter length of sediments involved in accretion and erosion is different for the each transects. For example, the upstream one-third (approximately) of the sandbar aggradates much more than the lower one-third. The two dimensional analysis conducted in this study is, therefore, inadequate to fully describe the aggradation/erosion process that is occurring on this sandbar. Examination of the survey profiles described in chapter 2 with respect to the stable seepage profile reveals that during the pre-research flow period, the low river stage was lower than that recorded during the research and interim low flow period. The lowest river stage elevation deduced

from geomorphic features is 92.0 m. The changes in volume corresponding to this volume is shown by the lower horizontal line in Figs 5.6 - 5.9.

Using the equilibrium volume of the pre-research flows, it is evident from Figs 5.6 - 5.9 that failures on sandbar 172L involve areas above the stable seepage profile (Figs. 5.6 to 5.9). Since there is some uncertainty in the lowest river stage elevation, it is difficult to ascertain the location of the stable sand volume in Figs. 5.6 - 5.9. However, most of the eroded sediments are located above the stable seepage profile.

The general pattern of aggradation/erosion on sandbar 172L is consistent with the general conceptual model of aggradation/degradation of sandbars in Grand Canyon proposed in Art. 5.2. Sediments deposited above the stable seepage profile will collapse back to the stable seepage profile. The agent triggering the collapse can be seepage or tractive force. The behavior of sandbar 172L during the different flow regimes indicates that, regardless of the flow regime, this sandbar will exhibit a pattern of accretion followed by erosion. Regulation of the dam discharge parameters alone will not be effective in reducing the occurrence of mass wasting events on the sandbars downstream of the Glen Canyon Dam since natural phenomena play a significant, if not the major, role in aggradation/erosion of sediments in Grand Canyon.

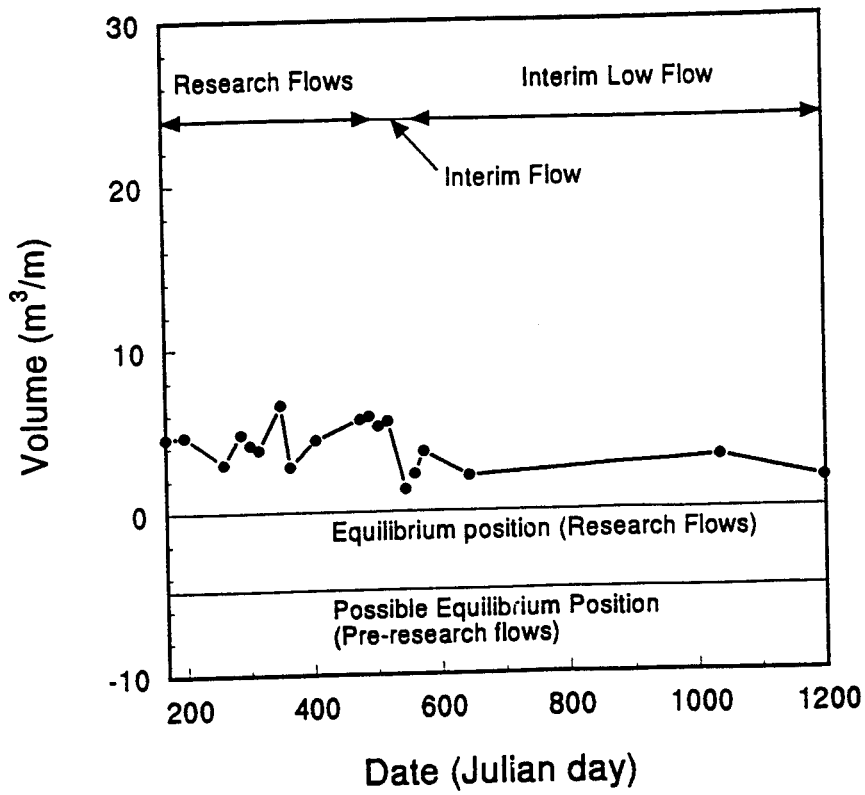


Fig. 5.6 Volume changes on profile 2, sandbar 172L.

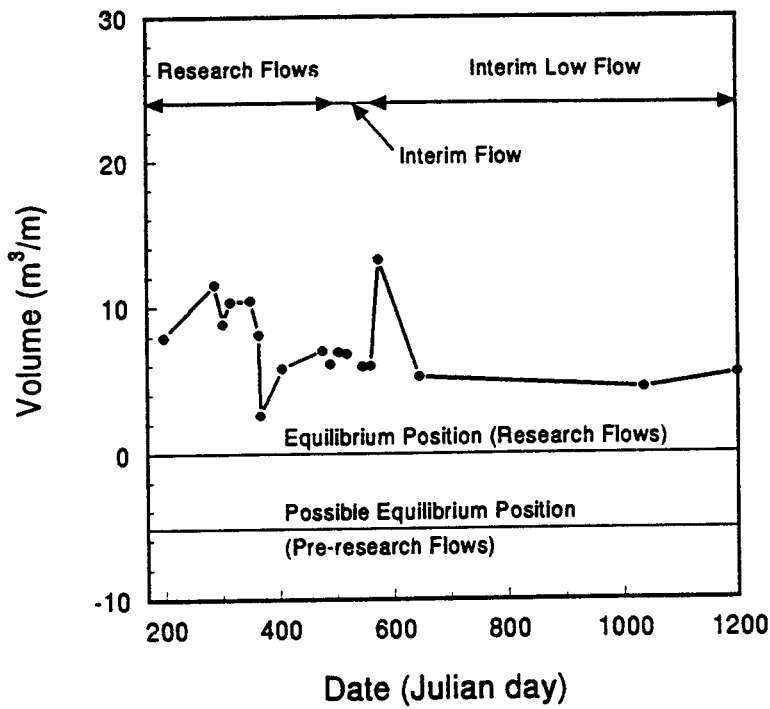


Fig. 5.7 Volume changes on profile 4, sandbar 172L.

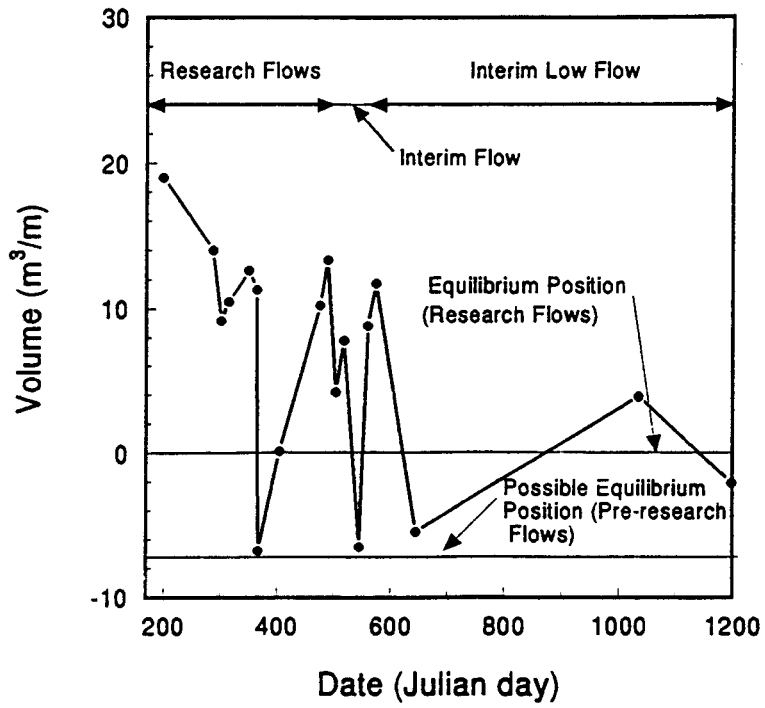


Fig. 5.8 Volume changes on profile 6, sandbar 172L.

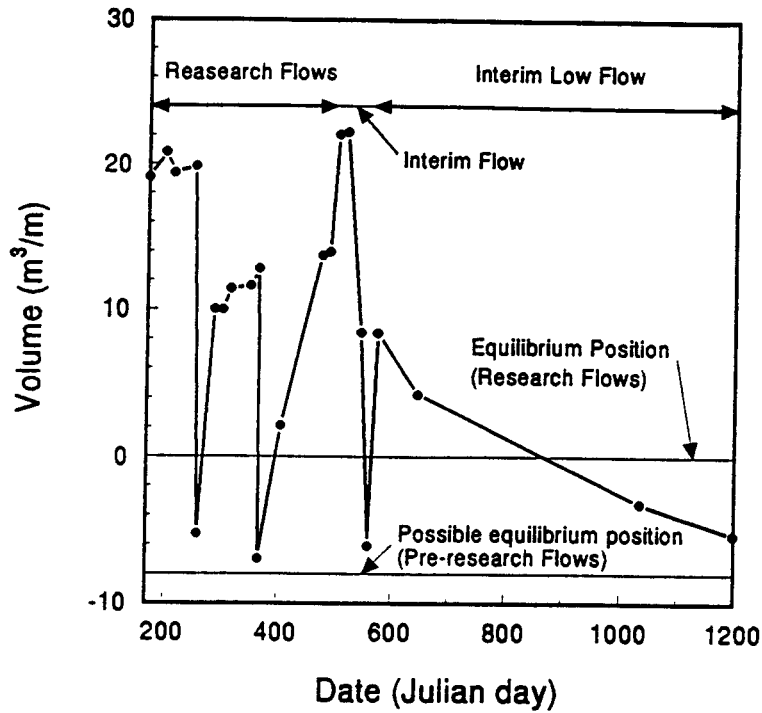


Fig. 5.9 Volume changes on profile 8, sandbar 172L.

5.4 Aggradation/Erosion Within Recirculating Zones

Many of the sandbars in Grand Canyon are in the vicinity of and/or are associated with recirculating zones. Each recirculating zone may consist of one or more eddies. Two modes of sandbar formation in recirculating zones in Grand Canyon were identified by Schmidt and Graf (1990). On the upstream end of the recirculating zone (Fig. 5.10), a separation bar, which consists of fine to very fine sediments, is formed. On the downstream side of the recirculating zone, a reattachment bar of coarser sediments than the separation bar, is formed. Reattachment bars are popular as campsites for boaters and hikers and usually exhibit cycles of aggradation and erosion. In this section, the mechanics of aggradation and erosion of reattachment bars (which are the subject of public scrutiny) within recirculating zones is presented.

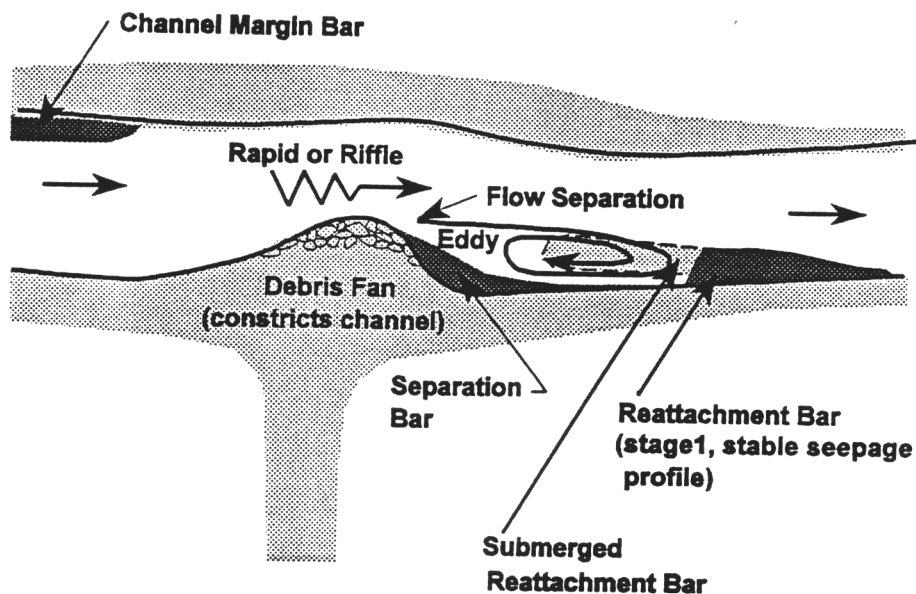


Fig. 5.10 Sandbar deposit at stage I

Consider a reattachment bar within a recirculating zone that had aggraded, as described by Schmidt and Graf (1990), to its maximum slope (Fig. 5.10). The flow regime compatible with the size of this recirculating zone is arbitrarily designated as X and this stage of the aggradational/erosion process is denoted as stage I. In Grand Canyon, the average maximum depositional slope is 28° (Table 2.1), the average angle of friction of the sediment is 30° and the average unit weight is 16 kN/m^3 (Budhu, 1992).

Under dam operation, the depositional slope becomes unstable under seepage forces as described in chapter 2. Using the simple model (chapter 2), the reattachment bar would fail (bank cuts, slope failures) from seepage forces, usually at low river stage, finally achieving an equilibrium profile as shown in Fig. 2.1. The mass of sand within the (theoretically) failed zone, ABCD (Fig. 4.1) would remain in the vicinity of the recirculating zone, becoming subaqueous sediments (Fig. 5.10). The sediments cannot be transported out of the recirculating zone because the flow velocity is low near the downstream end of the recirculating zone and the velocity in the main channel would be at its lowest value for the flow regime under consideration. Sediment concentration would be high and, according to Nelson (1991), water with high sediment concentration would move into the eddy near the streambed into the recirculating zone. The collapsed mass of sand (ABCD, Fig. 2.1) then fuels the recirculating zone and sediments are then redeposited on the equilibrium profile BCD (Fig. 2.1). The surface BCD is a surface of discontinuity and becomes the preferred failure surface. Once the redeposited sediments exceed the lower stable slope angle, α_s , slope failures would re-occur, and the failed mass of sediments

would then be entrapped in the recirculating zone again. If flow regime X is maintained, then the cyclic process of aggradation and erosion would perpetuate.

Suppose the dam discharge is changed from flow regime X to flow regime Y by increasing the discharge. Under flow regime, Y (stage II), the recirculating zone would stretch in the direction of flow (Schmidt and Graf, 1990) as shown in Fig. 5.11. The extreme upstream end of the extant reattachment bar (stable under flow regime X) would be subjected to tractive forces from the eddies and erode (Fig. 5.11). Part of the eroded volume of sediments would be trapped by the recirculating zone while the other part will be transported downstream by the main channel current. Some of the sediments trapped in the recirculating zone may be deposited on the upstream separation bar and on the downstream end of the reattachment bar (Fig. 5.11). Some of the eroded sediments

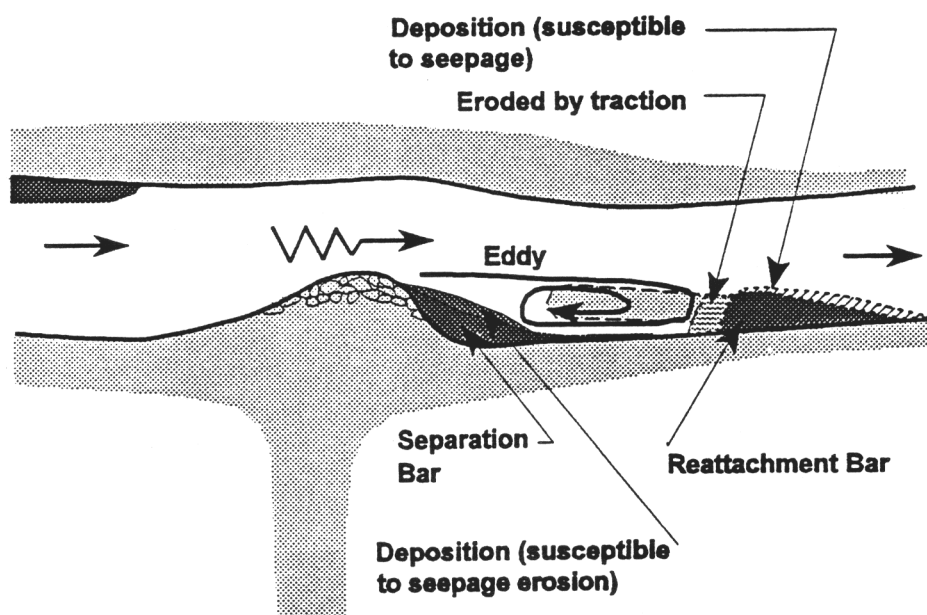


Fig. 5.11 Effects of an increase in discharge on sandbar stability - stage II.

transported by the main channel current may be deposited on the downstream end of the reattachment bar or taken further downstream. As the river stage is lowered the depositional slope, if greater than α_s , would fail along the surface BCD (Fig. 2.1). The failed mass of sediment would then enter the recirculating zone and is available for redeposition to continue the cycle of aggradation/erosion.

If the dam discharge is changed to flow regime, Z (stage III), so that the maximum discharge is lower than flow regime, X, then the recirculating zone would shrink as illustrated in Fig. 5.12. Deposition may now occur on the upstream side of the extant reattachment bar which had been eroded in stage II by tractive forces. Little or no deposition is likely at the downstream end of the reattachment bar. The sediments deposited on the separation bar during stage II may erode from seepage erosion at the end of stage II or by tractive forces at the beginning of stage III (Fig. 5.12).

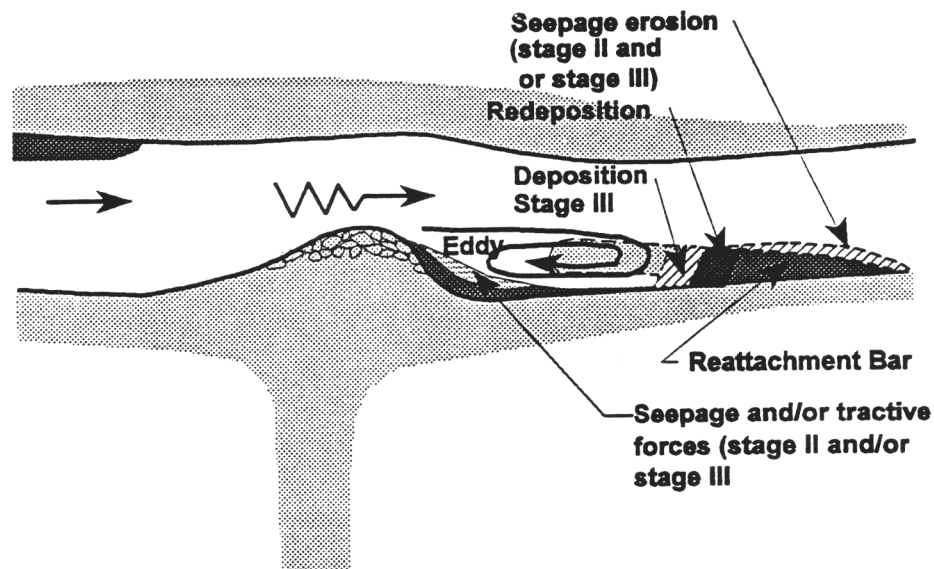


Fig. 5.12 Effects of a decrease in discharge on sandbar stability - stage III.

Unless some drastic changes in hydraulic conditions occur within or in the vicinity of the recirculating zone, such as debris flow in the recirculating zone, the surface BCD (Fig. 2.1) would be the preferred failure plane.

If the dam discharge then reverts to flow regime X (stage IV), the eddy system will rework the sediments (Fig. 5.13). Portions of the upstream end of the reattachment bar built up during stage III will now erode from tractive forces of the eddy system. The eroded sediments are likely to remain in the recirculating zone. The original area of the sand bar in stage I is regained in stage IV. Under stage II, there is a net loss of sediments from the recirculating zone. The implication is that if the cycle, stage I to stage IV, continues, and no new sediments are trapped in the recirculating zone, the reattachment bar will reduce in size.

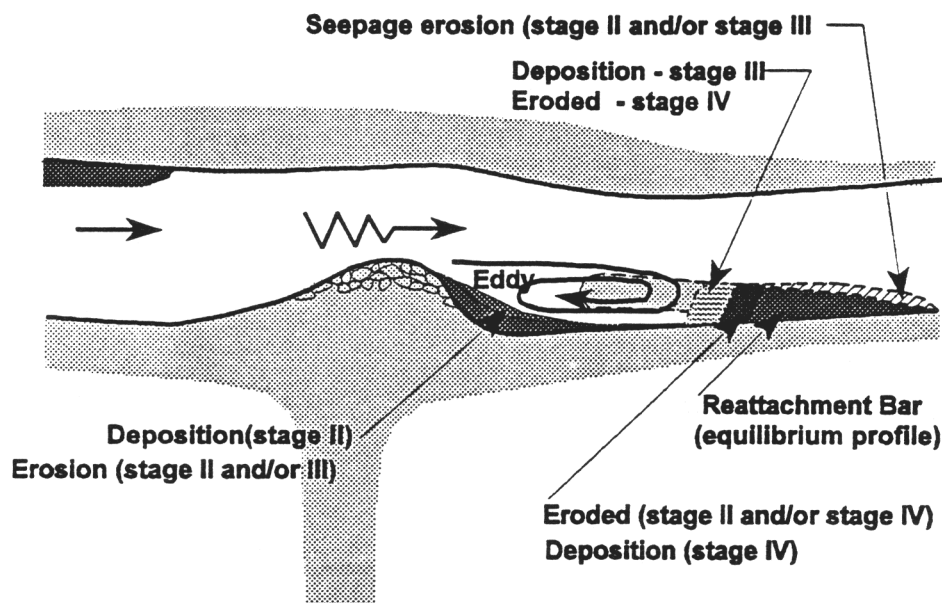


Fig. 5.13 Sandbar stability on completion of one cycle of changes in recirculating zone - stage IV.

There are other factors that contribute to the dynamics of the recirculating zones. For example, sediments transported by floods or high dam discharges from the tributaries to the main channel may also enter the recirculating zone adding another dimension to the aggradation/erosion process. The reattachment bars could be built wider and higher. Since the new geometry would be incompatible with the local dynamics of the recirculating zone, erosion by tractive forces and seepage will commence as soon as usual dam operation resumes. The influence of these sediments on the mechanics of the aggradation/erosion process in a recirculating zone is beyond the scope of this investigation.

Summary

The aggradation/erosion of sandbars in Grand Canyon is a complex process involving dam operation parameters and natural phenomena. For each dam discharge regime, the sediments on sandbars are reworked to either new equilibrium profiles or to previous equilibrium profiles if the range of dam discharge and duration of peak discharge are lower than historical highs. Sandbars in Grand Canyon have acquired equilibrium profiles congruous with dam operation parameters. Natural phenomena (for examples, debris flow, eddy dynamics, floods from snow melts) disturb the equilibrium profiles. Most sandbars are associated with recirculating zones whose sizes vary with changes in dam discharge regime. A cyclical process of aggradation/erosion occurs on reattachment sandbars in the recirculating zone. Sandbars, which are aggraded to slopes greater than

are permitted by seepage forces, collapse to an equilibrium profile and the collapsed mass of sand refuels the eddies in the recirculating zones to perpetuate the aggradation/erosion cycles. Sediments transported by flood or high dam discharge disturb the local dynamics of a recirculating zone by removing or adding sediments to the system. Upon resumption of 'normal' flow patterns the sandbar will be reworked to its new equilibrium position.

CHAPTER 6

SUMMARY AND CONCLUSIONS

Two mathematical two-dimensional models for seepage erosion were developed and validated in this study. The first model is a simple model that gives the extent of seepage erosion (bank cuts, mass wasting, slope instability) on sandbars in Grand Canyon. This model is intended to be used by dam operators and others to obtain an approximation of the effects of changes in dam operation on sandbar stability. The second model, based on finite element analysis, is a more elaborate than the simple model. It accounts for soil stratification, dam operation parameters (upramping and downramping rates, peak discharge holding time and total discharge), groundwater and stress changes due the river stage fluctatuations, soil failure and deformation. This finite element model is intended to provide detailed insights and understanding of the effects of dam operation parameters on the stability of sandbars. The predictions from both models compare favorably with field data. A conceptual model describing the aggradation/erosion cycles of sediments in sandbars in Grand Canyon due to dam operation and natural phenomena was proposed and validated by field data. Based on these models and the relevant field data, the following conclusions are presented.

► ***Equilibrium Profile***

The sandbars, studied in this report, have achieved equilibrium profiles compatible with the dam discharge regimes. For most of the sandbars, this equilibrium profile comprised two slopes - a lower stable seepage slope of angle between 11° and 14° (or lower) starting from the low river stage elevation and an upper slope of angle between 30° and 32°. When sufficient sediments are available in the main channel and the hydraulic conditions (low velocity) are favorable, sediments are deposited above the equilibrium profile. If the depositional slope is greater than the lower stable seepage slope, slope instability (mass wasting, bank cuts) would occur.

The interface between the equilibrium profile and the newly deposited sediments is a preferred plane of failure. Failure would occur on this preferred failure plane regardless of the agent that initiates the failure. Slope failure of sediments would progress up to the equilibrium profile, unless further erosion occurs from rilling and other agents of erosion, and remain there until re-deposition occurs. Evaluations of the field data reveal a cyclic pattern of deposition and erosion of sediments (transient sediments) above the equilibrium seepage profile.

► ***Effects of dam operation parameters on the equilibrium profile***

The dam parameters that affects the equilibrium profile are the range of discharge, the upramping rate and the duration of the peak discharge. An increase in the range of dam

discharge from a given low river stage level, or an increase in the duration of the peak discharge, would increase the amount of sediments involved in seepage erosion. Increasing the upramping rate would reduce the amount of sediments involved in seepage erosion. However, large upramping rates may increase the tractive forces the effects of which was not studied in this report. An equation is proposed, and a procedure was developed, in this study to determine the size of sandbar that would be negatively affected by changing the dam operation parameters.

▶ ***Research flows and interim low flows***

The various research flows introduced in the river system required the system to respond by reworking the sandbars to new equilibrium profiles compatible with each flow regime. For most sandbars, the range of dam discharge, the ramping rates and the peak discharge holding time were smaller than normal dam operation or historic highs. Thus, there was very little change in the established equilibrium profiles of the sandbars. The range of discharge for the interim low flow is lower than prior normal dam operation. Consequently, the amount of sediment participating in the aggradation/erosion cycles is lower than pre-interim low flow.

▶ ***Aggradation/erosion of sediments in Grand Canyon***

Erosion of sediments from sandbars in Grand Canyon occurs from dam operation and

natural phenomena. Dam operation is mainly responsible for seepage driven and tractive force erosion. The agents producing natural erosion are wind (wave forces and wind borne erosion), rock fall, debris flow, rains and snow melts. Recreational use and boat wakes also contribute to erosion but this appears to be significantly lower than dam operation and natural phenomena. The effect of dam operation and natural phenomena is to cause perturbations about the equilibrium profile. Sediments, transported from the tributaries during rainfall and snow melts into the main channel, are deposited on the equilibrium profile when the conditions are favorable. The depositional slopes are unstable under seepage forces and eventually collapsed back to the equilibrium profile under normal dam operation. Most sandbars are associated with recirculating zones and the cyclical process of aggradation/erosion occurring on them are related to the dynamics of these zones. The sand masses from slope failures on sandbars in the vicinity of the recirculating zones become subaqueous deposits and fuels the eddies in the recirculating zones. Sediment is then redeposited on the sandbars followed by erosion. The aggradation/erosion cycles on sandbars in Grand Canyon cannot be halted by changing dam operations because major perturbations in the system occur due to natural phenomena. The amount of sediments involved in the aggradation/erosion cycles can be reduced by reducing the range of discharge as currently practised for the interim low flow.

- ***Control Flood***

Provided that sufficient sediments are available in the main channel, a control flood may

cause deposition of sediments above the equilibrium profile. However, most of the sediments would be eroded during the recession of the flood and the commencement of normal dam operation. Because sandbars may be built wider and higher, larger volumes of sediments than during the proposed pre-flood aggradation/erosion cycles would collapse. The range of discharge and the ramping rates of the control flood can be predetermined using the finite element model to minimize the anticipated large scale collapse of the freshly deposited sediments from seepage forces and pore water pressures during the recession of the floods and the initiation of normal dam operation.

REFERENCES

- Amanullah., (1993). Experimental study of slope failure due to rapid drawdown, M.S. Thesis, University of Arizona.
- Bathe, K.J., and Khoshgoftaat, M.R., (1979). Finite element free surface seepage analysis without mesh iteration. *Int. J. Num. Anal. Methods Geomech.*, 3, 13-22.
- Bues, S.S., Avery, C.C., Stevens, L.E., Kaplanski, M.A., and Cluer, B.L., (1992). The influence of variable discharge regimes on Colorado River sand bars below Glen Canyon Dam, in S.S. Bues and C.C. Avery (eds.), *The influence of Variable Discharge on Colorado River Sand Bars Below Glen Canyon Dam: Final report to the National Park Service.*
- Bues, S.S., Avery, C.C., Stevens, L.E., Kaplanski, M.A., and Cluer, B.L., (1994). Private Communication.
- Biot, M. A., (1941). "Theory of elasticity and three dimensional consolidation." *J. of Applied Physics*, 12, 155-164.
- Booker, J.R., and Small, J.C., (1975). An investigation of the stability of numerical solution on Biot's consolidation. *Int. J. Solids Struct.* 11, 907-917.
- Budhu, M., (1992). Mechanisms of erosion and a model to predict seepage erosion due to transient flow, in S.S. Bues and C.C. Avery (eds.), *The influence of Variable Discharge on Colorado River Sand Bars Below Glen Canyon Dam: Final report to the National Park Service.*
- Budhu, M., Wu, C.S., and Contractor, D.N., (1994). Modelling ground water changes due to fluctuating dam discharge. *J. Applied Mathematical Modelling.*
- Carpenter, M.C., Carruth, R.L., Fink, J.B., Boling, J.K., and Cluer B.L., (1992). Hydrogeology of beaches 43.1L and 172.3L and the implications on flow alternatives along the Colorado River in the Grand Canyon, in S.S. Bues and C.C. Avery (eds.), *The influence of Variable Discharge on Colorado River Sand Bars Below Glen Canyon Dam: Final report to the National Park Service.*
- Carpenter, M.C., (1994). Private communication.
- Casagrande, A., (1937). Seepage through dams, Harvard University Publication 209, reprinted from *Journal of the New England Water Works Association.*

Cividini, A., and Gioda, G., (1989). On the variable mesh finite element analysis of unconfined seepage problems. *Geotechnique*, 2, 251-276.

Cluer, B.L., (1992). Daily responses of Colorado River sand bars to Glen Canyon Dam tests flows, Grand Canyon, Arizona, and Analysis of sand bar response along the Colorado River in Glen and Grand Canyons to test flows from Glen Canyon Dam, using aerial photograph, in S.S. Bues and C.C. Avery (eds.), *The influence of Variable Discharge on Colorado River Sand Bars Below Glen Canyon Dam: Final report to the National Park Service*.

Corps of Engineers, (1970). *Engineering and Design - Stability of Earth and Rock-Fill Dams*. Engineer Manual EM 1110-1902, Dept. Of the Army, Corps of Engineers, Office of the Chief Engineer.

Desai, C.S., (1976). Finite element residual schemes for unconfined flow. *Int. J. Num. Meth. Eng.*,5, 1415-1418.

Desai, C.S., (1984). Free surface flow through porous media using a residual flow procedure. In, *Finite elements in fluids*, 5, Chapter 18, Ed. Gallagher, R.H., Oden, J.T., Zienkiewicz, O.C., Kawai, T., and Hawahara (eds).

Desai, C.S., and Li, G. C., (1983). A residual flow procedure and application for free flow in porous media. *Advances in Water Resources*, 6, 27-35.

Duncan, M., Wright, S., and Kong, K.S., (1990). Slope stability during rapid drawdown. *Proc. H. Bolton Seed Memorial Symposium*, ed. J. Michael Duncan, Bitech Publishers Ltd., Vancouver, B.C., Canada, 2, 253-271.

Hagerty, D.J., (1991a) Piping/Sapping erosion: I: Basic considerations. *J. Hydr. Engrg.*, ASCE, 117, 8, 991-1008.

Hagerty, D.J., (1991b) Piping/Sapping erosion: II: Identification - diagnosis. *J. Hydr. Engrg.*, ASCE, 117, 8,1009-1025.

Harr, M.E., (1962). *Groundwater and seepage*. McGraw Hill, New York.

Hinton, E. And Owens, D.R.J., (1977). *Finite element programming*. Academic Press, London.

Howard, A.D., and Mclane, C.F., (1988). Erosion of cohesionless sediment by groundwater seepage, *Water Resource Research.*, 24, 1659-1674.

Howard, A.D., and Dolan, R., (1981). Geomorphology of the Colorado River in the Grand Canyon, *J. Geol.* 89: 269-298.

Iverson, R.M., and Major, J.J., (1986). Groundwater seepage vectors and the potential for hillside failure and debris flow mobilization, *Water Resource Research.*, 22, 1543-1548.

Janbu, N., (1954). Application of composite slip surface for stability analysis. *Proceedings European Conf. On stability of earth slopes, Sweden*, Vol. 3, 43-49.

Lacy, S.J., and Prevost, J.H., (1987). Flow through porous media: a procedure for locating the free surface. *Int. J. Num. Anal. Methods Geomech.* 11(6), 585-601.

Liggett, J.A., (1977). Location of free surface in porous media. *J. of Hydr. Division, ASCE*, 103(4), 353-365.

Lowe, J. III, and Karafiath, L., (1960). Stability of earth dams upon rapid drawdown. *Proc. 1st Panamerican Conf. On Soil Mech. And Found. Engrg.*, Mexico City, Mexico, Vol. 2, 537-552.

Marsily, de G., (1986). *Quantitative hydrogeology, Groundwater hydrology for engineers.* Academic Press Inc.

Nelson, J.M., (1991). Experimental and theoretical investigations of lateral separation eddies (abst.), in *AGU 1991 Fall Meeting Program and Abstracts.* American Geophysical Union EOS Transactions, supp. To vol. 72, no. 44, pp. 218-219.

Neuman, S.P., and Witherspoon, P.A., (1971). Analysis of non-steady flow with a free surface using the finite element method. *Water Resources Research*, 7(3), 611-623.

Neuman, S.P., (1973). Saturated-Unsaturated seepage by finite element method. *J. of Hydr. Division, ASCE*, 99(12), 2233-2251.

Roscoe, K.H., and Burland, J.B., (1968). On the generalised stress-strain behavior of a wet clay. In *Engineering Plasticity*, eds. Heyman, J., and Lechie, F.A., Cambridge University of Cambridge, 535-609.

Scofield, A.N., and Wroth, C.P., (1968). *Critical state soil mechanics.* McGraw Hill Book Company, London.

Schmidt, J. C., and Graf, J. B., (1990). "Aggradation and degradation of alluvial sand deposits 1965 to 1986, Colorado River, Grand Canyon National Park, Arizona." U.S. Geological Survey, Paper 1493.

Schmidt, J.C., Clark, J.J., Kyle, E.L., and Grams, P.E., (1992). Historic changes in sediment deposits in Grand Canyon, 1965-1990, in S.S. Bues and C.C. Avery (eds.), *The influence of Variable Discharge on Colorado River Sand Bars Below Glen Canyon Dam: Final report to the National Park Service.*

Smith, I.M., and Griffith, D.V., (1988). *Programming the finite element method.* Wiley and Sons, Inc., New York, N.Y.

Spencer, E., (1967). A method of analysis of the stability of embankments assuming parallel inter-slice forces. *Geotechnique*, London, England, 17(1), 11-26.

Stevens, L., (1983). *The Colorado River in the Grand Canyon, A Guide.* Red Lake Books, P.O. Box 1315, Flagstaff, AZ, USA.

Stevens, L. (1992) Private communication.

Taylor, D.W., (1948). *Fundamental of soil mechanics.* John Wiley & Sons, New York.

Taylor, R.L., and Brown, C.B., (1967). Darcy flow solution with a free surface, *J. of the Hydraulics Div., ASCE*, 93(2), 25-33.

Turner, R.M., and Karpiscak, M.M., (1980). Recent vegetation changes along the Colorado River between Glen Canyon Dam and Lake Mead, Arizona. *U.S. Geological Survey Professional Paper 1132.* Washington.

U.S. Department of Interior. (1988). *Glen Canyon Environmental Studies. Final Report.* Bureau of Reclamation, Washington, D.C.

Whitman, R.V., and Bailey, W.A., (1967). Use of computers for slope stability analysis. *J. Soil Mech. And Found. Div., ASCE*, 93(4), 475-497.

Zienkiewicz, O.C., (1966). *The finite element method.* McGraw-Hill, London.

LIST OF FIGURES

Fig. 1.1 Map of study area.

Fig. 2.1 Proposed stable seepage slope.

Fig. 2.2 Geological section of sandbar -6.5R.

Fig. 2.3 Comparison between model predictions and field data, Flow G.

Fig. 2.4 Comparison between model predictions and field data, Flow E.

Fig. 2.5 Comparison of predicted stable seepage slope with ground survey data for sandbar -6.5R.

Fig. 2.6 Geological section of sandbar 43L.

Fig. 2.7 Comparison of predicted stable seepage slope with ground survey data for sandbar 43L.

Fig. 2.8 Geological section of sandbar -6.5R.

Fig. 2.9 Comparison of predicted stable seepage slope with ground survey data for sandbar 172L.

Fig. 3.1 Relationship between groundwater surface and river stage variation.

Fig. 3.2 Variation of groundwater surface at high water level with rate of rising river stage.

Fig. 3.3 Plot of beta versus rate of rise of river stage.

Fig. 3.4 Plot of beta versus permeability

Fig. 3.5 Groundwater surface variation with time for downramp rate of 0.25 m/hr.

Fig. 3.6 Groundwater surface variation with time for downramp rate of 0.5 m/hr.

Fig. 3.7 Effects of duration of peak discharge on groundwater surface position.

Fig. 3.8 Stable seepage profile for the illustrative example.

Fig. 3.9 Geometry of width of sandbar affected by seepage erosion.

Fig. 3.10 Reduction of sandbar width with angle of friction.

Fig. 3.11 Variation of width with cohesion and angle of friction.

Fig. 3.12 Volume changes due to river stage fluctuations.

Fig. 3.13 Volume changes due to duration of peak discharge.

Fig. 4.1 Typical changes on the profile of sandbar 172L

Fig. 4.2 a Photograph of sandbar 172L on June 18, 1991 (courtesy of B. Cluer).

Fig. 4.2 b Photograph of sandbar 172L on June 19, 1991 (courtesy of B. Cluer).

Fig. 4.3 River stage and water level variation in well #63 from June 11 to June 15, 1991.

Fig. 4.4 Finite element approximation of river stage on June 14, 1991.

Fig. 4.5 Comparison between finite element prediction of groundwater and well #63 on June 18, 1991.

Fig. 4.6 Finite element approximation of river stage on June 18, 1991.

Fig. 4.7 Finite element prediction of failure zone when interface elements are included.

Fig. 4.8 Displacement vectors at low water level.

Fig. 4.9 Finite element prediction of failure zone without interface elements.

Fig. 5.1 General concept of erosion/aggradation.

Fig. 5.2 Instability of sediments due to seepage.

Fig. 5.3 Instability of sediments due to scour.

- Fig. 5.4 Plan of sandbar 172L
- Fig. 5.5 Diagram showing how the changes in profile area were determined.
- Fig. 5.6 Volume changes on profile 2, sandbar 172L.
- Fig. 5.7 Volume changes on profile 4, sandbar 172L.
- Fig. 5.8 Volume changes on profile 6, sandbar 172L.
- Fig. 5.9 Volume changes on profile 8, sandbar 172L.
- Fig. 5.10 Sandbar deposit at stage I.
- Fig. 5.11 Effects of an increase in discharge on sandbar stability - stage II.
- Fig. 5.12 Effects of an decrease in discharge on sandbar stability - stage III.
- Fig. 5.13 Sandbar stability on completion of one cycle of changes in recirculating zone - stage IV.
- Fig. I-1 Forces on an elemental volume of soil and ranges for Coulomb type failure and static liquefaction.
- Fig. I-2 Flow field in a homogeneous isotropic soil showing the exit velocity and its components.
- Fig. I-1 Slope angles for different seepage directions and the corresponding hydraulic gradient for $\phi = 30^\circ$.
- Fig. I-4 Forces on an elemental volume for a saturated-unsaturated soil.
- Fig. I-5 Plot of stable seepage slope as a function of Y/D ratio for $\phi = 30^\circ$.
- Fig. I-6 A sectional view of a flume used to investigate slope failures by emergent seepage.
- Fig. I-7 Observed stable seepage slope as a function of the number of drawdowns.
- Fig. II-1 Void ratio - $\ln(p)$ curve.

NOTATION

A	cross-sectional area of soil element
B	width of sand bar affected by seepage
B_i	body force
C_c	coefficient of curvature
C_u	coefficient of uniformity
c	cohesion
D	thickness of unsaturated zone
D_{50}	average grain size diameter
d	downramp rate
e	void ratio
F	factor of safety
G	specific gravity of soil
G_s	shear modulus
H_w	stage height (above low water level)
h_c	depth of tension crack
i	hydraulic gradient
i_{cr}	critical hydraulic gradient
j	seepage force per unit volume
K_a	coefficient of lateral active earth pressure
k	coefficient of permeability (hydraulic conductivity)
k_x, k_y, k_z	coefficient of permeability in x, y, z directions

N	normal force
$n_x, n_y, n_z,$	direction cosines
P_t	holding time
p	mean pressure
r	rate of rising river stage
S_r	degree of saturation
S	storativity
s	slope angle
R	resisting force
T	disturbing force
V	velocity
V_n	normal velocity
V_t	tangential velocity
w	weight per unit area
x	body position
z	depth of soil element
α_s	slope angle for stability under seepage
β	vertical projection of seepage slope
λ	direction of seepage vector
ϕ	angle of friction
p^t	mean total stress
e_v	volumetric strain

$\epsilon_1, \epsilon_2, \epsilon_3$	strains in the principal directions
κ	slope of unloading/reloading curve
μ	Poisson's ratio
ϵ_v^p	plastic volumetric strain
ϵ_v^e	elastic volumetric strain
δ_{ij}	Kronecker delta
σ_{ij}	effective stress
γ_c'	current effective unit weight
γ_{sat}	saturated bulk unit weight
γ'	effective unit weight
γ_t	total unit weight
γ_w	unit weight of water

APPENDIX I

Formulation of 'Simple' Model

Consider an elemental volume (V) of soil within a homogenous infinite slope of slope angle, α , and stress free boundaries, that is subjected to a seepage force, $i\gamma_w V$, where i is the magnitude of the seepage vector (hydraulic gradient) and γ_w is the unit weight of water. The direction of the seepage vector is assumed to make an angle λ with the plane normal to slope (Fig. I-1). The disturbing force down the slope (T) is

$$T = V(\gamma' \sin\alpha + i\gamma_w \sin\lambda) \quad (\text{I-1})$$

where the submerged (effective) unit weight of the soil is $\gamma' = \gamma_{\text{sat}} - \gamma_w$ and γ_{sat} is the saturated unit weight of the soil. The resisting force given by Coulomb's failure criterion is

$$R = cA + N \tan\phi \quad (\text{I-2})$$

where c is the cohesion of the soil, ϕ is effective friction angle, A is the cross sectional area of the element and N , the normal force given by

$$N = V(\gamma' \cos\alpha - i\gamma_w \cos\lambda) \quad (\text{I-3})$$

Substituting equation (I-3) into equation (I-2) we obtain

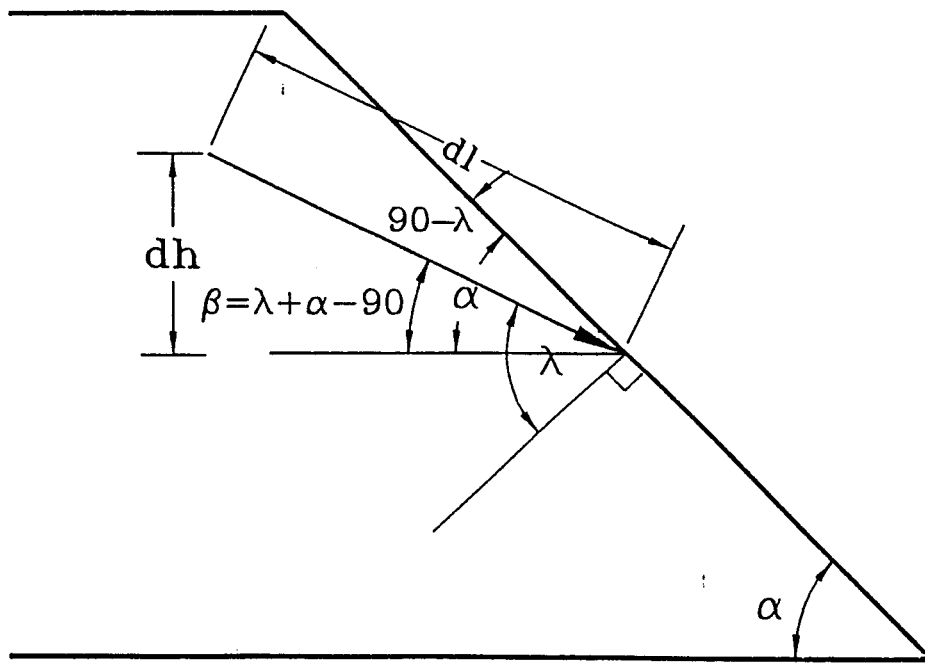


Fig. I-1. Forces on an elemental volume of soil and ranges of λ for Coulomb type failure and static liquefaction.

$$R = cA + V(\gamma' \cos\alpha - i\gamma_w \cos\lambda)\tan\phi \quad (I-4)$$

The factor of safety of the slope against a Coulomb type failure is

$$F = \frac{R}{T} = \frac{\frac{c}{\gamma_w z} + \left(\frac{\gamma'}{\gamma_w} \cos\alpha - i \cos\lambda\right)\tan\phi}{\frac{\gamma'}{\gamma_w} \sin\alpha + i \sin\lambda} \quad (I-5)$$

where z is depth of the element. Now, consider a flow net within a slope as shown in Fig. I-2. Harr (1962) showed that the tangential velocity (V_t) at a point C on the seepage face

AB, is

$$V_t = k \sin\alpha \quad (I-6)$$

and the normal (V_n) is

$$V_n = k \sin\alpha \cot\lambda \quad (I-7)$$

The resultant velocity (V) is

$$V = \sqrt{(V_t^2 + V_n^2)} = k \sin\alpha \sqrt{(1 + \cot^2\lambda)} = k \frac{\sin\alpha}{\sin\lambda} \quad (I-8)$$

From Darcy's law

$$V = ki = k \frac{\sin\alpha}{\sin\lambda} \quad (I-9)$$

and therefore

$$i = \frac{\sin\alpha}{\sin\lambda} \quad (I-10)$$

Thus, by substituting equation (I-10) into equation (I-5), we obtain

$$F = \frac{\frac{c}{\gamma_w z} + \left(\frac{\gamma'}{\gamma_w} \cos \alpha - \sin \alpha \cot \lambda\right) \tan \phi}{\sin \alpha \left(\frac{\gamma'}{\gamma_w} + 1\right)} \quad (I-11)$$

The minimum factor of safety for a particular soil type at a given slope is found by differentiating equation (I-7) with respect to λ and setting the resulting equation to zero. Thus,

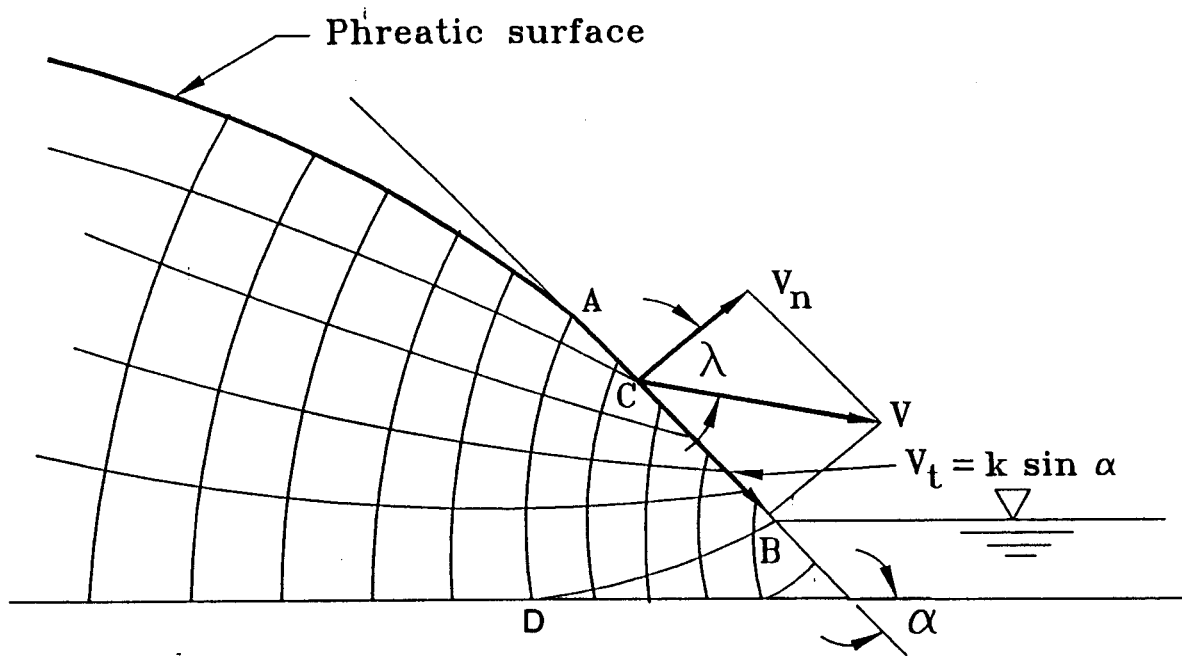


Fig. I-2. Flow field in a homogeneous isotropic soil showing the exit velocity and its components

$$\frac{\partial F}{\partial \lambda} = \frac{\operatorname{cosec}^2(\lambda)}{\frac{Y'}{Y_w} - 1} = 0 \quad (\text{I-12})$$

along the seepage face AB. The solution for equation (I-12) is $\lambda \rightarrow \infty$. Therefore, the theoretical minimum factor of safety is obtained when $\lambda \rightarrow \infty$. However, examination of Fig. I-1 shows that, for groundwater seepage out of the slope, λ varies from $\lambda = 90^\circ$ at A to $\lambda = 0^\circ$ at B. This then places limits on the factor of safety and also limits the magnitude of hydraulic gradient (equation I-5) that can provoke a Coulomb type failure to $\sin \alpha < i < \infty$. From equation (I-11), for a cohesionless soil, the condition

$$\frac{Y'}{Y_w} \cos \alpha > \sin \alpha \cot \lambda \quad (\text{I-13a})$$

or

$$\tan \lambda > \frac{Y_w}{Y} \tan \alpha \quad (\text{I-13b})$$

must be satisfied for a Coulomb type failure. At $\lambda = 90^\circ$, seepage is parallel to the slope, the hydraulic gradient is at its minimum value. Therefore, seepage parallel to slope will invoke a Coulomb type failure yielding the minimum stable seepage slope..

At limiting equilibrium, $F = 1$, equation (I-5) reduces to

$$\tan\phi = \frac{\frac{Y'}{Y_w} \sin\alpha + i \sin\lambda - \frac{c}{Y_w Z}}{\frac{Y'}{Y_w} \cos\alpha - i \cos\lambda} \quad (\text{I-14})$$

For a cohesionless soil ($c = 0$), equation (I-14) further reduces to

$$\tan\phi = \frac{\frac{Y'}{Y_w} \sin\alpha + i \sin\lambda}{\frac{Y'}{Y_w} \cos\alpha - i \cos\lambda} \quad (\text{I-15})$$

or, by substituting equation (I-10), to

$$\tan\phi = \frac{\sin\alpha \left(\frac{Y'}{Y_w} + 1\right)}{\frac{Y'}{Y_w} \cos\alpha + \sin\alpha \cot\lambda} \quad (\text{I-16})$$

For seepage parallel to the slope, $\lambda = 90^\circ$, equation (I-14) reduces further to the Taylor (1948) equation

$$\alpha = \tan^{-1}\left(\frac{Y'}{Y_{sat}} \tan\phi\right) \quad (\text{I-17})$$

Iverson and Major (1986) obtained equation (I-15) following a more rigorous analysis using differential calculus. They discussed various scenarios for slope instability and static liquefaction depending on the direction and magnitude of the seepage vector. The magnitude

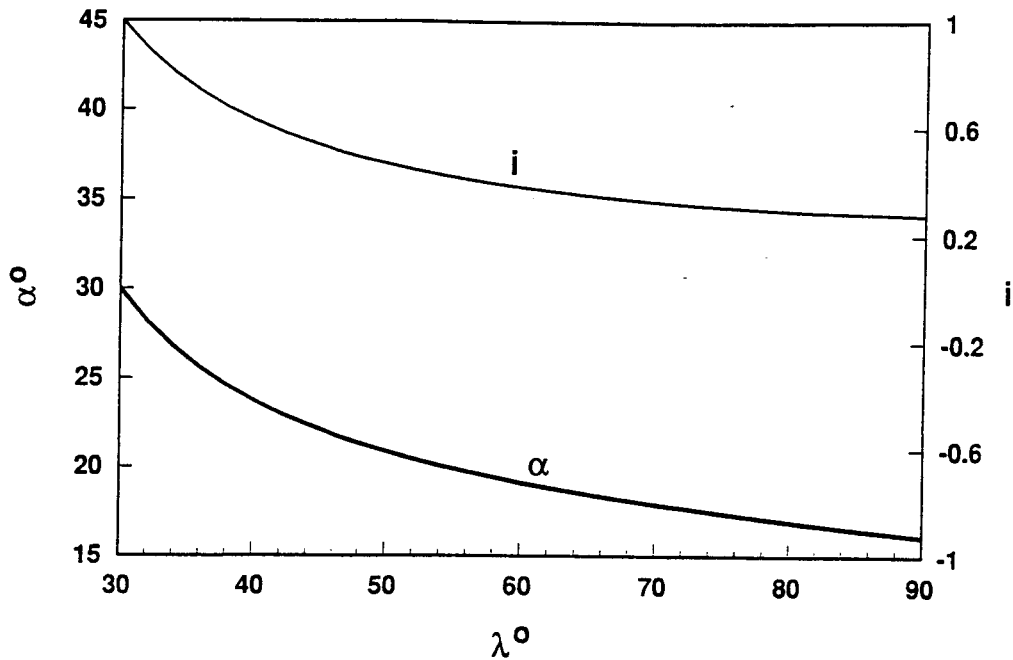


Fig. I-3 Slope angles for different seepage directions and the corresponding hydraulic gradient for $\phi = 30^\circ$.

of the seepage vector, i , and its direction, λ , are uniquely related at the seepage face (AB, Fig. I-2) for a given slope angle (equation I-10) and not independent as shown in plots of equation (I-15) by Iverson and Major (their figures 3, 4 and 5). Changes in i result in changes in λ , or for a given value of i , there is a unique value of λ as expressed by equation (I-10).

For most soils, $\gamma'/\gamma_w = 1$, which by substitution in equation (I-15) results in

$$\tan \alpha = \frac{\tan \phi}{2 - \tan \phi \cot \lambda} \quad (\text{I-18})$$

A plot of equation (I-18) for $\phi = 30^\circ$ is shown in Fig. I-3 for the valid range of λ , i.e., from a maximum value of 90° to $\tan^{-1}(\gamma_w/\gamma' \tan \alpha) = \tan^{-1}(1 \tan 30^\circ) = 30^\circ$. Only a single curve is generated and not a family of curves as described by Iverson and Major (1986). For example,

if $\alpha = 30^\circ$ and seepage is horizontal, then $\lambda = (90 - \alpha) = 60^\circ$ and $i = 0.577$; only one value of i is consistent with this direction of seepage. The value of i corresponding to the appropriate value of λ from equation I-10, is shown by the light line in Fig. I-3. The minimum stable seepage slope, as expected from the preceding discussion, occurs when $\lambda = 90^\circ$, that is, seepage is parallel to the slope.

In Fig. I-3, the slope, originally at its angle of friction ($\alpha = \phi = 30^\circ$), will remain stable (at limiting equilibrium) until λ exceeds 30° . If, for example, $\lambda = 60^\circ$ (horizontal seepage), the slope will collapse from $\alpha = 30^\circ$ to $\alpha = 19^\circ$. In general, the stable seepage slope decreases with increasing λ reaching its minimum value, for a Coulomb type failure, when $\lambda = 90^\circ$. Observed failures outside of the range $30^\circ \leq \lambda \leq 90^\circ$ are caused by mechanisms other than a Coulomb type. Generally, the lower limit of λ is $\tan^{-1}(\gamma_w/\gamma' \tan \alpha)$. The stable seepage slope angle (α_s) for a Coulomb type failure is given by equation (I-11). Thus, slope angles within the range $0 < \alpha < \alpha_s$ would not fail by a Coulomb type mechanism under seepage forces.

The direction of seepage varies within a soil mass. Typically, the face of the slope will be a tangent to the groundwater surface at contact point A (Fig. I-1), i.e. $\lambda = 90^\circ$, while a streamline, such as DB, intersects the slope at right angles, i.e. $\lambda = 0^\circ$. The stable seepage slope, at a given time, will then depend on the predominant seepage direction. Slope failures under seepage is, therefore, progressive and the minimum stable seepage slope is reached when the predominant seepage direction is parallel to the slope.

Effects of Cohesion

The factor of safety for a purely cohesive soil is obtained from (I-11) by setting $\phi = 0$.

Thus,

$$F = \frac{\frac{c}{\gamma_w Z}}{\sin \alpha \left(\frac{\gamma}{\gamma_w} + 1 \right)} \quad (I-19)$$

At limiting equilibrium, $F = 1$, equation (I-19) reduces to

$$\sin \alpha = \frac{c}{\gamma_{sat} Z} \quad (I-20)$$

Therefore, a purely cohesive soil, seepage directions do not influence the stable slope for an infinite slope failure.

Seepage in an Unsaturated-Saturated Sand Mass

The stable seepage slope for seepage in an unsaturated - saturated sand mass (Fig. I-4) can be obtained by using the appropriate value for the soil weight, W . Consider an element at a depth Z below the ground surface in the saturated region and assuming that a capillary zone of thickness, d , exists just above the groundwater surface. The weight per unit area, w , is

$$w = \gamma_t D + \gamma_{sat} d + \gamma h \quad (I-21)$$

where D is the thickness of the unsaturated region, γ_t is the bulk unit weight, and $h = Z - D - d$ is the depth from the groundwater surface to the element. Following the procedures used to obtain equation (I-15), the corresponding equation for seepage in an unsaturated-saturated sand mass is

$$\tan \phi = \frac{\sin \alpha + \frac{i \sin \lambda}{\xi}}{\cos \alpha - \frac{i \cos \lambda}{\xi}} \quad (I-22)$$

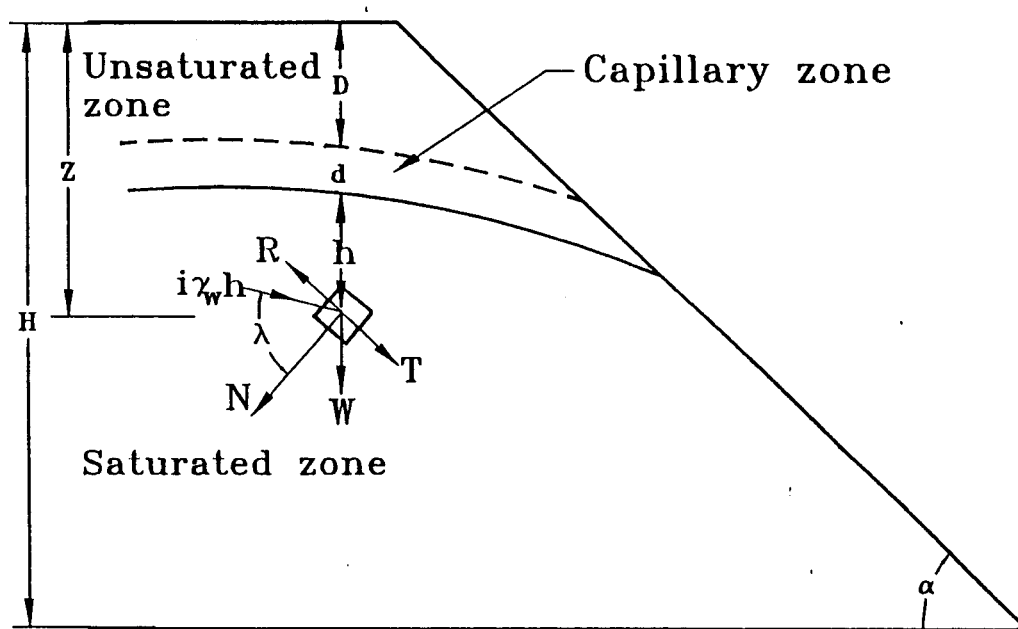


Fig. I-4. Forces on an elemental volume for a saturated-unsaturated soil.

or, by substituting equation (I-10), is

$$\tan\phi = \frac{\sin\alpha (\xi - 1)}{\xi \cos\alpha - \sin\alpha \cot\lambda} \quad (\text{I-23})$$

where

$$\xi = \frac{\gamma D}{\gamma_w h} + \frac{\gamma_{sat} d}{\gamma_w h} + \frac{\gamma'}{\gamma_w} \quad (\text{I-24})$$

and

$$\frac{\gamma}{\gamma_w} = \frac{G + S_r \rho}{1 + e} \quad ; \quad \frac{\gamma_{sat}}{\gamma_w} = \frac{G + e}{1 + e} \quad ; \quad \frac{\gamma'}{\gamma_w} = \frac{G - 1}{1 + e} \quad (\text{I-25})$$

where G is the specific gravity of the soil, e is void ratio and S_r is the degree of saturation.

For seepage parallel to the slope, λ = 90°, equation (I-24) reduces to

$$\tan\alpha = \left(\frac{\xi}{1 + \xi} \right) \tan\phi \quad (\text{I-26})$$

Assuming d = 0 (no capillary zone), S_r = 0 (dry soil mass above ground water surface), γ'/γ_w = 1 (equivalent to e = 0.7 for G = 2.7) and φ = 30°, then

$$\xi = 1.588 \left(\frac{1}{\frac{Z}{D} - 1} \right) + 1 \quad ; \quad \frac{Z}{D} \geq 1 \quad (\text{I-27})$$

A plot of the stable seepage slope using equation (I-22) and (I-23) is shown in Fig. I-5. From the ground water surface to the ground surface, $Z/D \leq 1$, the slope angle is ϕ . As Z/D increases, the slope angle decreases rapidly until about $Z/D = 10$, then slowly decreases to $\tan^{-1}(0.5 \tan\phi)$ as $Z/D \rightarrow \infty$. For practical purposes, slopes with $Z/D > 10$ in an unsaturated-saturated cohesionless soil can reasonably be assumed to be infinite.

Comparison of Analysis with Laboratory Experiments

A sand mass was deposited in water over a 3 m length in a flume 5.5 m long, 0.61 m wide and 0.76 m in height. The water in the flume was lowered very slowly so that seepage erosion was minimized. A slope of angle $\alpha = 32^\circ$ was constructed (Fig. I-6) in the flume. The properties of the sand, determined from laboratory geotechnical tests following American

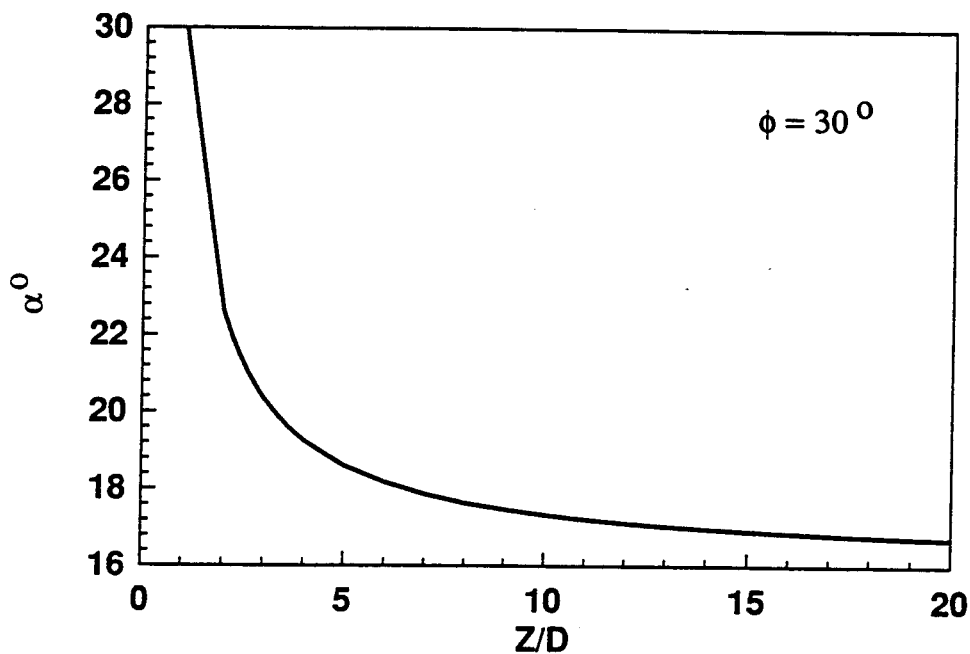


Fig. I-5 Plot of stable seepage slope as a function of Z/D ratio for $\phi = 30^\circ$.

Standard Testing Methods, are as follows: (ASTM D 421-422) average grain size, $D_{50} = 0.73\text{mm}$, coefficient of uniformity, $C_u = 3.9$, coefficient of concavity, $C_c = 1.1$, $\gamma_{\text{sat}} = 19 \text{ kN/m}^3$, (ASTM D 2424-68) coefficient of permeability = $5.0 \times 10^{-3} \text{ cm/s}$, and (ASTM D 3080-90) $\Phi = 32^\circ$. One of the longitudinal sides of the extant flume was constructed from glass so that we were able to observe and measure changes in slope resulting from seepage.

The external water level (water level in front of the slope) was raised to the top of the slope and kept there until equilibrium was achieved with the water level in the slope. As the external water level was lowered at a rate of 0.1m/min (maximum withdrawal rate permitted by the outflow valve, Fig. I-6), cracks appeared on the slope. When the external water level reached an elevation 7.5 cm from the base of the slope (low water level), the slope failed. A vertical face, 27 cm in depth from the top of the slope, was followed by a slope of 22° after the failure (insert diagram, Fig. I-7). The above procedure of raising and lowering the external water level was repeated several times. Further slope failures were observed after each drawdown until the 8th drawdown. After the 8th drawdown, the slope remained stable at an angle of 18° (Fig. I-7). During the second rise of the external water level, the vertical face collapsed indicating that this face was formed by capillary action.

The results indicate that slope failures under seepage is progressive until a minimum stable seepage slope is achieved. From equation (I-15), the predicted minimum stable seepage slope for the sand mass is $\alpha_{\text{min}} = \tan^{-1} \left[\left\{ \frac{19-9.81}{19} \right\} \tan 32^\circ \right] = 17^\circ$ which is in good agreement with the observed value of 18° . The experimental arrangement and procedures were kept very simple to obtain gross behavior. Instrumentation, such as pore water pressure

transducers, was not inserted into the sand mass so as to prevent interference with the development of the failure surface. The direction of seepage could not be determined from the experiments. However, from equation (I-14), the predominant seepage direction to cause the first slope failure, for example, is $\lambda = 52^\circ$. A more detailed series of experiments was conducted by Amanullah (1993) using various initial slopes, and rates of rise and drawdown of the external water level. His observations and conclusions are similar to the preceding.

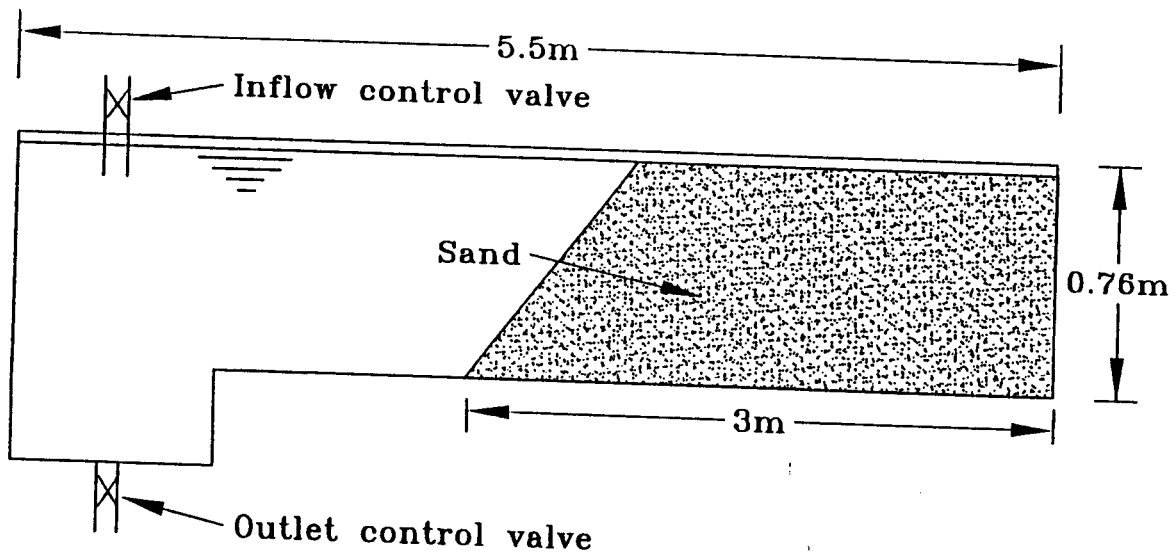


Fig. I-6. A sectional view of the flume used to investigate slope failures by emergent seepage

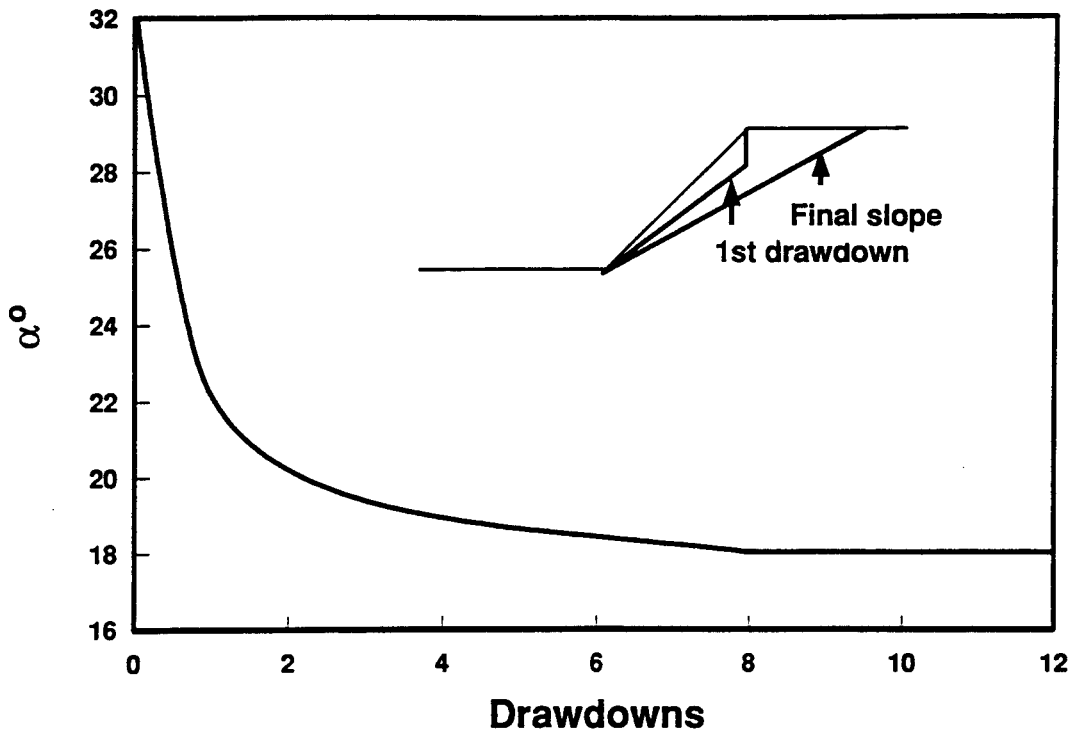


Fig. I-7 Observed stable seepage slope as a function of the number of drawdowns.

APPENDIX II

Formulation of Finite Element Model for Seepage Erosion

A numerical model for seepage erosion using Biot (1941) consolidation theory is formulated in the following. The groundwater level (free surface) within a sandbar fluctuates with transient river stage. Thus, the effective stresses, consolidation ratio and the permeability of the soil mass can vary with river stage. The advantage of utilizing Biot's theory is that stress changes, pore water pressures, seepage stresses, slope (bank) stability and the free surface can be solved simultaneously.

Biot (1941) presented a coupled theory for consolidation in which pore water pressures and total stresses are linked by the principle of effective stresses.

$$\sigma_{ij}^t = \sigma_{ij} + \delta_{ij}u \quad (\text{II-1})$$

where σ_{ij}^t is the total stress, σ_{ij} is the effective stress, δ_{ij} is the Kronecker delta and u is the pore water pressure. The equations of equilibrium are

$$\frac{\partial \sigma_{ij}^t}{\partial x_j} + B_i = 0 \quad (\text{II-2})$$

where B_i is the body force unit volume and x is the position of the body. The equation of continuity together with Darcy's law results in

$$\frac{1}{\gamma_w} \left\{ k_x \frac{\partial^2 u}{\partial x^2} + k_y \frac{\partial^2 u}{\partial y^2} + k_z \frac{\partial^2 u}{\partial z^2} \right\} + \frac{\partial \epsilon_v}{\partial t} = 0 \quad (II-3)$$

where k_x , k_y , k_z are the coefficients of permeability in the x, y and z Cartesian directions and γ_w is the unit weight of water which is assumed to remain constant. The volumetric strain ϵ_v is

$$\epsilon_v = \epsilon_1 + \epsilon_2 + \epsilon_3 \quad (II-4)$$

where ϵ_1 , ϵ_2 , ϵ_3 are the principal strains. Compressive volumetric strains are taken as positive. Equation (II-3) can be compared with the conventional equation used in groundwater modeling, that is,

$$\left\{ k_x \frac{\partial^2 h}{\partial x^2} + k_y \frac{\partial^2 h}{\partial y^2} + k_z \frac{\partial^2 h}{\partial z^2} \right\} - S \frac{\partial h}{\partial t} \quad (II-5)$$

where h is head ($h = u/\gamma_w$), and S is storativity. Thus, equations (II-3) and (II-5) are identical provided

$$- \frac{\partial \epsilon_v}{\partial t} = S \frac{\partial h}{\partial t} \quad (II-6)$$

Under transient flow, the soil can undergo both elastic and plastic volumetric change. Thus, a soil model has to be chosen that would allow the evolution of elastic and plastic strains. There are many models in the literature to select from. The soil model selected is the modified Cam-clay (Roscoe and Burland, 1968) because only a few soil

parameters are required to use the model and these can be easily obtained from conventional soil tests.

Let us consider the volume changes from transient changes in groundwater level in a sandbar within the framework of the modified Cam-clay model. The inset diagram in Fig. II.1 shows a soil layer with the groundwater level at a distance y from the ground surface at time, t_0 . The initial state of a typical element, X , located at a distance z is represented by B on the void ratio - $\ln(p)$ curve (Fig. II.1), as approximated by Schofield and Wroth (1968). The curve AM is the loading curve with a slope of λ and MC is the unloading/reloading curve with a slope of κ . We assumed, for simplicity, that the soil is normally consolidated in its existing state. If it were not, then B would lie on the curve MC . Suppose the phreatic surface drops to a new position M , the mean effective stress on a typical element will increase from, say, an initial value of p_0 to p_m . The soil consolidates and the total change in void ratio is

$$\delta e = \lambda \ln \frac{p_m}{p_0} \quad (II-7)$$

and the total change in volumetric strain is

$$\delta e_v^t = \frac{\lambda}{1+e_0} \ln \frac{p_m}{p_0} \quad (II-8)$$

where e_0 is the initial void ratio. In the Soil Mechanics literature, compression is taken as positive, so λ is positive. The total change in volumetric strain can be decomposed into two parts, an elastic part, δe_v^e , and a plastic part, δe_v^p , such that

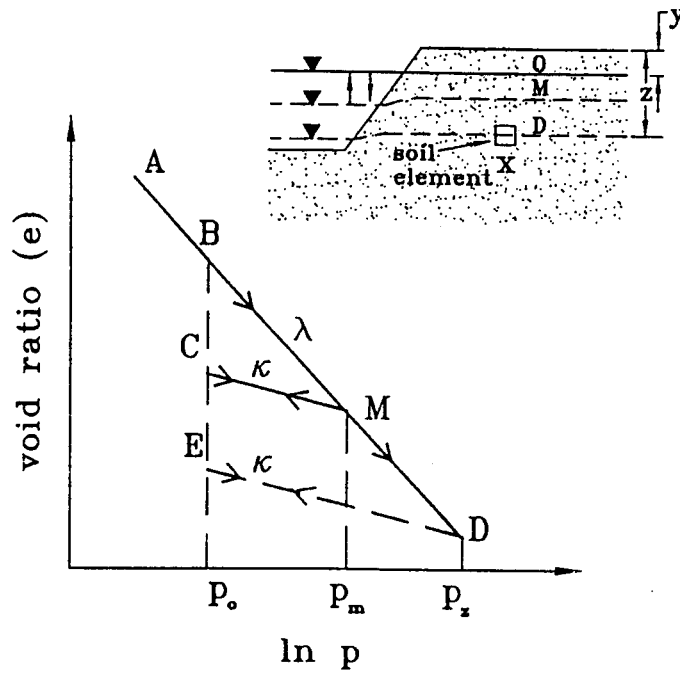


Fig. II-1 Void ratio - $\ln(p)$ curve.

$$\delta e_v = \delta e_v^e + \delta e_v^p \quad (II-9)$$

If the groundwater level were to rise to its original position, the path followed will not be MB but MC (Fig. II.1), because the soil had previously undergone changes in both elastic and plastic volumetric strains. The elastic volumetric strain component is obtained from the slope of the line MC whereby

$$\delta e_v^e = \frac{\kappa}{1+e_o} \ln \frac{p_m}{p_o} \quad (II-10)$$

where κ is taken as positive for compression, and the plastic component is

$$\delta e_v^p = \frac{\lambda - \kappa}{1+e_o} \ln \frac{p_m}{p_o} \quad (II-11)$$

Suppose that the groundwater level now drops below its original position. The mean effective stress will then increase to a value p_z which is greater than the maximum past mean effective stress p_m . The total change in volumetric strain as a result of this loading condition (path CMD) is

$$\delta \epsilon_v = \frac{1}{1+e_o} \left\{ \kappa \ln \left(\frac{p_m}{p_o} \right) + \lambda \ln \left(\frac{p_z}{p_m} \right) \right\} \quad (\text{II-12})$$

If a rise in water level were to subsequently occur up to the original groundwater level, the soil would follow path DE. The changes in elasto-plastic volumetric strains resulting from transient conditions can now be incorporated into equation (II-5). For example, if the groundwater level fluctuations are within the elastic region, MC, equation (II-5) becomes

$$\left(k_x \frac{\partial^2 h}{\partial x^2} + k_y \frac{\partial^2 h}{\partial y^2} + k_z \frac{\partial^2 h}{\partial z^2} \right) = \frac{\kappa}{p_o(1+e_o)} \frac{\partial p_o}{\partial t} \quad (\text{II-13})$$

and if the past maximum mean effective stress is exceeded, the governing elasto-plastic equation is

$$\left(k_x \frac{\partial^2 h}{\partial x^2} + k_y \frac{\partial^2 h}{\partial y^2} + k_z \frac{\partial^2 h}{\partial z^2} \right) = \frac{1}{1+e_o} \left\{ \frac{\kappa}{p_o} \frac{\partial p_o}{\partial t} - \frac{\lambda}{p_z} \frac{\partial p_z}{\partial t} \right\} \quad (\text{II-14})$$

The soil parameters κ and λ can be found by conducting a consolidation test on the soil and finding the slopes of the loading and unloading lines. If the changes in stress from groundwater level fluctuations lie within the unloading/reloading line then the soil is

overconsolidated and an elastic analysis can be used as an approximation. In this case, κ can be found from the shear modulus of the soil (G_s) through the relationship

$$\kappa = \frac{p(1 + e_0)}{K} = \frac{1.5p(1 + e_0)(1 - 2\mu)}{(1 + \mu)G_s} \quad (II-15)$$

where p is the mean effective stress, K is the bulk modulus and μ is Poisson's ratio.

The solution for equation (II-5), over the whole domain, is found using standard numerical techniques. For example, for a finite element solution, using variational principles, equation (II-3) becomes

$$\begin{aligned} \frac{1}{V_w} \int_V \left(k_x \frac{\partial(\delta u)}{\partial x} \frac{\partial u}{\partial x} + k_y \frac{\partial(\delta u)}{\partial y} \frac{\partial u}{\partial y} + k_z \frac{\partial(\delta u)}{\partial z} \frac{\partial u}{\partial z} \right) dV + \int_V \delta u \frac{\partial \epsilon_u}{\partial t} dV \\ - \int_A \left(k_x(\delta u) \frac{\partial u}{\partial x} n_x + k_y(\delta u) \frac{\partial u}{\partial y} n_y + k_z(\delta u) \frac{\partial u}{\partial z} n_z \right) dA \end{aligned} \quad (II-16)$$

where n_x , n_y and n_z are direction cosines of the unit outward normal vector, V is volume, A is the surface area of the domain, and δ is a small increment.

In order to solve this time-marching problem, the following approximation is made

$$\int_{t_n}^{t_{n+1}} u(t) dt = \{(1 - \alpha)u(t_n) + \alpha u(t_{n+1})\} \Delta t \quad (II-17)$$

where α is a constant with a magnitude chosen to yield optimum stability. The virtual work equation is

$$\int_V \sigma_{ij}^t \delta \epsilon_{ij} dV - \int_A \sigma_{ij}^t n_j \delta X_i dA + \int_V B \delta X dV \quad (II-18)$$

where ϵ_{ij} is the strain tensor and X_i is the displacement. The coupled equations (II-17) and (II-18) can now be used in a finite element scheme to solve the transient seepage-stress-consolidation problem. The finite element method and programming methodology occur extensively in the literature (for example, Zienkiewicz et al., 1966, Hinton and Owen, 1977) and will not be repeated here. In our formulation, we specify a value of $\alpha = 1$; Booker and Small (1975) showed that the coupled equations are unconditionally stable provided $\alpha \geq 0.5$.